Centralized Control of Power System Stabilizers

Gerardo A. Sánchez Ayala

Dissertation submitted to the faculty of the Virginia Polytechnic Institute and State University in partial fulfillment of the requirements for the degree of

Doctor of Philosophy

in

Electrical Engineering

Virgilio A. Centeno, Chair

James S. Thorp

Jaime De La Ree Lopez

Daniel J. Stilwell

Werner E. Kohler

September 19, 2014
Blacksburg, Virginia

Keywords: Centralized Control, Gain Scheduling, Phasor Measurement Unit (PMU), Power System Stabilizer (PSS), Wide Area Measurement Systems (WAMS), Dynamic Reduction, Decision Trees, Small Signal Analysis

Centralized Control of Power System Stabilizers

Gerardo A. Sánchez Ayala

Abstract

This study takes advantage of wide area measurements to propose a centralized nonlinear controller that acts on power system stabilizers, to cooperatively increase the damping of problematic small signal oscillations all over the system. The structure based on decision trees results in a simple, efficient, and dependable methodology that imposes much less computational burden than other nonlinear design approaches, making it a promising candidate for actual implementation by utilities and system operators.

Details are given to utilize existing stabilizers while causing minimum changes to the equipment, and warranting improvement or at least no detriment of current system behavior. This enables power system stabilizers to overcome their inherent limitation to act only on the basis of local measurements to damp a single target frequency. This study demonstrates the implications of this new input on mathematical models, and the control functionality that is made available by its incorporation to conventional stabilizers.

In preparation of the case of study, a heuristic dynamic reduction methodology is introduced that preserves a physical equivalent model, and that can be interpreted by any commercial software package. The steps of this method are general, versatile, and of easy adaptation to any particular power system model, with the aggregated value of producing a physical model as final result, that makes the approach appealing for industry. The accuracy of the resulting reduced network has been demonstrated with the model of the Central American System.

To my family.

Acknowledgements

From its beginning this project has found essential supporters that have made this achievement possible. Especially I express my deepest gratitude to Dr. Virgilio Centeno who has been an academic and life advisor, and continue as a friend. His generous assistance has gone from technical and academic discussions, to fixing car problems and being there for family needs. Not only has his contribution greatly enriched this experience as a graduate student, but also lets a mark that will remain.

I am very grateful to Dr. James Thorp for his participation in this research project from the very moment of idea inception, and to Dr. Jaime De La Ree for his genuine interest and incessant efforts to boost my accomplishments integrally. All discussions, comments, and scrutiny from Dr. Daniel Stilwell, Dr. Yaman Evrenosoğlu, and Dr. Werner Kohler contributed to shape and polish this dissertation and are greatly appreciated.

To my family members, especially my father Gabriel and my wife Jane, that continuously and unconditionally were by my side, and to many good friends that often lightened the load, I am particularly thankful. Finally I would like to extend my gratitude to the Fulbright Program, and to the Department of Electrical and Computer Engineering of Virginia Tech, for enabling this doctoral project with the necessary financial support.

Table of Contents

List of Figures

List of Tables

CHAPTER 1 Introduction

1.1 Overview and Objective

Poorly damped small signal oscillations in power systems can harm regular operation and are capable of obstructing planning decisions to the extent of preventing the interconnection of remote areas, causing serious deviations from scheduled power transfers, and resulting in blackouts, as was the case in the 1996 blackout of the North America Western interconnection system [1]. This phenomenon is always present, to some degree, in power systems and the best approach to counter act it seeks to improve awareness of oscillations by identifying oscillating frequencies along with their respective damping, and to instigate actions towards augmented damping of hazardous oscillations.

Power System Stabilizers (PSSs) were originally designed to introduce a damping torque component in the excitation system of generators, such that the damping of a specific oscillation frequency can be increased. PSSs are installed following either a detailed measurement of frequency deviations all over the system, or modal analysis based on mathematical system models to determine oscillation frequencies, damping, and participation factors. In the best cases, both studies are done to verify discrepancies between model and reality. This allows the determination of the generators where the stabilizers should be placed; lastly, PSS parameters are tuned to increase the effective damping of selected frequencies.

The effectiveness of the PSS is indubitable provided if the device is properly tuned, but as a consequence of model imprecisions and system variations, the PSS' constituting filters are often tuned to damp frequencies different to the actual frequencies observed in real system conditions. This weakness has been of concern to power system engineers, and has led to robust PSS designs that are not yet commonly used. One of the factors that is changing the local measurements focus of these robust stabilizer designs is the growing accessibility to Wide Area Measurement (WAM), from Phasor Measurement Units (PMUs).

Small signal oscillations [2], [3], are tightly related to network topology, geographic distribution, and other physical parameters of the power grid. The time synchronization of PMUs effectively solves the disparity problem of measurements taken at distant locations; this feature has been taken advantage of in the study of implementations of Flexible AC Transmission Systems (FACTS) devices, as well as PSSs for damping control of inter-area oscillations, using feedback from remote measurements.

This dissertation proposes a centralized controller that employs PSSs to act cooperatively to increase damping of small signal oscillations in the system. The suggested state feedback controller receives real time synchronized measurements from generation plants disseminated all over the system, and sends control signals to all the PSSs that are to participate in the control loop.

Instead of modeling uncertainties, an enumeration method is used in this work to account for robustness in a gain scheduling approach. A nonlinear controller is built for the nonlinear power system plant by assembling a set of linear controllers that are coordinated in real time via switching. Decision trees are implemented as coordinating entities in charge of the gain scheduling. This methodology is simple and imposes much less computational burden than other nonlinear design approaches, making it a promising candidate for actual implementation by utilities and independent system operators (ISOs).

1.2 Literature Review

Centralized control of power system oscillations became feasible with the advent of PMUs, but even before that, research efforts emerged towards robust control actions to damp sustained oscillations. In the early nineties, [4] analyzed the applicability of robust, adaptive, and nonlinear control to various classes of power system control problems, paying attention to how uncertainties were modeled (either structured or unstructured), the magnitude of disturbances (either small or large), and the domain of action of the controller (either centralized or decentralized). More recently, in 2009 a survey on robust control methods in power systems is presented in [5], highlighting characteristics of gain scheduling, linear matrix inequalities (LMI), and linear parameter varying (LPV) control methods.

Modified power system stabilizers have been proposed to expand the capabilities of these devices in providing damping torque components to the excitation systems. In 1996, [6] proposed a PSS design with two inputs, one receiving local rotor speed measurements to damp local oscillations, and the other receiving remote measurements from a point in the system sensitive to a specific inter-area oscillation. This method is simulated on a 19-machine system resembling the Western North American Grid. Another approach of PSS design was made by Electricité de France in the mid-nineties [7], [8], introducing the desensitized method which obtains a robust controller so that its performance does not significantly deteriorates when the operating point changes. This structure was proved to be equivalent to the standard structure of an automatic voltage regulator with a stabilizer (AVR+PSS). An extended desensitized four-loop regulator (EDFLR) is proposed in [9] designed to address local and inter-area oscillations on the European Power System.

Different types of flexible AC transmission system (FACTS) devices have the capacity of influencing oscillation damping. [10] uses time-optimal control to act on a series capacitor placed in a carefully selected transmission line to damp inter-area modes, showing simulated results on a six-machine system. A 24-machine model is used in [11] to present a linear controller that acts on a thyristor controlled series capacitor (TCSC) and on a thyristor controlled phase angle regulator (TCPAR) to increase the damping of inter-area oscillations, relying on selected measurements.

To damp small signal oscillations, a linear optimal controller is implemented on a two-machine system in [12], the study includes RTDS simulations with control actions applied to Variable Series Compensators (VSCs). In [13], post disturbance damping is increased by PID controllers acting on a TCSC. The study accounts for robustness by designing multiple system models and scheduling the control actions with a Bayesian probability-weighted average. The method was tested on a 4-machine system.

HVDC lines are used to increase the damping of targeted inter-area oscillations in [14]. The authors apply a state feedback control method, and perform simulations on the Southern Chinese system. Robustness is accounted for by Relative Gain Array (RGA). HVDC lines are also used in [15] and [16], acting from H_2/H_∞ controllers implemented with polytopic LMI to damp small signal oscillations; in addition to HVDCs, [17] also uses energy storage devices and remote PMU frequencies as added inputs to selected power system stabilizers. With the same goal, [18] controls TCSCs with state feedback control, [19] uses a static synchronous series compensator (SSSC) to interact with a Fuzzy Logic controller, and [20] applies modal linear quadratic Gaussian control methodology to act on an HVDC on the 16-Machine New England-New York System. In a similar work, [21] proposes a neural network based controller to act on a convertible static compensator.

Power System Stabilizers have also been proposed by several authors as mechanisms to receive control signals from a centralized controller, to enhance their influence on oscillations. In 2002, [22] proposed a supervisory power system stabilizer (SPSS) coordinated with local PSSs (LPSS) to detect online system oscillations. The control of the SPSS is done by LMI-H_∞, and the interaction with the local PSSs is coordinated with multi-agent system technology. It relies on WAMs and demonstrates the results on a 29-machine system.

More recently, [23] uses PSSs to damp oscillations with a centralized controller based on linear matrix inequalities. Similarly to [17], [24] uses HVDC lines, Energy storage devices and remote PMU frequencies as added inputs to selected power system stabilizers, with a combination of H_2/H_∞ robust control, and federated Kalman filters to define the most suitable controller for different operating conditions. A combination of controllers is used when the system is not exactly in one of the predefined operating points. The New England-New York System is the test system for this study. A hybrid controller consisting of a feed forward neural network-based controller, and a model reference adaptive controller, is used to interact with selected augmented PSSs to damp inter-area oscillations in [25]; this method is tested on a 5-machine system. In other applications, [26] proposes a wide area based damping controller that tunes PSSs, and in [27] an inter-area mode oriented pole shifting method is introduced to coordinate control actions of TCSC and PSSs in the New England-New York System.

Automatic voltage regulators have been considered as receivers of centralized control actions for damping oscillations in [28]. In this study a state feedback controller is designed to act on selected AVRs while accounting for changes in the system by a proposed external loop to adjust the control parameters in a near-real-time way aimed to accommodate varying operation conditions based on state estimation. The method was implemented on a 262 machine reduced model of the Chinese system. In another AVR application, [29] proposes a H_2/H_∞ centralized controller resolved by linear matrix inequalities optimization in the New England System with 10 machines.

The effect of latency that unavoidably would take place in a centralized control system has been studied in [30], where a predictor approach is adopted to formulate the damping-control design. In [31] an approach based on inverse system algorithm and linear matrix inequalities is proposed to design a nonlinear robust integrated controller. [32] finds the limits of time delay that can be tolerated for a specific LMI controller design.

The development of the centralized control method in this dissertation relies on several concepts and analytical tools that currently are in a mature stage of development and have found numerous applications in power systems. The following references list the publications relevant to this study on Prony Method, Genetic Algorithms, Decision Trees, and Dynamic Reduction applied to power system analysis and design cases.

Applications of Prony method in power systems

- Supervision of transient harmonics, and characterization of waveform distortions: [33], [34]
- Estimation of fundamental frequency, and phasor calculations: [35], [36]
- Evaluation of performance of PSSs and identification of dominant modes: [37], [38]
- Comparison of Prony with other methods: [39], [40]
- Tracking of voltage variations: [41]
- Model reduction, and system transfer functions: [28], [42]

Applications of genetic algorithms in power systems

- Optimal power flow, economic load dispatch and planning: [43], [44], and [45]
- Power system planning: [46], [47], and [48]
- Parameter tuning and system performance: [43], [49], [50], [51], and [52]

Decision Trees in power systems

- Adaptive protection, and security assessment: [53], [54], [55], [56], [57]
- Islanding detection, identification, and classification of disturbances: [58], [59], [60]
- Adaptation to complex synchrophasor data: [61]
- Prediction of stochastic residual demand curves, estimation of daily load pattern of units, prediction of reactor and capacitor values: [62]

Dynamic reduction in power systems

- Reduction by artificial neural networks: [63]
- Software applications: [64], [65], [66]
- Reduction by computation of observability and controllability Gramians: [67]
- Coherency-based mathematical reduction: [68]
- Coherency identification: [69]
- Optimization-based reduction: [70], [71]
- Kinetic energy-based reduction: [72]
- Reduction by selective modal analysis: [73], [15]

1.3 Outline

The remainder of this dissertation is organized as follows. Chapter 2 looks at the fundamental concepts of tools and techniques that are well developed and have found numerous applications in several fields

of science and engineering, and are used as well in the development of this study. The chapter starts with a discussion of the concept of stability in power systems, and a presentation of the structure and operation of power system stabilizers that at a later stage are proposed as receivers of the control signals.

State feedback control and a review of controllability are equally discussed in Chapter 2. These concepts are essential for the pole displacement design of feedback gains at selected operation points. This discussion is followed by a review of the basic fundaments of optimization by genetic algorithms that are used in the dynamic reduction process of the Central American system. The chapter continues with a mathematical review of Prony analysis, presented as a base for its implementation in the classification of stable and unstable responses, followed by an introduction to the concepts of eigenvector and participation factor analysis indispensable in small signal studies. The chapter concludes with a review of the fundaments of decision trees that are later applied as coordinating agents for gain scheduling.

Chapter 3 details how standard PSSs can be adapted, with minimum disruption to existing installations, to receive an external control signal incoming from the centralized controller. The proposed adaptation emphasizes the preservation of existing parameters to guarantee minimum detriment on the expected behavior accomplished with utilities' settings; the effectiveness of this methodology is verified by simulations. After, details are provided on the variable transformations required to migrate existing system model from traditional settings to the one that is suitable for the proposed controller implementation. The chapter also introduces the design of a state feedback controller, and demonstrates its behavior when applied on the New England-New York model to increase the damping of problematic oscillation modes.

Chapter 4 describes the incorporation of robustness to the centralized controller, exemplified with the model of the Central American system. Although the proposed control implementation is capable of coping with large order system models, the chapter begins with a heuristic methodology for dynamic reduction applied to the system under study, so that the demonstration of this method is expedited. Next, a comprehensive description of the anticipated range of operation of the Central American system is laid out, based on practices of the Central American System Operator (EOR is acronym in Spanish for Ente Operador Regional). A set of representative operation points is selected to proceed with the design of the respective state feedback gains, and decision trees are trained and validated to act as schedulers. The chapter ends with considerations of the effect of communications latency in the feedback loop. The final chapter summarizes the project achievements, and defines lines for future research.

CHAPTER 2 Fundaments

The development of the proposed centralized controller relies on some basic concepts that need to be introduced in advance to allow a fluent discussion of results in the chapters to follow. This chapter presents basic notions on control systems applied in current power grids; it reviews the state feedback control methodology and the genetic algorithm used for optimization in Section 4.1. The Prony analysis used for classification of waveforms is also covered, as well as the decision trees concepts that are the basis for gain scheduling in Section 4.4.

2.1 Power System Stabilizers

Power System Stabilizers or PSSs play an important role in current power systems due to their potential to affect low frequency electromechanical oscillations and their contribution to increase damping on the large rotor angle excursions that follow certain contingencies. Understanding the strengths and weaknesses of these devices requires a closer study of the small signal stability problem, and the enhancement of control technologies in this matter.

This section starts with an outlook of how the stability problem is treated in power systems, and continues with a description of the role and characteristics of PSSs.

2.1.1 The Study of Stability in Power Systems

Control mechanisms in current power systems are crucial to keep a continuous and trustworthy availability of electric energy. Their function aims to smoothly accommodate the system to the requirements of the desired operating conditions, and simultaneously enhance its general stability.

The size of typical power systems, the number of variables at play, and the actual shortage of accurate universal models capable of describing power systems in a compact mathematical form, puts the problem out of reach for stability analysis in a unified way as it is done with other complex systems. Instead, the issue of stability in a power system is studied by focusing on specific behavioral characteristics, one at a time.

These domains of stability analysis are related to the type of disturbances exciting the system's dynamics. When the system is subject to quasistatic changes on power demand, transient responses are not considered and **voltage stability** is studied. This type of stability is related to a monotonically decreasing voltage magnitude that takes place to the extent that power transfer is increased. It is dealt with transmission reinforcements such as reactive compensation, static VAR compensators, transmission line upgrading, or grid reconfiguration.

Transient stability refers to the ability of the system to not loose synchronism when sudden changes or contingencies ensue upon the system. The consequences of large disturbances are reduced mainly through protection systems that promptly isolate faulty zones, and remedial actions that reduce the stress on affected generators. In parallel, as demonstrated in [74], automatic voltage regulators and power system stabilizers are installed in generation plants to increase damping torque on generators, not only for low frequency oscillations, but also for fast angle variations following disturbances.

When a power system is in steady state, it still is continuously influenced by relatively small disturbances that originate from normal demand and generation changes. These random occurrences persistently excite the system's dynamics and its modes, causing oscillatory behavior that may or may not be sufficiently damped. **Small signal stability** regards these circumstances, and its study suggests the use of power system stabilizers to avoid small signal instability. This dissertation proposes a new mechanism that can be used to support small signal stability as presented in Chapter 3 and 4.

2.1.2 Structure and Operation of Power System Stabilizers

The dynamic model of a power system typically includes mathematical representations of all generator types with their control components, FACTS, HVDCs, and loads with significant dynamic contribution. When the system is to be analyzed subjected only to small disturbances, it can be characterized using linearized versions of the complete model, computed about a specified operating point. Once a state space model is available, linear analysis techniques can be implemented to understand the system's behavior and to design suitable control mechanisms to improve stability and performance.

The action of PSSs at this stage can be explained from the linearized model of a synchronous machine. This model was originally developed by Heffron and Phillips [75], and it was modified for PSS applications by DeMello and Concordia in [76]. The block diagram representation is shown in Figure 2.1, where the parameter values depend on electromechanical properties of the machine, the transfer functions of the control components (AVR and PSS), and the particular operating point of the complete system. A detailed development of the linearized model, and the analytical method to find exact expressions of the model constants, can be studied following the guidelines in [74].

In Figure 2.1 H is the inertia constant, K_D is the damping coefficient, and ω_0 is the synchronous speed. G_{PSS} represents the transfer function for the stabilizer and G_{exc}, the transfer function for the automatic voltage regulator. The mechanical torque is T_m, and V_{ref} is the exciter reference voltage. The model also shows the following system variables:

ω_r	:	Rotor speed
δ	:	Rotor position
T_e	:	Electromagnetic torque

ψ_{fd} : Field winding flux linkage

E_{fd} : Exciter output voltage

V_{PSS} : Stabilizer output voltage

E_t : Terminal voltage

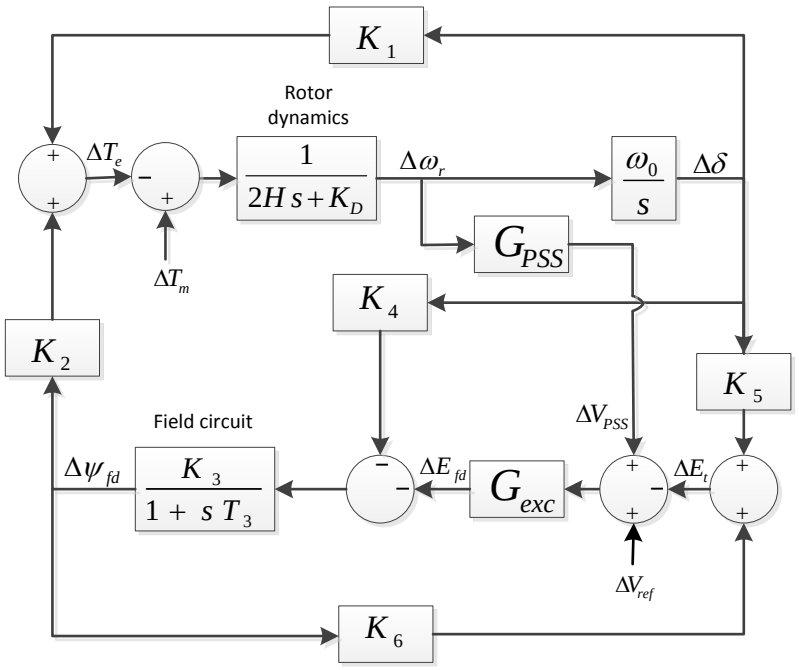

Figure 2.1 Block diagram representation of the synchronous machine including Automatic Voltage Regulator and Power System Stabilizer

Since the goal of the PSS is to introduce damping torque, and this torque is directly related to rotor speed, then the speed deviation is the natural choice of input variable to the PSS for each machine. Ideally the torque produced by the PSS should be in exact opposition to the torque produced by the sub-damped oscillations of the rotor, but as can be seen in Figure 2.1, the transfer function between the exciter input and the resulting electromagnetic torque will inevitably introduce a phase lag that will be a function of the oscillation frequency. For this reason, the transfer function of every PSS must be tuned to have a high gain at the frequency of interest and to compensate for the phase lag that will occur at that frequency. Simultaneously the PSS is also required to have very small gain at low frequencies, and to contribute to damp other local or inter-area modes. If the frequency response of the stabilizer does not exhibit the described characteristics, its action may result in a decrement of damping torque and consequently increased oscillations.

The basic model of a PSS uses only one input, which is normally the local rotor speed, and is composed by a washout stage, one or more phase compensation stages, and a saturation function as shown in Figure 2.2. The washout block is a high-pass filter whose function is to

prevent PSS operation in quasi steady state conditions that could allow slow frequency variations as in islanded operation, systems with frequency based pricing policies, or systems where the lack of governor control prevails. Figure 2.3 depicts a Bode plot for a washout transfer function with $T_W = 10$, and $K_{PSS} = 100$; the linear frequency scale allows to see the regular frequency range of PSS operation.

The lead-lag blocks in Figure 2.2 compensate for the phase lag introduced in the path between the PSS output and the electromagnetic torque. Several compensation stages may be applied to increase the phase–frequency and gain–frequency slopes of the combined frequency response. Figure 2.4 shows the Bode graph with a linear frequency scale for two cascaded lead-lag blocks, where $T_{n1} = 0.1$, $T_{d1} = 0.02$, $T_{n2} = 0.08$ and $T_{d2} = 0.02$. The phase response in a PSS is generally designed for a slight undercompensation of about ten degrees for the whole range of frequencies where the stabilizer will act. This practice is to prevent the reduction of damping torque that would result if overcompensation occurred [74]. Imprecise modeling is unfortunately a common problem in many power systems. Logically this results in incorrect tuning of PSSs and a latent risk of loss of synchronism. As it will be shown later, deficiencies in PSS tuning can be compensated with the proposed centralized control technique.

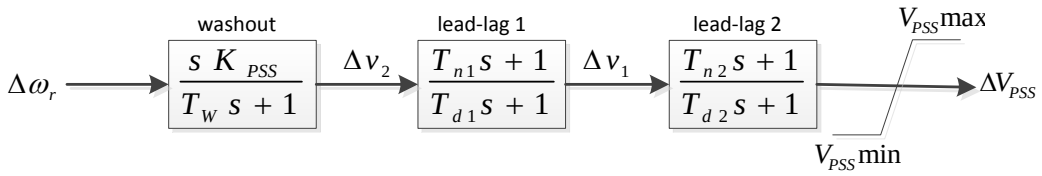

Figure 2.2 Basic structure for a single input PSS with two lead-lag blocks

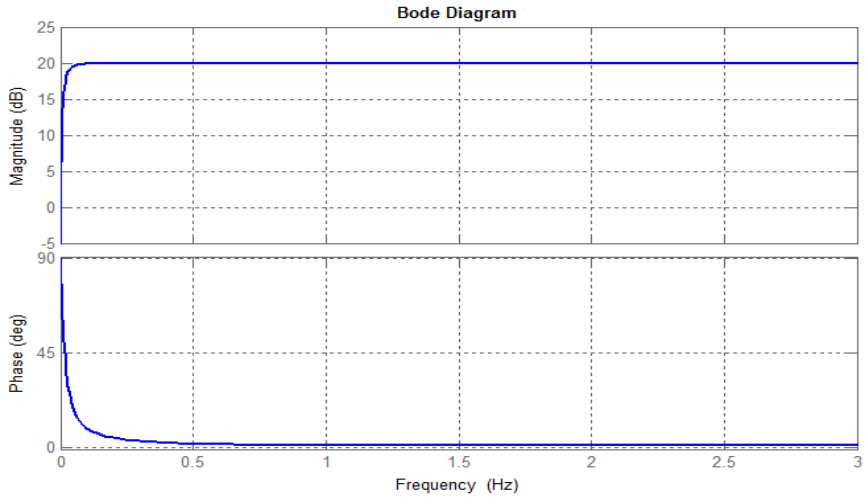

Figure 2.3 Bode plot with linear frequency scale for a washout block with $T_W = 10$ and $K_{PSS} = 100$

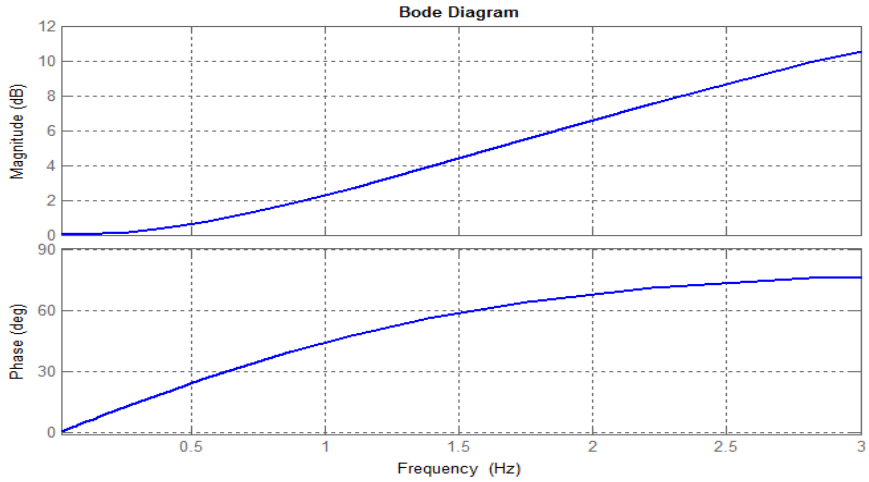

Figure 2.4 Bode plot with linear frequency scale for two cascaded lead-lag blocks where $T_{n1} = 0.1$, $T_{d1} = 0.02$, $T_{n2} = 0.08$ and $T_{d2} = 0.02$

2.2 State Feedback Control

In Linear Control, if a system is controllable then all its eigenvalues can be allocated at will by state feedback. When full controllability is theoretically granted, in practice the pole placement is achieved through control actions that will be limited by operational constraints on actuators or on controlled devices. This section reviews the concepts and results of state feedback control, a well-developed technique that is exploited in this study for a centralized controller in power systems. The material of this section follows the lines of linear system theory as presented in [77], [78], [74], and [79].

2.2.1 Controllability

Since the output does not play a role in controllability, at this point an n^{th} order, *p*-inputs linearized system is sufficiently described by the state equation,

$$\dot{\boldsymbol{x}} = \mathbf{A}\boldsymbol{x} + \mathbf{B}\boldsymbol{u} \qquad (2.1)$$

where $\mathbf{A}$ is the square state matrix of order n, and $\mathbf{B}$ is the input matrix of order $n \times p$.

For (2.1), controllability is defined as [77],

"The state equation (2.1), or the pair $(\mathbf{A}, \mathbf{B})$ *is said to be controllable if for any initial state* $\boldsymbol{x}(\mathbf{0}) = \boldsymbol{x}_0$ *and any final state* $\boldsymbol{x}_1$*, there exists an input that transfers* $\boldsymbol{x}_0$ *to* $\boldsymbol{x}_1$ *in a finite time. Otherwise (2.1) or* $(\mathbf{A}, \mathbf{B})$ *is said to be uncontrollable."*

The n right eigenvectors of $\mathbf{A}$ are the n^{th} order vectors $\boldsymbol{\phi}_i$, $i = 1 \ldots n$, that have the property of scalar amplification on $\mathbf{A}$ according to,

$$\mathbf{A}\boldsymbol{\phi}_i = \lambda_i \boldsymbol{\phi}_i \tag{2.2}$$

where λ_i, $i = 1, \dots n$, are the eigenvalues of $\mathbf{A}$.

Similarly, the n^{th} order vectors $\boldsymbol{\psi}_i$, $i = 1 \dots n$, that have the property of scalar amplification on $\mathbf{A}$ according to,

$$\boldsymbol{\psi}_i \mathbf{A} = \lambda_i \boldsymbol{\psi}_i \tag{2.3}$$

are the left eigenvectors of $\mathbf{A}$.

The collection of right and left eigenvectors of $\mathbf{A}$ gives rise respectively to the modal matrices $\boldsymbol{\Phi}$ and $\boldsymbol{\Psi}$ as,

$$\boldsymbol{\Phi} = [\boldsymbol{\phi}_1 \quad \boldsymbol{\phi}_2 \quad \dots \quad \boldsymbol{\phi}_n] \tag{2.4}$$

$$\boldsymbol{\Psi} = [\boldsymbol{\psi}_1^T \quad \boldsymbol{\psi}_2^T \quad \dots \quad \boldsymbol{\psi}_n^T]^T$$

The right and left eigenvectors are orthogonal, following that $\boldsymbol{\psi}_i \boldsymbol{\phi}_j = 0$ if $i \neq j$, and $\boldsymbol{\psi}_i \boldsymbol{\phi}_j = C_i$ if $i = j$. Besides, from (2.2) given that $\boldsymbol{\phi}_i$ is an eigenvector of $\mathbf{A}$, then any scalar k multiplied by $\boldsymbol{\phi}_i$ also is an eigenvector of $\mathbf{A}$. This allows to say that the eigenvectors can be normalized such that $\boldsymbol{\psi}_i \boldsymbol{\phi}_j = C_i/k = 1$, and in general the modal matrices (2.4) can be expressed as,

$$\boldsymbol{\Psi}\boldsymbol{\Phi} = \mathbf{I} \quad , \quad \boldsymbol{\Psi} = \boldsymbol{\Phi}^{-1} \tag{2.5}$$

Using the modal matrix $\boldsymbol{\Phi}$ to perform the transformation $\boldsymbol{x} = \boldsymbol{\Phi}\boldsymbol{z}$, (2.1) yields,

$$\boldsymbol{\Phi}\dot{\boldsymbol{z}} = \mathbf{A}\boldsymbol{\Phi}\boldsymbol{z} + \mathbf{B}\boldsymbol{u}$$

$$\dot{\boldsymbol{z}} = \boldsymbol{\Phi}^{-1}\boldsymbol{A}\boldsymbol{\Phi}\boldsymbol{z} + \boldsymbol{\Phi}^{-1}\mathbf{B}\boldsymbol{u} \tag{2.6}$$

(2.2) can be expanded to,

$$\mathbf{A}\boldsymbol{\Phi} = \boldsymbol{\Phi}\boldsymbol{\Lambda} \quad , \quad \boldsymbol{\Phi}^{-1}\mathbf{A}\boldsymbol{\Phi} = \boldsymbol{\Lambda} \tag{2.7}$$

where $\boldsymbol{\Lambda}$ is a diagonal matrix with the eigenvalues λ_i, $i = 1, \dots, n$ in the diagonal.

Then (2.6) can be written in the Jordan normal form as,

$$\dot{\boldsymbol{z}} = \boldsymbol{\Lambda}\boldsymbol{z} + \mathbf{B}_n\boldsymbol{u} \tag{2.8}$$

where $\mathbf{B}_n = \boldsymbol{\Phi}^{-1}\mathbf{B}$ is referred to as the mode controllability matrix.

Since $\boldsymbol{\Lambda}$ is a diagonal matrix then every state in the transformed state vector $\boldsymbol{z}$ in (2.8) is decoupled from the rest, implying that every row of $\mathbf{B}_n$ is related to only one mode of $\mathbf{A}$, and that the only way to affect the i^{th} transformed state $\boldsymbol{z}_i$, from an input $\boldsymbol{u}$, is by having a nonzero i^{th} row of $\mathbf{B}_n$.

This observation leads to the concept of modal controllability, where the i^{th} non-repeated mode of (2.8) is controllable if and only if the i^{th} row of $\mathbf{B}_n$ is different than zero; otherwise the mode is uncontrollable. Considering that the property of controllability is invariable with similarity transformations, the controllability of the original state space model (2.1) can be assessed by evaluating the controllability of (2.8) [77].

2.2.2 State Feedback

A constant gain negative state feedback method was selected to demonstrate the centralized control of system modes. Here, the input $\boldsymbol{u}$ of the system (2.1) is replaced by,

$$\boldsymbol{u} = \boldsymbol{r} - \mathbf{F}\boldsymbol{x} \tag{2.9}$$

where $\boldsymbol{r}$ is the reference input and $\mathbf{F}$ is the constant feedback matrix.

In the small signal model under study the states are deviations from the equilibrium point, and the control goal is to keep the system in the state of equilibrium, thus the reference input is zero in this case. Combining (2.9) and the state equation (2.1) leads to the closed loop state feedback model,

$$\begin{aligned} \dot{\boldsymbol{x}} &= (\mathbf{A} - \mathbf{BF})\boldsymbol{x} + \mathbf{B}\boldsymbol{r} \\ \dot{\boldsymbol{y}} &= \mathbf{C}\boldsymbol{x} \end{aligned} \tag{2.10}$$

This system is represented in Figure 2.5.

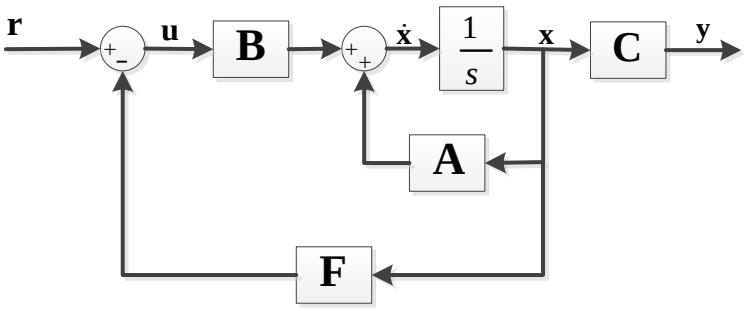

Figure 2.5 Block diagram representation of the state feedback model

The specific method that was applied in this project is a robust pole placement algorithm that minimizes the sensitivity of the poles to variations in the closed loop state matrix; it is fully described and theoretically supported in [79]. There the pole placement problem is stated as follows:

"Given real matrices $(\mathbf{A}, \mathbf{B})$ *of orders* $(n \times n)$ *and* $(n \times m)$ *respectively, and a set of* n *complex numbers,* $\mathcal{L} = \{\lambda_{c1}, \lambda_{c2}, \dots, \lambda_{cn}\}$*, closed under complex conjugation, find a real* $(n \times m)$ *matrix* $\mathbf{F}$ *such that the eigenvalues of* $\mathbf{A} - \mathbf{BF}$ *are* $\lambda_{cj}, j = 1, 2, \dots, n$*".*

The problem can be solved even if the pair $(\mathbf{A}, \mathbf{B})$ is not completely controllable, as long as the set $\mathcal{L} = \{\mathcal{L}_u, \mathcal{L}_c\}$ contains $\mathcal{L}_u$, the set of all uncontrollable modes of $(\mathbf{A}, \mathbf{B})$.

In the same reference it is stated that if $\mathbf{M} = \mathbf{A} - \mathbf{BF}$ is non-defective, that is, $\mathbf{M}$ has n linearly independent eigenvectors, then $\mathbf{M}$ is diagonalizable and the sensitivity of a closed loop eigenvalue λ_{cj} to perturbations in the components of $\mathbf{M}$ depends upon the magnitude of the condition number c_j, where,

$$c_j = \frac{\|\boldsymbol{\psi}_{cj}\|_2 \|\boldsymbol{\phi}_{cj}\|_2}{|\boldsymbol{\psi}_{cj}^T \boldsymbol{\phi}_{cj}|} \geq 1$$

$\boldsymbol{\psi}_{cj}$ is the j^{th} left eigenvector and $\boldsymbol{\phi}_{cj}$ is the j^{th} right eigenvector, both of the closed loop state matrix $\mathbf{M}$.

A restriction is applied to the definition of $\mathcal{L}$ in order to assure that the resulting matrix $\mathbf{M}$ is non-defective, that is the multiplicity of the eigenvalues $\lambda_j \in \mathcal{L}$ to be assigned must be less than or equal to the number of linearly independent inputs. Once this is granted, robustness is added by reformulating the pole placement problem to find a real matrix $\mathbf{F}$ and a nonsingular matrix $\mathbf{X}$ satisfying,

$$(\mathbf{A} - \mathbf{BF})\mathbf{X} = \mathbf{X}\boldsymbol{\Lambda}_c$$

where,

$$\boldsymbol{\Lambda}_\mathbf{c} = \begin{bmatrix} \lambda_{c1} & 0 & 0 & 0 \\ 0 & \lambda_{c2} & 0 & 0 \\ 0 & 0 & \ddots & 0 \\ 0 & 0 & 0 & \lambda_{cn} \end{bmatrix}$$

such that some robustness measure $\boldsymbol{\nu}$ is optimized, for example $\boldsymbol{\nu} = \|\boldsymbol{c}\|_\infty$, where $\boldsymbol{c}^T = [c_1 \quad c_2 \quad \cdots \quad c_n]$ is the vector of condition numbers corresponding to the selected matrix $\mathbf{X}$ of eigenvectors. This problem is equivalent to find a non-defective system of eigenvectors, given by $\mathbf{X}$, such that it is as well conditioned as possible.

The Matlab function `place(A,B,p)` computes a feedback gain matrix $\mathbf{F}$ that achieves the desired closed-loop pole locations `p`, assuming all the inputs of the plant are control inputs. Precise details on this methodology and its implementation algorithms for robust pole placement can be found in [79].

2.3 Optimization by Genetic Algorithm

In Chapter 4, the dynamic reduction of the Central American System involves the optimization of PSS parameters to attain slight corrections on the damping of selected oscillation modes. An optimization method by a genetic algorithm was employed for this task due to its aptitude to solve a variety of

optimization problems that are not well suited for standard optimization algorithms, including highly complex optimization functions.

A genetic algorithm mimics the process of natural selection of biological organisms to find the fittest individual among a vast population, as a function of inherited characteristics evolving on their environment. The adaptability of the natural selection process makes it applicable to solve optimization problems by being able to efficiently process multivariable problems of any nature, without demanding previous knowledge of their features, and being independent of the selected initial point [80]. Following the genetic algorithm presentation in [81], the most remarkable concepts behind this application are described next.

The system under study —the electric power system — represents the environment on which individuals play. Every individual is constituted by a set of parameters to optimize, which related to this study would refer to a set of scalar values for the transfer functions of the stabilizers being modified; for convenience an individual is arranged as a vector. A fitness or objective function of all the parameters to optimize is defined beforehand, such that it reflects the qualities of an individual performance in the environment.

The following paragraphs outline the basic genetic algorithm depicted in Figure 2.6. It starts by producing the first generation: a population of random elements, regardless of the range of choice for this initial set. Subsequently, two individuals are sifted out from among the initial population to become the parents of the new generation; this is the first rule of the genetic algorithm denominated as *Selection*. Afterwards the algorithm proceeds with the other two rules: *Crossover*, and *Mutation*.

Selection

The selection rule is in charge of deciding which individuals are to be used as parents to produce the next generation. Emulating nature, the most apt individuals are granted with better chances to hand down their characteristics, and therefore the selection of an individual will be related to their fitness evaluation in the objective function. However, less fitted individuals must not be left out of reproduction chances to prevent that the population becomes homogenous. A common strategy is to select one of the parents based on its fitness while the other parent is selected randomly.

Several selection methods are available for genetic algorithms [82], [83], one of the most common is the Roulette or Montecarlo selection, which assigns a probability between 0 and 1 to every individual in proportion to its own fitness value. According to this probability, every individual is allotted a fraction of the roulette, and is allocated in descending order. The selection of an individual is achieved by generating a random number between 0 and 1, locating this value on the roulette, and thus selecting the individual belonging to that position.

Another method for selection is known as Tournament, where a number n of individuals is randomly chosen and one of them is selected on a basis that may be deterministic, or stochastic. An example of the deterministic selection would be if the individual with highest fitness value is selected, and then again a stochastic approach could be followed by generating a random number between 0 and 1, and if

this number surpasses a predefined threshold, the most apt individual is selected, otherwise, select the one that follows in aptitude.

Crossover [81]

The idea behind the crossover relies on the natural combination of parent genes, to result in children who inherit part of the characteristics of every parent. Depending on how the crossover takes place, the descendants can exhibit either better or worse fitness than the originating individuals, but since the parents were well adapted individuals, there will be a chance that the children inherit the precise genes responsible for the parents' fitness.

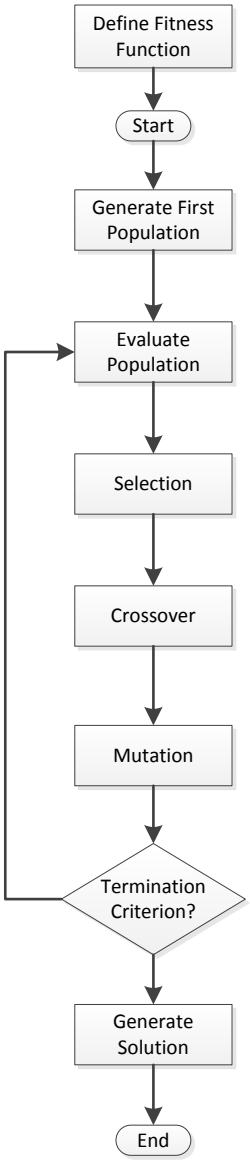

Figure 2.6 Basic diagram of the genetic algorithm

When the good characteristics of individuals are shared, the descendants, or at least part of them will likely have a higher fitness than their parents. If this does not happen to be the case and the population

of children is not as fit as the parents', this won't mean that progress has not been obtained because somehow the good genes are there, and in future generations they may resurge, regaining the apparently lost fitness.

The crossover methods that best illustrate the concept are:

1. **Single point crossover**

   This method consists in generating a random partition to each parent, splitting them in heads and tails, and then swapping each other's tails to generate the children. To illustrate this, let the parents be two strings of seven parameters each.

   Parent 1: $\{\alpha_1\ \alpha_2\ \alpha_3\ \alpha_4\ \alpha_5\ \alpha_6\ \alpha_7\}$
   Parent 2: $\{\beta_1\ \beta_2\ \beta_3\ \beta_4\ \beta_5\ \beta_6\ \beta_7\}$

   Assuming that the random division is generated at the second position, the resulting heads and tails are:

   Head 1: $\{\alpha_1\ \alpha_2\}$ Tail 1: $\{\alpha_3\ \alpha_4\ \alpha_5\ \alpha_6\ \alpha_7\}$
   Head 2: $\{\beta_1\ \beta_2\}$ Tail 2: $\{\ \beta_3\ \beta_4\ \beta_5\ \beta_6\ \beta_7\}$

   From here the exchange of tails results in the following children:

   Child 1: $\{\alpha_1\ \alpha_2\ \beta_3\ \beta_4\ \beta_5\ \beta_6\ \beta_7\}$
   Child 2: $\{\beta_1\ \beta_2\ \alpha_3\ \alpha_4\ \alpha_5\ \alpha_6\ \alpha_7\}$

2. **Double point crossover**

   This method is similar to the single point crossover, except that instead of one random partition point, two of them are generated to divide each parent in three segments; next, the central elements are swapped.

   In the previous example, assuming that the random divisions are the third and the fifth positions, the partitions of the parent would be:

   Parent 1: Part 1: $\{\alpha_1\ \alpha_2\ \alpha_3\}$ Part 2: $\{\alpha_4\ \alpha_5\}$ Part 3: $\{\alpha_6\ \alpha_7\}$
   Parent 2: Part 1: $\{\beta_1\ \beta_2\ \beta_3\}$ Part 2: $\{\beta_4\ \beta_5\}$ Part 3: $\{\beta_6\ \beta_7\}$

   After exchanging the central portions the resulting children would be:

   Child 1: $\{\alpha_1\ \alpha_2\ \alpha_3\ \beta_4\ \beta_5\ \alpha_6\ \alpha_7\}$
   Child 2: $\{\beta_1\ \beta_2\ \beta_3\ \alpha_4\ \alpha_5\ \beta_6\ \beta_7\}$

3. **Uniform crossover**

   With the uniform crossover method, every element of the children has the same probability of belonging to either of the parents. It consists in generating a random binary array of the same length as the number of parameters, and then using it as a mask on the parents. To form the first child, the locations of the ones in the mask will indicate the elements that should be taken from Parent 1, and the locations of the zeroes mark the elements that should be taken from

Parent 2. The formation of the Child 2 is done by repeating the same actions after the ones and the zeroes have been swapped in the mask.

Following the same example, if the randomly generated mask is:

Mask: $\{1\ 1\ 0\ 1\ 0\ 0\ 1\}$

then the children would be:

Child 1: $\{\alpha_1\ \alpha_2\ \beta_3\ \alpha_4\ \beta_5\ \beta_6\ \alpha_7\}$
Child 2: $\{\beta_1\ \beta_2\ \alpha_3\ \beta_4\ \alpha_5\ \alpha_6\ \beta_7\}$

Mutation [81]
A complementary way of generating children is the introduction of mutations on the descendants. This is a necessary measure to have the possibility of creating new genes to explore thoroughly the search space, and to avoid reaching a premature solution caused by the lack of diversity in the population.

A mutation is done by applying random changes to a single individual in the current generation to create a child. These changes are usually random replacements of usually one single attribute of the parents, and the process is repeated until the desired proportion of mutation children is completed.

The genetic algorithm ends when a termination criterion has been reached. This can be the completion of the maximum number of generations, achieving a fitness minimum limit, exceeding the maximum time for optimization, or stall of generations or fitness value.

2.4 Prony Analysis

The Prony's estimation method decomposes a signal in a sum of exponentially damped and phase displaced sinusoids, corresponding to the frequency components of the original signal [84], [85]. This method is appropriate to determine if a given signal includes or not exponentially growing components, which would be a proper indication of unstable behavior.

Prony analysis is used in this project for the design of decision trees for gain scheduling in Section 4.4, and the study of latency effects on the centralized controller covered in Section 4.5. Both applications rely on the detection of unstable behavior by signal analysis.

From (2.8), the natural response of an n^{th} order Linear Time Invariant system expressed in terms of the variable transformation $\boldsymbol{x} = \boldsymbol{\Phi z}$ is,

$$\dot{\boldsymbol{z}} = \begin{bmatrix} \dot{z}_1 \\ \dot{z}_2 \\ \vdots \\ \dot{z}_n \end{bmatrix} = \begin{bmatrix} \lambda_1 & 0 & 0 & 0 \\ 0 & \lambda_2 & 0 & 0 \\ 0 & 0 & \ddots & 0 \\ 0 & 0 & 0 & \lambda_n \end{bmatrix} \begin{bmatrix} z_1 \\ z_2 \\ \vdots \\ z_n \end{bmatrix} = \boldsymbol{\Lambda z} \tag{2.11}$$

Every transformed state $\boldsymbol{z}$ is decoupled from the rest, and (2.11) can be put as n independent differential equations as,

$$\dot{z}_i = \lambda_i z_i\,, \qquad i = 1, 2, \dots, n \tag{2.12}$$

The solution to (2.12) depends only on the initial condition of the transformed state z_i, and on its respective eigenvalue:

$$z_i(t) = z_i(0)e^{\lambda_i} \tag{2.13}$$

(2.4) can be used to return the solution to the state vector $\boldsymbol{x}$, as:

$$\begin{bmatrix} x_1 \\ x_2 \\ \vdots \\ x_n \end{bmatrix} = [\boldsymbol{\phi}_1 \quad \boldsymbol{\phi}_2 \quad \dots \quad \boldsymbol{\phi}_n] \begin{bmatrix} z_1 \\ z_2 \\ \vdots \\ z_n \end{bmatrix} = \boldsymbol{\phi}_1 z_1 + \boldsymbol{\phi}_2 z_2 + \cdots + \boldsymbol{\phi}_n z_n \tag{2.14}$$

where $\boldsymbol{\phi}_i, i = 1, 2, \dots, n$ are the right system eigenvectors of order $(n \times 1)$.

Combining (2.13) and (2.14) leads to,

$$\begin{aligned} [x_1 \quad x_2 \quad \dots \quad x_n]^T &= \boldsymbol{\phi}_1 z_1(0)e^{\lambda_1 t} + \boldsymbol{\phi}_2 z_2(0)e^{\lambda_2 t} + \cdots \\ &+ \boldsymbol{\phi}_n z_n(0)e^{\lambda_n t} = \sum_{i=1}^{n} \boldsymbol{\phi}_i z_i(0)e^{\lambda_i t} \end{aligned} \tag{2.15}$$

From (2.14) and (2.5) it follows that,

$$\begin{bmatrix} z_1 \\ z_2 \\ \vdots \\ z_n \end{bmatrix} = \boldsymbol{z} = \boldsymbol{\Phi}^{-1}\boldsymbol{x} = \boldsymbol{\Psi}\boldsymbol{x} = \begin{bmatrix} \boldsymbol{\psi}_1 \\ \boldsymbol{\psi}_2 \\ \vdots \\ \boldsymbol{\psi}_n \end{bmatrix} \begin{bmatrix} x_1 \\ x_2 \\ \vdots \\ x_n \end{bmatrix} \tag{2.16}$$

or,

$$z_i = \boldsymbol{\psi}_i \begin{bmatrix} x_1 \\ x_2 \\ \vdots \\ x_n \end{bmatrix} \tag{2.17}$$

where $\boldsymbol{\psi}_i,\ i = 1, 2, \dots, n$ are the left system eigenvectors of order $(1 \times n)$.

From (2.17) if follows that $z_i(0) = \boldsymbol{\psi}_i \boldsymbol{x}(0)$, and (2.15) becomes,

$$\boldsymbol{x}(t) = \sum_{i=1}^{n} \boldsymbol{\phi}_i \boldsymbol{\psi}_i \boldsymbol{x}(0)e^{\lambda_i t} \tag{2.18}$$

In this last equation, the product $\boldsymbol{\psi}_i \boldsymbol{x}(0) := b_i \in \mathbb{C}$ is a scalar, where the subscript i takes values from 1 to n. Since the eigenvalue $\lambda_i = \sigma_i \pm j\omega_i$ is in general a complex number, then the response in time of every state $x_i(t)$ behaves in fact as a linear combination of complex exponentials, where each of them

may be non-oscillatory in the case of real eigenvalues, or oscillatory with an exponential envelope when the eigenvalues are complex. The response in time of the k^{th} state would be,

$$x_k(t) = \phi_{1,k} b_1 e^{\sigma_1 t} e^{j\omega_1 t} + \phi_{1,k}^* b_1^* e^{\sigma_1 t} e^{-j\omega_1 t} + \cdots + \phi_{n,k} b_n e^{\sigma_n t} e^{j\omega_n t} + \phi_{n,k}^* b_n^* e^{\sigma_n t} e^{-j\omega_n t} \quad (2.19)$$

where $\phi_{i,k}$ for $i = 1, \dots, n$ is the k^{th} element of the i^{th} right eigenvector, and $\phi_{i,k}^*$ is its conjugate.

Defining $B_{i,k} := \phi_{i,k} b_i \in \mathbb{C}$ for $i = 1, \dots, n$, (2.19) can be rewritten as,

$$x_k(t) = |B_{1,k}| e^{\sigma_1 t} e^{j(\omega_1 t + \theta_{1,k})} + |B_{1,k}| e^{\sigma_1 t} e^{-j(\omega_1 t + \theta_{1,k})} + \cdots + |B_{n,k}| e^{\sigma_n t} e^{j(\omega_n t + \theta_{n,k})} + |B_{n,k}| e^{\sigma_n t} e^{-j(\omega_n t + \theta_{n,k})}$$

where $B_{i,k}$ for $i = 1, \dots, n$ being a complex number, is represented in polar form as $|B_{i,k}| e^{j\theta_{i,k}}$, and $\theta_{i,k}$ is the argument of $B_{i,k}$.

Using Euler's Identity the last expression can be simplified to,

$$\begin{aligned} x_k(t) = |B_{1,k}| e^{\sigma_1 t} & \left[\left(\cos(\omega_1 t + \theta_{1,k}) + j \sin(\omega_1 t + \theta_{1,k}) \right) \right. \\ & \left. + \left(\cos(\omega_1 t + \theta_{1,k}) - j \sin(\omega_1 t + \theta_{1,k}) \right) \right] + \cdots \\ & + |B_{n,k}| e^{\sigma_n t} \left[\left(\cos(\omega_n t + \theta_{n,k}) + j \sin(\omega_n t + \theta_{n,k}) \right) \right. \\ & \left. + \left(\cos(\omega_n t + \theta_{n,k}) - j \sin(\omega_n t + \theta_{n,k}) \right) \right] \end{aligned}$$

$$\begin{aligned} x_k(t) & \quad (2.20) \\ & = 2|B_{1,k}| e^{\sigma_1 t} \cos(\omega_1 t + \theta_{1,k}) \\ & + \cdots \\ & + 2|B_{n,k}| e^{\sigma_n t} \cos(\omega_n t + \theta_{n,k}) \end{aligned}$$

Equation (2.20) reveals that the time response of the LTI system is constituted by a weighted sum of damped sinusoids shifted in phase. The goal of the Prony Method is to find the coefficients $B_{i,k}$, as well as the complex frequencies $\sigma_i \pm j\omega_i$ for $i = 1, \dots, n$ (the order of the system), and for k being the specific state to be constructed.

The estimation of the complex frequencies is accomplished by recognizing that (2.20) is the solution to some differential equation and that for the n^{th} order system at the discrete instant m, the homogeneous part is expressed in a linear, constant coefficient difference equation as [86]:

$$\sum_{i=0}^{n} a_i x_k[m - i] = 0 \quad (2.21)$$

where a_i, for $i = 0, \dots n$ are the scalar coefficients of its characteristic polynomial in the discrete domain of the z-Transform.

(2.21) can be reordered as,

$$a_0 x_k[m] + a_1 x_k[m-1] + \cdots + a_n x_k[m-n] = 0$$

or in recursive form,

$$x_k[m] = -\frac{1}{a_0}\sum_{i=1}^{n} a_i x_k[m-i] = \sum_{i=1}^{n} \alpha_i x_k[m-i] \tag{2.22}$$

where $\alpha_i = -a_i/a_0$ for $i = 1, \ldots n$.

The reconstruction of the signal x_k will rely on p samples taken at a sampling period T. Expanding (2.22), $p - n$ equations are formed and expressed in matrix form as,

$$\begin{bmatrix} x_k[n-1] & x_k[n-2] & \ldots & x_k[0] \\ x_k[n] & x_k[n-1] & \ldots & x_k[1] \\ x_k[n+1] & x_k[n] & \ldots & x_k[2] \\ \vdots & \vdots & \ldots & \vdots \\ x_k[p-2] & x_k[p-3] & \ldots & x_k[p-n-1] \end{bmatrix} \begin{bmatrix} \alpha_1 \\ \alpha_2 \\ \vdots \\ \alpha_n \end{bmatrix} = \begin{bmatrix} x_k[n] \\ x_k[n+1] \\ x_k[n+2] \\ \vdots \\ x_k[p-1] \end{bmatrix} \tag{2.23}$$

or,

$$\mathbf{D}\boldsymbol{\alpha} = \mathbf{d} \tag{2.24}$$

where,

$$\mathbf{D} := \begin{bmatrix} x_k[n-1] & x_k[n-2] & \ldots & x_k[0] \\ x_k[n] & x_k[n-1] & \ldots & x_k[1] \\ x_k[n+1] & x_k[n] & \ldots & x_k[2] \\ \vdots & \vdots & \ldots & \vdots \\ x_k[p-2] & x_k[p-3] & \ldots & x_k[p-n-1] \end{bmatrix}, \quad \boldsymbol{\alpha} := \begin{bmatrix} \alpha_1 \\ \alpha_2 \\ \vdots \\ \alpha_n \end{bmatrix}, \quad \mathbf{d} := \begin{bmatrix} x_k[n] \\ x_k[n+1] \\ x_k[n+2] \\ \vdots \\ x_k[p-1] \end{bmatrix}$$

In order to permit the identification of all the coefficients of the characteristic polynomial, the number of samples has to be at least the order of the system, i.e. $p \geq 2n$, often resulting in an over determined problem. (2.23) can then be solved for the α_i coefficients by linear regression.

Let $X_k(z)$ be the z-Transform of $x_k[m]$. Then the transformed version of (2.22) is,

$$X_k(1 - \alpha_1 z^{-1} - \alpha_2 z^{-2} - \cdots - \alpha_n z^{-n}) = 0 \tag{2.25}$$

with the characteristic polynomial $F(z) = (1 - \alpha_1 z^{-1} - \alpha_2 z^{-2} - \cdots - \alpha_n z^{-n})$.

This polynomial can be solved by numerical analysis methods returning its roots z_i for $i = 1, \ldots, n$, each of them can be mapped through $z_i = e^{\lambda_i T}$ to the pursued complex frequencies $\lambda_i = \sigma_i \pm j\omega_i$ in (2.18) to (2.20).

By sampling (2.18) with a sampling period T, the k^{th} state signal at the discrete time instant m, or at $t = mT$ can be rewritten as,

$$x_k[m] = B_{1,k} e^{\lambda_1 mT} + B_{2,k} e^{\lambda_2 mT} + \cdots + B_{n,k} e^{\lambda_n mT} \tag{2.26}$$

Where λ_i for $i = 1, \dots, n$ is the solutions of the characteristic polynomial in (2.25) mapped back to the continuous domain of t, and n the order of the system.

As in the case of (2.23), p samples are taken and (2.26) can be expanded and arranged in matrix form as,

$$\begin{bmatrix} L_1^0 & L_2^0 & \dots & L_n^0 \\ L_1^1 & L_2^1 & \dots & L_n^1 \\ L_1^2 & L_2^2 & \dots & L_n^2 \\ \vdots & \vdots & \dots & \vdots \\ L_1^{p-1} & L_2^{p-1} & \dots & L_n^{p-1} \end{bmatrix} \begin{bmatrix} B_{1,k} \\ B_{2,k} \\ \vdots \\ B_{n,k} \end{bmatrix} = \begin{bmatrix} x_k[0] \\ x_k[1] \\ x_k[2] \\ \vdots \\ x_k[p-1] \end{bmatrix} \tag{2.27}$$

where $L_i = e^{\lambda_i T}$ for $i = 1, \dots, n$.

Again, (2.27) is an over determined system that can be solved by linear regression leading to the complex coefficients $B_{i,k}$ for $i = 1, \dots, n$, and thus completing the construction of x_k in (2.20).

The implementation of the Prony Method involves the solution of the arbitrarily large linear regression problems in (2.24) and (2.27), as well as finding the roots of the characteristic polynomial in (2.25). In this project the Matlab function `pronytool.m` was used for this purpose.

2.5 Eigenvectors and Participation Factors

Many of the mathematical tools required for small signal analysis have already been introduced in previous sections to prepare the way for the introduction of the concept of participation factor, and the physical interpretation of the right and left eigenvalues on small signal oscillations studies. This section reviews these concepts that will be applied vigorously in Chapter 3 and 4 to analyze the small signal behavior of the New England-New York and of the Central American power systems.

In the following discussion it will be assumed that the system under study is already linearized and is represented by (2.1)[1]. In the previous section the transformation $\boldsymbol{x} = \boldsymbol{\Phi z}$ lead to (2.11), a decoupled system where every transformed state z_i is independent from the rest, with the solution (2.13). This transformation is expanded in (2.14) and rewritten here as,

$$\begin{bmatrix} x_1 \\ x_2 \\ \vdots \\ x_n \end{bmatrix} = \boldsymbol{\phi}_1 z_1 + \boldsymbol{\phi}_2 z_2 + \cdots + \boldsymbol{\phi}_n z_n$$

From here it can be concluded that since the i^{th} mode affects only z_i, then the i^{th} right eigenvector ϕ_i weights the contribution of the i^{th} mode on every state in $\boldsymbol{x}$. In other words it is said that the right eigenvector defines the mode shape, i.e. the magnitudes of the elements in ϕ_i give the extent of the activity of the n state variables when the i^{th} mode is excited, and the angles of the elements of ϕ_i quantify the phase displacements between the states affected by the same mode. From here it can be

[1] A description on linearization process is included in section 3

established if there are groups of states acting in opposition at a certain oscillation frequency, for example.

The left eigenvector also contributes with useful information for modal analysis. To see this, consider (2.16) rewritten here:

$$\begin{bmatrix} z_1 \\ z_2 \\ \vdots \\ z_n \end{bmatrix} = \boldsymbol{z} = \boldsymbol{\Phi}^{-1}\boldsymbol{x} = \boldsymbol{\Psi}\boldsymbol{x} = \begin{bmatrix} \boldsymbol{\psi}_1 \\ \boldsymbol{\psi}_2 \\ \vdots \\ \boldsymbol{\psi}_n \end{bmatrix} \begin{bmatrix} x_1 \\ x_2 \\ \vdots \\ x_n \end{bmatrix}$$

The product of the i^{th} left eigenvector with the state vector $\boldsymbol{\psi}_i\boldsymbol{x}$ weights the contribution of every state on the i^{th} mode, represented by z_i. Thus the k^{th} element of $\boldsymbol{\psi}_i$ establishes the activity of x_k on the i^{th} mode.

Combining the virtues of the right and the left eigenvector gives rise to the participation factors $p_{ki} = \phi_{ki}\psi_{ik}$ [87], where ϕ_{ki} corresponds to the k^{th} element of the i^{th} right eigenvector, and ψ_{ik} is the k^{th} element of the i^{th} left eigenvector. This is a measure of the net participation of the k^{th} state variable on the i^{th} mode, and vice versa. Unlike the eigenvectors, the participation factors are dimensionless, and if the eigenvectors are normalized as in (2.5) the sum of all the participation factors corresponding to a mode, or associated to any state variable, equals one [74].

Many power systems analysis tools are capable of performing small signal analysis. On this project three software packages were used: SSAT from DSA Tools, DigSILENT Power Factory, and the Matlab Power Systems Toolbox (PST). PST v3 runs on the Matlab environment and was developed by Dr. Kwok W. Cheung and Prof. Joe Chow from Rensselaer Polytechnic Institute [88].

2.6 Decision Trees for Classification

In Chapter 4, decision trees are implemented as a means to make an informed decision on gain scheduling, such that robustness is provided to the centralized control task for a wide range of operational conditions expected from the system under consideration. The decision is made from the classification of a large set of time-synchronized voltage measurements, resulting in an estimated outcome determining if a particular scheduled gain would result in secure conditions or not. This section presents an outlook of decision trees and their application for classification; a complete description of this subject can be found in [89].

2.6.1 Terminology of Decision Trees

A set of individual observations or instances is called the training set. Here every instance is fully described by a number of attributes common to all the entries of the training set, paired with an additional attribute that has the form of an outcome to the combination of attributes of the instance; this outcome attribute is called a classification.

Thus the training set can be expressed in a tabular form as it is shown in Table 2-1, where *m* instances and *n* attributes are represented by the data entries $D(i,j)$ and by the classification outcomes $C(i)$ for the i^{th} instance and for the j^{th} attribute.

Every attribute, depending on its nature can be either categorical or continuous. The first type is associated to attributes that can be described in a finite number of ways, for example, the attribute "Weather" on a given day can be tagged as sunny, cloudy, or rainy, defining this way three categories. The continuous attributes are those that are described in terms of infinite categories such as the set of real numbers. For instance, "Temperature" conditions on a given day can be a continuous attribute that could be classified with inequalities such as $Temperature \geq T$ or $Temperature < T$, where T is some threshold.

Table 2-1 Typical arrangement of the training set

		Attribute Number				
		1	2	…	n	**Class**
Instance	1	D(1,1)	D(1,2)	…	D(1,n)	C(1)
	2	D(2,1)	D(2,2)	…	D(2,n)	C(2)
	⋮	⋮	⋮	…	⋮	⋮
	m	D(m,1)	D(m,2)	…	D(m,n)	C(m)

A decision tree aims to construct classification rules that compress the training set to a reduced number of instructions, disregarding redundant or meaningless attributes that do not contribute to the determination of the outcome. Even with this reduced number of classification rules and with no apparent information on all the instances, the decision tree is able to take any data entry of the training set and reproduce the resulting outcome.

More importantly, a decision tree is capable of predicting the classification of unseen data entries with a definite accuracy. This allows the rapid creation of inferences from pattern recognition, whose quality depends on the richness of information contained in the training set. As an illustration, consider The Golf Example [89], [90] in the following example.

Example 2.1

A golf player consistently makes a decision of playing or not playing depending on four factors:

- *Weather*. It can be sunny, cloudy or rainy. Categorical attribute.
- *Temperature*. It takes a numerical value. Continuous attribute.
- *Humidity*. It takes a numerical value. Continuous attribute.
- *Wind*. It can be either windy or not windy. Categorical attribute.

A daily observation is done during fourteen days, and the results are compiled in Table 2-2. The derived decision tree is shown Figure 2.7.

In order to determine the classification, first the Weather attribute is observed. If the weather is cloudy, then the decision is to play. However if the weather is sunny, the decision of playing or not will depend on whether the attribute Humidity is greater than 75% or not. Similarly, if the

weather is rainy the decision of playing will be contingent to the wind conditions. This decision tree is capable of reproducing all the instances of Table 2-2, and therefore is a compression of the training set. Note that the attribute Temperature is not determinant on the player's decision.

The decision tree of Figure 2.7 is also capable of predicting what the payer's decision could be in circumstances not observed in the training set, for instance if a given day the conditions are: Sunny, temperature of 74F, humidity of 77%, and there is no wind, then according to the tree in Figure 2.7 the decision would probably be to play.

Table 2-2 Training Data for the Golf Example

Weather	Temp. [F]	Hum. [%]	Windy	Class
sunny	75	70	yes	play
sunny	80	90	yes	don't play
sunny	85	85	no	don't play
sunny	72	95	no	don't play
sunny	69	70	no	play
cloudy	72	90	yes	play
cloudy	83	78	no	play
cloudy	64	65	yes	play
cloudy	81	75	no	play
rainy	71	80	yes	don't play
rainy	65	70	yes	don't play
rainy	75	80	no	play
rainy	68	80	no	play
rainy	70	96	no	play

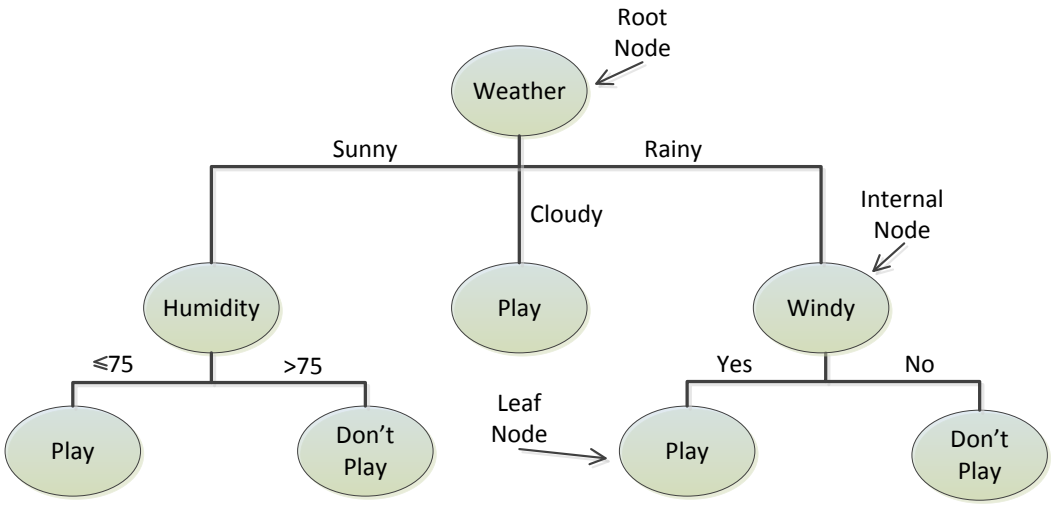

Figure 2.7 Decision tree for the Golf Example

□

2.6.2 Construction of a Decision Tree

In this section, one of the most commonly used methods to build decision trees is introduced; this is the Top-Down Induction of Decision Tree (TDIDT) algorithm combined with the Information Gain strategy for attribute selection. The TDIDT generates decision trees by repeatedly splitting the values of attributes, a process known as recursive partitioning. The basic TDIDT algorithm is as follows [89], [90]:

IF All the instances in the training set belong to the same class

THEN Return the value of the class

ELSE
- Select an attribute A to split on
- Sort the instances in the training set into subsets, one for each value of attribute A
- Return a tree with one branch for each non-empty subset, each branch having a descendant sub-tree or a class value produced by the algorithm recursively

This algorithm is guaranteed to terminate and any selection of attributes will produce a decision tree as long as the following conditions are met:

- One attribute should not be selected more than once in the same branch
- No two instances with the same values of all attributes may belong to different classes

The TDIDT algorithm by itself is underdetermined since no attribute selection rule is established. This makes the algorithm effective in generating trees that reproduce the training set, but in general these resulting trees won't be compact nor will they be capable of predicting classes for unseen instances.

Choosing splitting attributes can be done in any arbitrary way, but none of these selections will produce a satisfactory tree. One of the most commonly used strategies to select the next splitting attribute in the TDIDT algorithm is the Information Gain method, which is based on the concept of Entropy.

Entropy is an information-theoretical measure of the uncertainty contained in a training set, due to the presence of more than one possible classification. The smaller the entropy of a training set, the greater is the gain of information [89]. The proportion of instances with a certain classification divided by the total number of instances in the training set is denoted by p_i, where i is the index of a given classification. If there are K classes, then the entropy of the training set is defined as,

$$E = -\sum_{i=1}^{K} p_i \log_2 p_i$$

A selection of the next attribute to split is done by initially computing the entropy of the training set. Then an attribute is selected, a training set table is arranged for every value the selected attribute can take, and the respective entropy of every newly created training set is computed. Finally a weighted sum of the specific attribute entropies is obtained, where the weighting factors are the original proportions of every classification. The same process is followed for every possible splitting attribute, and the one selected to perform the split will be the one that produces the maximum reduction of entropy, with respect to the entropy of the original training set.

As it was seen in the Golf Example, some attributes may be categorical like the weather, or wind conditions, and some other attributes may be continuous like temperature or humidity. Although the previously described TDIDT algorithm and the Information Gain strategy are thought for categorical attributes, continuous attributes can be discretized so that the same decision tree induction method can be applied.

Discretization of a continuous attribute is done simply by segmenting the range of the continuous attribute either in equal width intervals, in equal frequency intervals, or using other division strategy that defines border values that can be used in inequality expressions. The resulting inequalities partition the continuous range in an integer number of classes for which the TDIDT algorithm and the Information gain strategy can be used. Details on these decision tree induction methods and on a variety of other approaches can be found in [89], [90] or [91]. The implementation of the decision trees algorithm in Chapter 4 was accomplished using the function `classregtree.m` built in in the Statistics Toolbox of Matlab.

CHAPTER 3 Centralized Control of Power System Stabilizers

Small signal oscillations in power systems are triggered by the random power variations that are characteristic of the natural behavior of an electric power network. These variations range from the almost imperceptible ones produced by the switching of distribution load and distributed generation, to the significant changes due to industrial load changes, large generation and large contingencies. Whatever the origin and magnitude of the disturbances may be, they often are sufficient to excite natural modes of generators and their controls, leading to low frequency oscillations that may or may not be damped enough to produce noxious effects in the overall system operation.

The machines involved in a particular oscillation mode may be neighboring generation units in the same plant, units electrically distant but in the same area, or units that belong to different control areas. This proximity measure of the participating machines gives rise to respectively classify the oscillation modes as intraplant, local, or inter-area [92]. The frequency of oscillation is also related to this proximity, where higher frequencies (from 2 to 3 Hz) can be expected for short inter-plant electrical distance, and lower frequencies are associated to inter-area modes (below 1Hz). When these low frequency oscillations are present with insufficient damping, the impact on the power system may range from inconvenient power fluctuations that complicate energy markets, to massive blackouts.

The mechanisms that are currently used to handle small signal oscillations are power system stabilizers (PSS), static VAR compensators (SVC) and high voltage DC transmission lines (HVDC). All of them show a degree of effectiveness to damp oscillations and all have their own limitations. HVDC transmission lines are built to interconnect distant control areas and allow energy transfers while impeding inter-area oscillations, in cases where AC links would not allow small signal stability. These power system components strongly reject frequency oscillations between the interconnected areas and also can act on other oscillation modes by means of supplementary control signals. However, the high financial cost of HVDCs limits their use to only situations where there will be a significant economic benefit of interconnecting two areas by direct current; damping other oscillation modes in practice can only be attempted using existing HVDC infrastructure.

SVCs are primarily placed to aid on voltage and transient stability in sensitive locations of the system. Voltage control is effectively achieved by the combination of fixed capacitors and thyristor controlled reactors. As in the case of HVDCs, SVCs are also capable of handling supplementary control signals to enable the damping of system oscillations, nevertheless their contribution to this secondary function is subordinated to the location of the SVC. The installation of an SVC will be subject to voltage and transient stability requirements, and to its advantages upon other lower cost alternatives.

Unlike the two components previously described, PSSs are designed to deal exclusively with small signal oscillations. They are installed (not necessarily enabled) in the majority of generation units in current power systems, and their relatively low cost allows their placement in any synchronous generation plant. The PSS is disseminated throughout modern power systems, and in many cases it is only by its proper implementation that normal operation can be accomplished. However, to this day the PSS is only used as a local controller, enabling it to act only on previously defined oscillation modes which cannot be expected to remain unchanged in evolving power grids.

This Chapter lays the foundation for the development of a robust centralized controller based on PSSs and Wide Area Measurements. It states that WAMs permit PSSs to act in a coordinated manner to increase small signal stability in a given system, demonstrates how a centralized controller can be designed to this end, and discusses implementation aspects regarding the incorporation of new control signals to existing PSSs. The design of a robust controller and the repercussion of latency on PMU measurements are left for later chapters.

3.1 Centralized Control through Stabilizers

This dissertation proposes that PSSs can be coordinated simultaneously from a centralized controller to increase the damping of low frequency oscillation modes caused by small signal disturbances. Figure 3.1 shows the proposed control structure, where it is assumed to be p generators in the system, m of which possess automatic voltage regulators, and n have power system stabilizers. Thick lines represent multiple signal channels, and thin lines represent single signal channels. All state measurements are feedback to the controller, and the controller in turn produces n control signals to be feed as external inputs to the stabilizers. The figure also shows that stabilizers and voltage regulators receive the traditional terminal voltage and rotor speed signals.

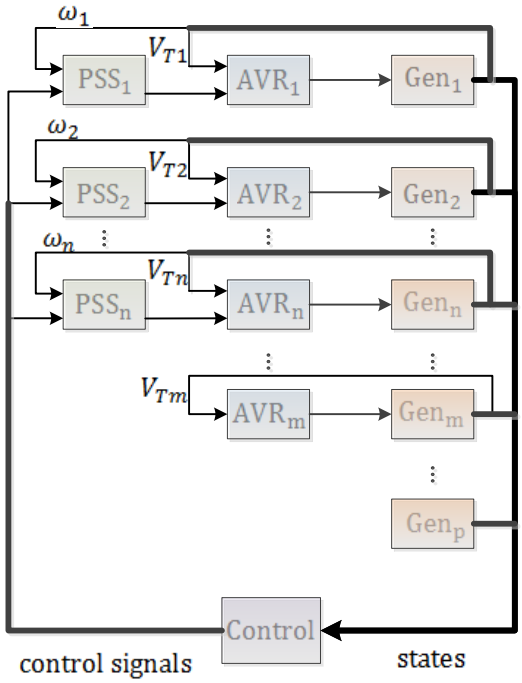

Figure 3.1 Structure of the centralized control of PSSs

To attain this control scheme, first it is necessary to determine a way to access the PSS with an external signal, then the repercussions of this new input must be evaluated and quantified in the linearized model. Once the controllability from these inputs has been verified the design of a suitable controller follows. To begin this task it is illustrative to briefly review the process of model linearization that is commonly used in power systems analysis tools.

3.1.1 Modeling Considerations

The linearized dynamic model of the complete power system is attained by individually building:

a) The dynamic equations of every synchronous generator along with its governor, automatic voltage regulator and stabilizer,
b) The models of other generation sources like wind or solar including their power electronics interphases,
c) The models of HVDC lines, representative dynamic loads, and all FACTS devices such as SVCs, controllable series compensators or mechanically switched capacitors.

The dynamic component of transmission lines, transformers and generator stators are neglected in the process, since the time constant associated with their behavior is much smaller than the time constant of shaft oscillation dynamics. Finally all dynamic models are interrelated by algebraic equations symbolizing the links provided by transmission lines and transformers. A complete description of this methodology can be found in [93].

An n^{th} order dynamic model of a particular machine with its local control systems can be expressed as n first order differential equations,

$$\begin{aligned} \dot{x}_1(t) &= f_1\left(t, x_1(t), \dots, x_n(t), u_1(t), \dots, u_p(t)\right) \\ \dot{x}_2(t) &= f_2\left(t, x_1(t), \dots, x_n(t), u_1(t), \dots, u_p(t)\right) \\ &\vdots \\ \dot{x}_n(t) &= f_n\left(t, x_1(t), \dots, x_n(t), u_1(t), \dots, u_p(t)\right) \end{aligned} \qquad (3.1)$$

where $\mathrm{x_i(t)}$ for $\mathrm{i} = 1, \dots, \mathrm{n}$ is the i^{th} state variable and $\mathrm{u_j(t)}$ for $\mathrm{j} = 1, \dots, \mathrm{p}$ is the j^{th} input.

(3.1) is written in vector form as:

$$\dot{\boldsymbol{x}}(t) = \boldsymbol{f}\left(t, \boldsymbol{x}(t), \boldsymbol{u}(t)\right) \qquad (3.2)$$

where $\mathrm{x(t)} = [\mathrm{x_1(t)} \quad \dots \quad \mathrm{x_n(t)}]^{\mathrm{T}}$ and $\mathrm{u(t)} = [\mathrm{u_1(t)} \quad \dots \quad \mathrm{u_p(t)}]^{\mathrm{T}}$ are the state and input vectors.

Given an equilibrium point $\left(\mathrm{u_0(t)}, \mathrm{x_0(t)}\right)$ that corresponds to $\mathrm{f}\left(\mathrm{t}, \mathrm{x_0(t)}, \mathrm{u_0(t)}\right) = 0$, (3.2) can be linearized for the disturbed state vector $\Delta\mathrm{x}$ and the disturbed input vector $\Delta\mathrm{u}$ using Taylor series, leading to:

$$\boldsymbol{\Delta\dot{x}}(t) = \boldsymbol{A}(t)\boldsymbol{\Delta x}(t) + \boldsymbol{B}(t)\boldsymbol{\Delta u}(t) \qquad (3.3)$$

where $\mathrm{A}(\mathrm{t})$ and $\mathrm{B}(\mathrm{t})$ are the Jacobians defined as:

$$\boldsymbol{A}(t) := \partial \boldsymbol{f}/\partial \boldsymbol{x}(\boldsymbol{t}) := \begin{bmatrix} \partial f_1/\partial x_1(t) & \dots & \partial f_1/\partial x_n(t) \\ \vdots & \vdots & \vdots \\ \partial f_n/\partial x_1(t) & \dots & \partial f_n/\partial x_n\,(t) \end{bmatrix}, \text{ and}$$

$$\boldsymbol{B}(t) := \partial \boldsymbol{f}/\partial \boldsymbol{u}(\boldsymbol{t}) := \begin{bmatrix} \partial f_1/\partial u_1(t) & \dots & \partial f_1/\partial u_p(t) \\ \vdots & \vdots & \vdots \\ \partial f_n/\partial u_1(t) & \dots & \partial f_n/\partial u_p\,(t) \end{bmatrix}$$

Since it is likely that the resulting model of the power system will involve several thousands of state variables, usually linearization is performed numerically by sequentially creating small disturbances to each state variable and input $\left(\Delta \mathrm{x_i} \text{ and } \Delta \mathrm{u_j}\right)$, and registering the propagated effect in the rest of the system $(\Delta \mathrm{f_i})$. At each step the effect of the variations is weighted against the originating disturbance in order to get an approximation of the respective column of the Jacobian.

3.1.2 Accessing the PSS with External Signals

All components of a power system are classified as critical infrastructure assets, and as such, clearance for experimentation is rarely granted. Whatever implementation is to be done must be failsafe, preferably not interfere with energy supply or other equipment, and above all, it must point towards a demonstrated improvement in system operation and stability. The parameters of a PSS are adjusted during their installation, and normally the settings are preserved until oscillation modes change following grid expansion or reconfiguration. When evaluating the present approach, care has been taken to propose actions that imply minimum disruption to the system and according to this, existing PSSs configuration should be kept and no parameter changes must be attempted. However, slight internal (software) or external (hardware) reconfiguration might be necessary to receive the new control signals.

Nowadays PSSs are manufactured either for standalone applications or integrated with automatic voltage regulators. Power plants worldwide are constantly upgrading excitation systems including PSSs, adopting digital technologies with embedded functionality for easy tuning and configuration, but in spite of this, analog excitation systems are still present in many power stations, and therefore these must be considered in the present study. Regardless of the model or the type of technology (analog or digital), PSSs are generally designed to receive one or two input signals from the following set [94]:

- Rotor speed deviation
- Local bus frequency deviation
- Generator electrical power
- Accelerating power
- Bus voltage
- Derivative of bus voltage

These signals are usually synthesized from terminal voltage and current measurements as shown in Figure 3.2. Digital PSSs would need to be software configured in order to receive a new nonstandard control signal, depending on how many input ports are being used, or on the availability of spare inputs. The introduction of an external control signal to an analog PSS can be accomplished by cascading an adding block that combines two signals, the local and the external.

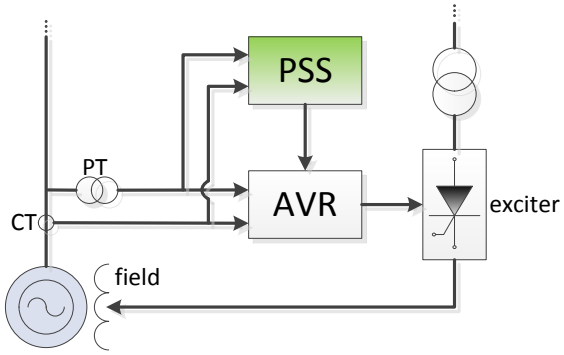

Figure 3.2 Configuration of the Excitation System

Figure 3.3 shows the proposed configuration to introduce the external control input (u) into the PSS. In the following sections it is assumed that the conventional input is the rotor speed deviation, but the same analysis is applicable to other signals.

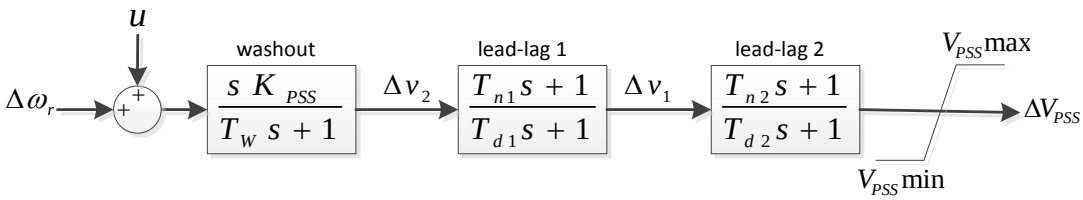

Figure 3.3 Introduction of an external control signal (u) to the PSS

3.1.3 Correcting Action of the External Control Signal

In this study it is assumed that the system is linear and time invariant. The added input u shown in Figure 3.3, has the potential of acting as a corrective signal to eliminate tuning deficiencies that may be present, and therefore, if appropriately designed it can be sufficient to control at least the oscillation modes in which such machine participates. To visualize this, consider a generating unit in steady state with a sinusoidal shaft speed deviation,

$$\Delta\omega_r(t) = k_o \sin(\omega_o t) \qquad (3.4)$$

where ω_o is the frequency of oscillation.

Regarding Figure 2.1, it is assumed that the transfer function from the PSS output to the electromagnetic torque, and the transfer function of the PSS, both evaluated at ω_o, and expressed in phasor form are:

$$\left.\frac{\Delta T_e(s)}{\Delta V_{PSS}(s)}\right|_{s=j\omega_o} = G_M e^{-j\theta}$$

$$G_{PSS}(s) = \left.\frac{\Delta V_{PSS}(s)}{\Delta \omega_r(s)}\right|_{s=j\omega_o} = G_{PSS} e^{j\phi} \qquad (3.5)$$

where $\phi > 0$ and $\theta > 0$.

This means that the machine is introducing a gain G_M and a phase lag θ to the exciter input, and the PSS is compensating with a gain G_{PSS} and a phase lead ϕ in an attempt to produce a damping torque (in phase with $\Delta\omega_r$). Then the torque produced by PSS action is:

$$\Delta T_e(j\omega_o) = G_M G_{PSS} k_o e^{j(\phi-\theta)} \Delta\omega_r(j\omega_o) \qquad (3.6)$$

In the time domain this can be written as:

$$\Delta T_e(t) = G_M G_{PSS} k_o \sin(\omega_o t + \phi - \theta) \qquad (3.7)$$

Therefore an effective damping torque component will be produced for the oscillation mode ω_o only if $\phi = \theta$; otherwise the PSS would operate inefficiently and could compromise the integrity of the system. If a sinusoidal input $u(t)$ is added to the PSS as in Figure 3.3, with the goal of putting ΔT_e in phase with $\Delta\omega_r$, then according to (3.4) and (3.5),

$$\Delta T_e(t) = k_o \sin(\omega_o t) = G_M G_{PSS}\big(k_o \sin(\omega_o t + \phi - \theta) + u(t + \phi - \theta)\big)$$

Rearranging,

$$u(t + \phi - \theta) = \frac{k_o}{G_M G_{PSS}} \sin(\omega_o t) - k_o \sin(\omega_o t + \phi - \theta)$$

$$u(t) = \frac{k_o}{G_M G_{PSS}} \sin(\omega_o t - \phi + \theta) - k_o \sin(\omega_o t) \qquad (3.8)$$

Then adding of $u(t)$ as in (3.8) enables the PSS to overcome tuning deficiencies in magnitude or in phase, to damp a single oscillation mode. Since the system under study is assumed linear and time invariant, the superposition principle allows counteracting other sinusoidal components in the speed deviation, with correspondent components in the external input, and thus the same logic can be applied if the generator was participating in more than one oscillation mode.

The action of an additional input to the PSS is illustrated by applying a proportional-integral (PI) control block to a single machine as depicted in Figure 3.4. The PI block produces an external signal for the PSS, seeking to minimize the difference between the rotor speed deviation and the reference (zero in this case). In order to simulate shaft oscillations, a mechanical torque input constituted by sinusoidal signals of three different frequencies ($\omega = 1, 2$ and 3 rad/s) is introduced as shown in Figure 3.5. The effect of the external signal applied to the PSS is

demonstrated in Figure 3.6, where a reduction in two orders of magnitude is registered in the oscillations by the action of the control signal u.

This reasoning demonstrates that the proposed location of the external control signal is suitable for influencing the oscillation modes of the machine, and therefore can be used reliably in a centralized control scheme.

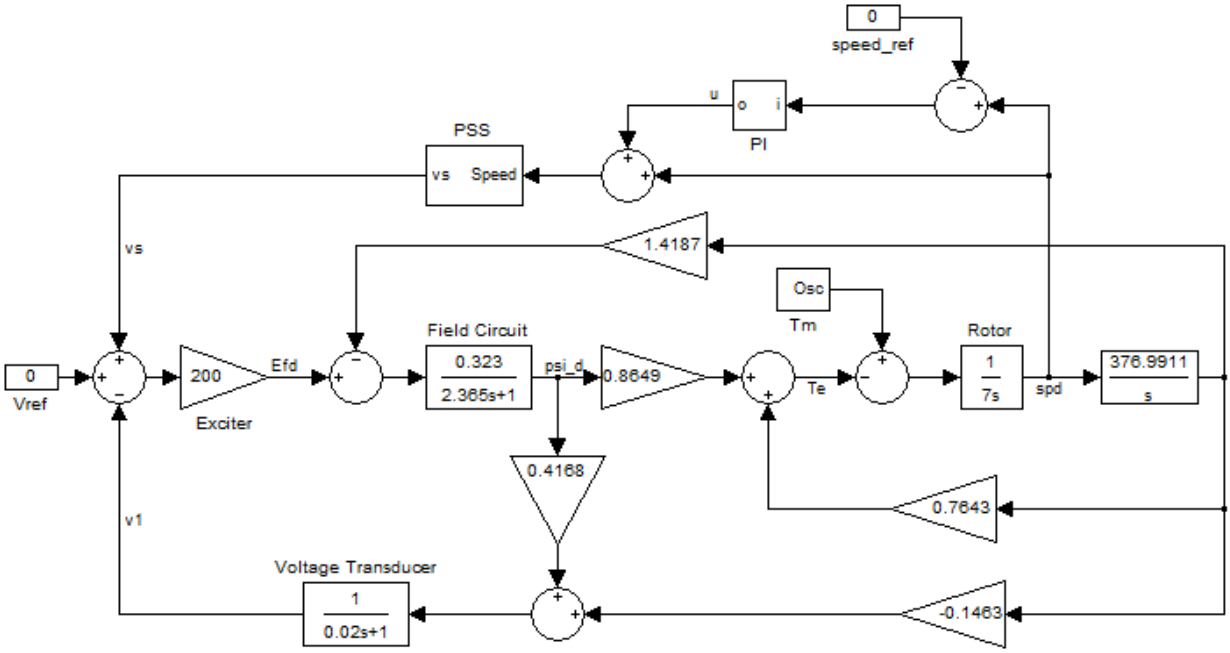

Figure 3.4 Linearized model of a synchronous machine including a PI control block

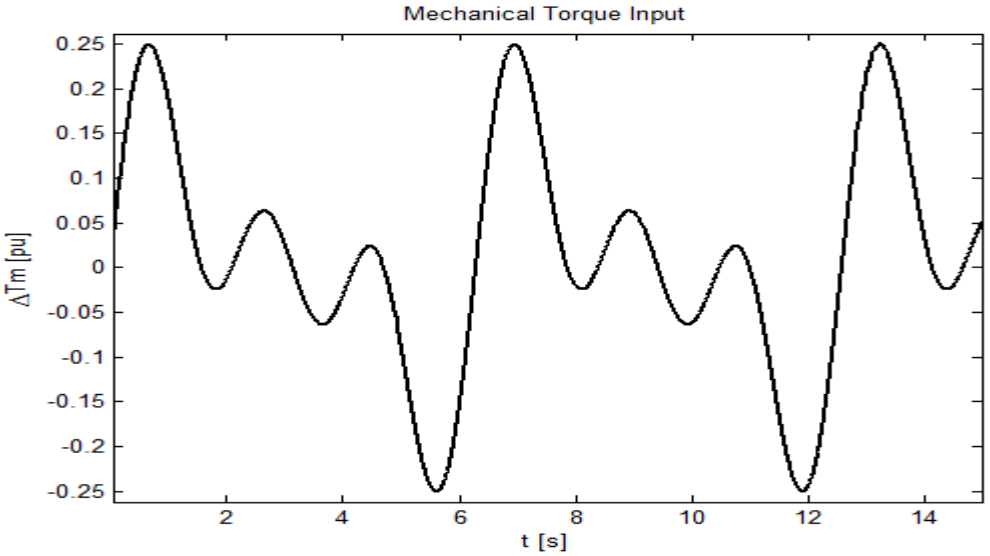

Figure 3.5 Mechanical torque input to simulate shaft oscillations

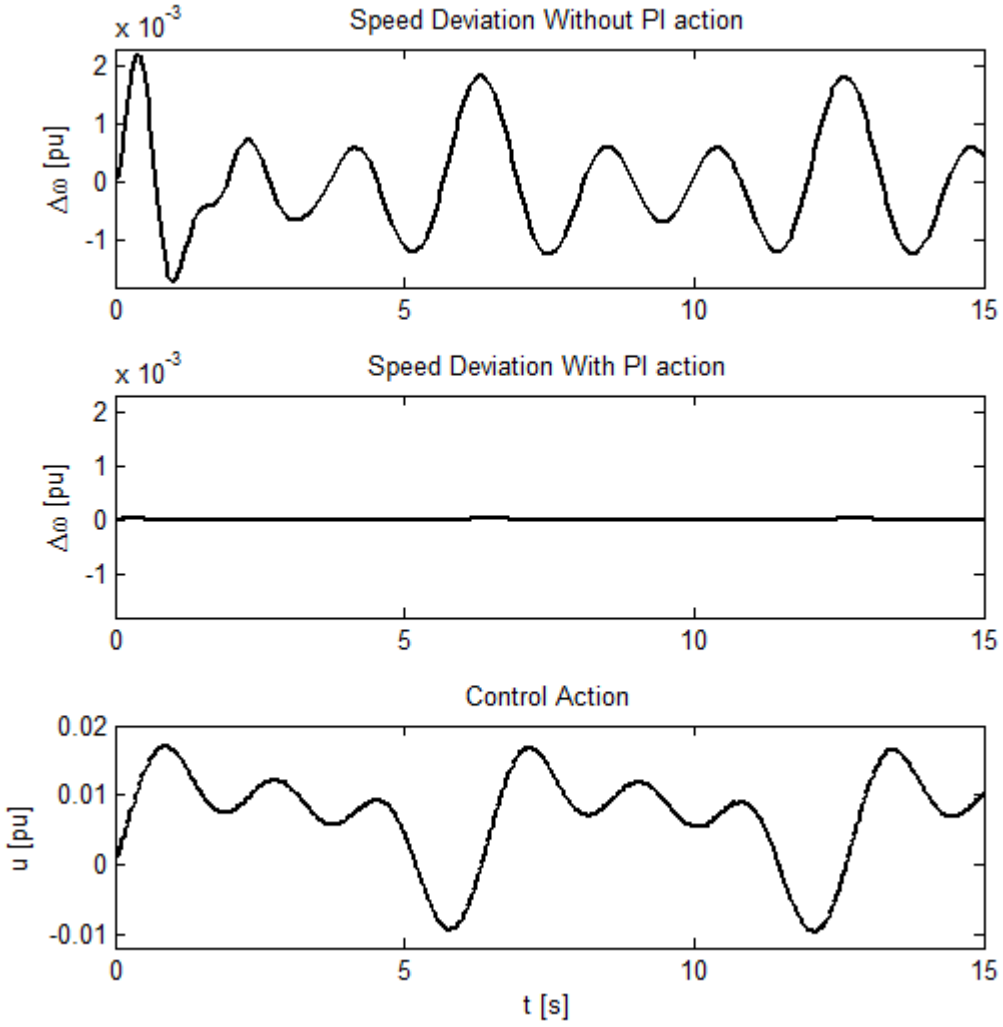

Figure 3.6 Effect of the external control input in the speed deviation oscillations

3.1.4 Modifications in the Linearized Model Caused by the External Input

Once the new signal has been assigned to the PSS the state space model will be affected. Consider the transfer function of the washout block of Figure 3.3, and rearrange it to uncover the state equation associated with Δv_2:

$$\frac{\Delta v_2(s)}{\Delta\omega_r(s) + u(s)} = \frac{sK_{PSS}}{T_W s + 1}$$

$$\Delta v_2(s)(T_W s + 1) = sK_{PSS}\big(\Delta\omega_r(s) + u(s)\big)$$

$$s\Delta v_2(s) = \frac{K_{PSS}}{T_W} s\Delta\omega_r(s) - \frac{1}{T_W}\Delta v_2(s) + \frac{K_{PSS}}{T_W} su(s) \qquad (3.9)$$

Since $\Delta\omega_r$ is always a state variable in machine models, then an expression of $s\Delta\omega_r$ is always available as a function of other state variables; on the other hand the term $su(s)$ is not, and its direct inclusion in the linearized model would require the addition of one state variable per PSS. This inconvenience can be bypassed by partitioning the washout block as shown in Figure 3.7 and replacing the state variable Δv_2 by another internal state Δv_{i2} as follows:

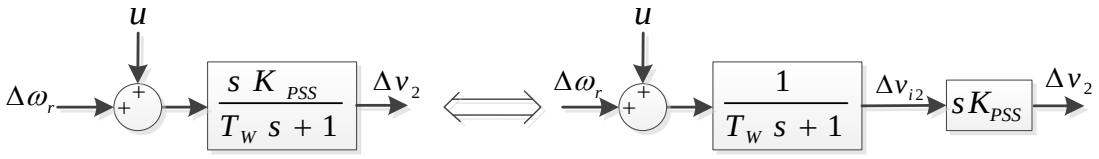

Figure 3.7 Partition of the washout block

$$\frac{\Delta v_{i2}(s)}{\Delta\omega_r(s)+u(s)} = \frac{1}{T_W s+1}$$

$$\Delta v_{i2}(s)(T_W s+1) = \Delta\omega_r(s)+u(s)$$

$$s\Delta v_{i2}(s) = \frac{1}{T_W}\left(\Delta\omega_r(s) - \Delta v_{i2}(s) + u(s)\right) \qquad (3.10)$$

(3.10) is the updated state equation for Δv_{i2}. Also, $\Delta v_2(s) = K_{PSS} s\Delta v_{i2}$, and substituting (3.10) into this expression results in,

$$\Delta v_{i2}(s) = \Delta\omega_r(s) - \frac{T_W}{K_{PSS}}\Delta v_2(s) + u(s) \qquad (3.11)$$

which represents the new state variable as a function of the original one. In a similar fashion and with the same purpose of avoiding the increment in the number of state variables, an internal state (Δv_{i1}) can be defined for the first lead – lag block of Figure 3.3 as shown in the next figure and subsequent derivation:

$$\frac{\Delta v_{i1}(s)}{\Delta v_2(s)} = \frac{1}{T_{d1}s+1}$$

$$s\Delta v_{i1}(s) = \frac{1}{T_{d1}}\Delta v_2(s) - \frac{1}{T_{d1}}\Delta v_{i1}(s) \qquad (3.12)$$

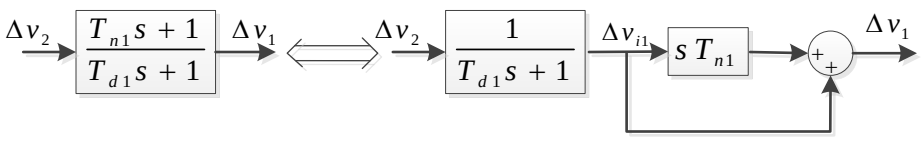

Figure 3.8 Partition of the first lead – lag block

Substituting (3.11) in the last equation:

$$s\Delta v_{i1}(s) = \frac{K_{PSS}}{T_{d1}T_W}\left(\Delta\omega_r(s) - \Delta v_{i2}(s) + u(s)\right) - \frac{1}{T_{d1}}\Delta v_{i1}(s) \qquad (3.13)$$

is the updated state equation for Δv_{i1}. Next, the equation for the change of variable is found by substituting (3.12) in $\Delta v_1(s) = T_{n1} s \Delta v_{i1}(s) + \Delta v_{i1}(s)$, resulting in:

$$\Delta v_1(s) = \frac{T_{n1}}{T_{d1}} \Delta v_2(s) + \left(\frac{T_{d1} - T_{n1}}{T_{d1}} \right) \Delta v_{i1}(s)$$

or,

$$\Delta v_{i1}(s) = \frac{T_{d1}}{T_{d1} - T_{n1}} \Delta v_1(s) - \frac{T_{n1}}{T_{d1} - T_{n1}} \Delta v_2(s) \quad (3.14)$$

The second lead – lag block is treated in the same way (Figure 3.9), producing the analog equations:

$$s\Delta V_{iPSS}(s) = \frac{T_{n1} K_{PSS}}{T_{d1} T_{d2} T_W} \left(\Delta \omega_r(s) - \Delta v_{i2}(s) + u(s) \right) + \frac{T_{d1} - T_{n1}}{T_{d1} T_{d2}} \Delta v_{i1}(s) - \frac{1}{T_{d2}} \Delta V_{iPSS}(s) \quad (3.15)$$

$$\Delta V_{iPSS}(s) = \frac{T_{d2}}{T_{d2} - T_{n2}} \Delta V_{PSS}(s) - \frac{T_{n2}}{T_{d2} - T_{n2}} \Delta v_1(s) \quad (3.16)$$

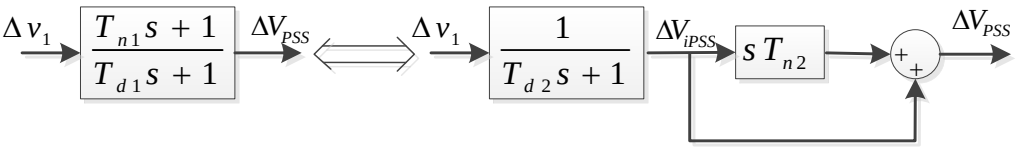

Figure 3.9 Partition of the second lead – lag block

Although this development has been done for the PSS structure of Figure 2.2, the same reasoning can be extend to any other type of stabilizer to avoid adding state variables to the system, and to facilitate the incorporation of $u(t)$ to the model. Equations (3.10), (3.13) and (3.15) summarize the modifications in matrices A and B of the state – space model (3.3) for the rows corresponding to the respective state variables. Since variations in the mechanical torque (ΔT_m) and in the reference voltage (ΔV_{ref}) are null in this particular analysis, the only nonzero input to the system is the control signal $u(t)$; the only terms of the input matrix B that are affected by the external PSSs inputs will be the factors multiplying $u(s)$ in (3.10), (3.13) and (3.15).

Usually small signal analysis tools produce state – space models based on Δv_1, Δv_2 and ΔV_{PSS}, instead of Δv_{i1}, Δv_{i2} and ΔV_{iPSS} as PSS state variables. In this cases a change of variables must be performed according to (3.11), (3.14) and (3.16) to convert the state – space model in an equivalent that is capable of handling the control signal $u(t)$. This change of variables is performed as a similarity transformation that ensures that the eigenvalues of the original model are preserved.

Example 3.1

To illustrate the modifications that are imposed on the linearized system, consider a classic model of a machine including a PSS with one lead – lag block, a proportional exciter and a terminal

voltage transducer as drawn in Figure 3.10. This model was taken from [74] and after analysis, using $\Delta\omega_r$ as the only PSS input, it produced the state – space model $\Delta\dot{x}(t) = A\Delta x(t)$, where,

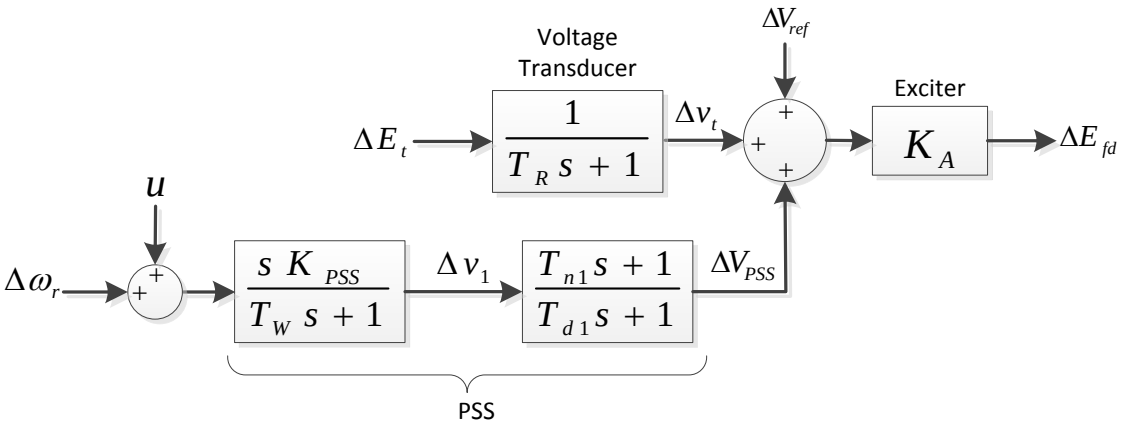

Figure 3.10 Machine excitation system used to demonstrate the model transformation

$$\mathbf{A} = \begin{bmatrix} 0 & -0.1092 & -0.1236 & 0 & 0 & 0 \\ 376.99 & 0 & 0 & 0 & 0 & 0 \\ 0 & -0.1938 & -0.4229 & -27.3172 & 0 & 27.3172 \\ 0 & -7.3125 & 20.8391 & -50 & 0 & 0 \\ 0 & -1.0372 & -1.1738 & 0 & -0.7143 & 0 \\ 0 & -4.8404 & -5.4777 & 0 & 26.9697 & -30.303 \end{bmatrix}, \quad \boldsymbol{\Delta x(t)} = \begin{bmatrix} \Delta\omega(t) \\ \Delta\delta(t) \\ \Delta\psi_{fd}(t) \\ \Delta v_t(t) \\ \Delta v_1(t) \\ \Delta V_{PSS}(t) \end{bmatrix}$$

Since ΔV_{ref} and ΔT_m are so far the only inputs and both are zero, then the matrix B does not have any impact on the system dynamics. If the signal $u(t)$ is added to the PSS input, equations (3.11) and (3.14) must be used to transform the state vector into,

$$\boldsymbol{\Delta x_i(t)} = \begin{bmatrix} \Delta\omega(t) \\ \Delta\delta(t) \\ \Delta\psi_{fd}(t) \\ \Delta v_t(t) \\ \Delta v_{i1}(t) \\ \Delta V_{iPSS}(t) \end{bmatrix}$$

Adapting (3.11) and (3.14) to the state variables x_i, and evaluating the parameters $T_W = 1.4$ s, $K_{PSS} = 9.5$, $T_{n1} = 0.154$ s and $T_{d1} = 0.033$ s, the conversion equations result in[2]:

$$\Delta v_{i1}(t) = \Delta\omega_r(t) - \frac{T_W}{K_{PSS}}\Delta v_1(t) = \Delta\omega_r(t) - 0.1474\Delta v_1(t)$$

$$\Delta V_{iPSS}(t) = \frac{T_{d1}}{T_{d1} - T_{n1}}\Delta V_{PSS}(t) - \frac{T_{n1}}{T_{d1} - T_{n1}}\Delta v_1(t) = -0.2727\Delta V_{PSS}(t) + 1.2727\Delta v_1(t)$$

[2] Since at this point the only interest is in the forced response, when evaluating the inverse Laplace transforms to (3.11) and (3.14), zero initial conditions have been assumed.

Similarly (3.10) and (3.13) are evaluated to determine the contributions of $\mathrm{u(t)}$ that will appear in the input matrix B:

$$\Delta\dot{v}_{i1}(t)|_{\boldsymbol{x_i=0}} = \frac{1}{T_W}u(t) = 0.7143u(t)$$

$$\Delta\dot{V}_{iPSS}(t)\big|_{\boldsymbol{x_i=0}} = \frac{K_{PSS}}{T_{d1}T_W}u(t) = 205.6277u(t)$$

This can also be written in the form of a similarity transformation $\mathrm{x_i(t) = Px(t)}$ as:

$$\underbrace{\begin{bmatrix}\Delta\omega(t)\\ \Delta\delta(t)\\ \Delta\psi_{fd}(t)\\ \Delta v_t(t)\\ \Delta v_{i1}(t)\\ \Delta V_{iPSS}(t)\end{bmatrix}}_{\boldsymbol{x_i}(t)} = \underbrace{\begin{bmatrix}1 & 0 & 0 & 0 & 0 & 0\\ 0 & 1 & 0 & 0 & 0 & 0\\ 0 & 0 & 1 & 0 & 0 & 0\\ 0 & 0 & 0 & 1 & 0 & 0\\ 1 & 0 & 0 & 0 & -0.1474 & 0\\ 0 & 0 & 0 & 0 & 1.2727 & -0.2727\end{bmatrix}}_{\boldsymbol{P}} \underbrace{\begin{bmatrix}\Delta\omega(t)\\ \Delta\delta(t)\\ \Delta\psi_{fd}(t)\\ \Delta v_t(t)\\ \Delta v_1(t)\\ \Delta V_{PSS}(t)\end{bmatrix}}_{\boldsymbol{x}(t)}$$

And the transformed state equation becomes, $\boldsymbol{\dot{x}_i}(t) = \boldsymbol{A_i x_i}(t) + \boldsymbol{B_i}u(t)$, where

$$\boldsymbol{A_i = PAP^{-1}} = \begin{bmatrix}0 & -0.1092 & -0.1236 & 0 & 0 & 0\\ 376.99 & 0 & 0 & 0 & 0 & 0\\ 865.0447 & -0.1938 & -0.4229 & -27.3172 & -865.0447 & -100.1631\\ 0 & -7.3125 & 20.8391 & -50 & 0 & 0\\ 0.7143 & 0.0437 & 0.0494 & 0 & -0.7143 & 0\\ 205.6273 & 0 & 0 & 0 & -205.6273 & -30.303\end{bmatrix}$$

and the input matrix[3] is, $\boldsymbol{B_i} = [\ 0 \quad 0 \quad 0 \quad 0 \quad 0.71 \quad 205.6]^T$. The eigenvalues of $\boldsymbol{A}$ are the same as the ones of $\boldsymbol{A_i}$ and therefore small signal analysis can be performed on the transformed model, which also allows to realize control actions through $u(t)$. □

3.2 Case Study: New England – New York Reduced Model

A verification of effectiveness of the proposed control input is done by designing a state feedback controller to alter the oscillation modes of the New England – New York transmission system. The data for this model was obtained from [95] and it is summarized in Appendix A. The model was built using Power System Toolbox © (PST) which allows the linearization of a dynamic model according to the exposed in Section 3 and includes analysis tools for the computation of eigenvalues, eigenvectors, participation factors, dynamic simulation, and PSS tuning among others.

3.2.1 The New England – New York Model

As it is implicit in its name, the model consists of two main areas interconnected by two transmission lines and one transformer, and other three equivalent areas which are represented

[3] Normally the input matrix B will have its first two columns associated to mechanical torque (governor reference) and to reference voltage (AVR reference). In this case only the third column is relevant since it is the one associated to the external input to PSSs, and therefore the first two columns are not shown.

by their respective load consumption and generation capability; a diagram of this system is shown in Figure 3.11 includes 68 buses and 16 generators. The New York Area comprehends nine generators located in buses 53 to 61, which in this particular scenario has a power consumption of 5,182 MW including load and transmission losses. The New England Area has a consumption of 6,442 MW and four generators installed in buses 62 to 65. The power exchange between areas summarized in Figure 3.12 and it is an indicative of the level of stress in interconnecting links that will be useful to evaluate the critical nature of inter-area oscillation modes. Generators 53 to 64 use IEEE DC1 exciters [96] whose model is represented in Figure 3.13, along with the state variables that will be used in the linearized model:

ΔE_{fd}: Output of the AVR which is used as a reference for the power electronics components feeding the field winding

ΔV_R: Output of the regulation stage

ΔR_f: Output of the stabilizing stage

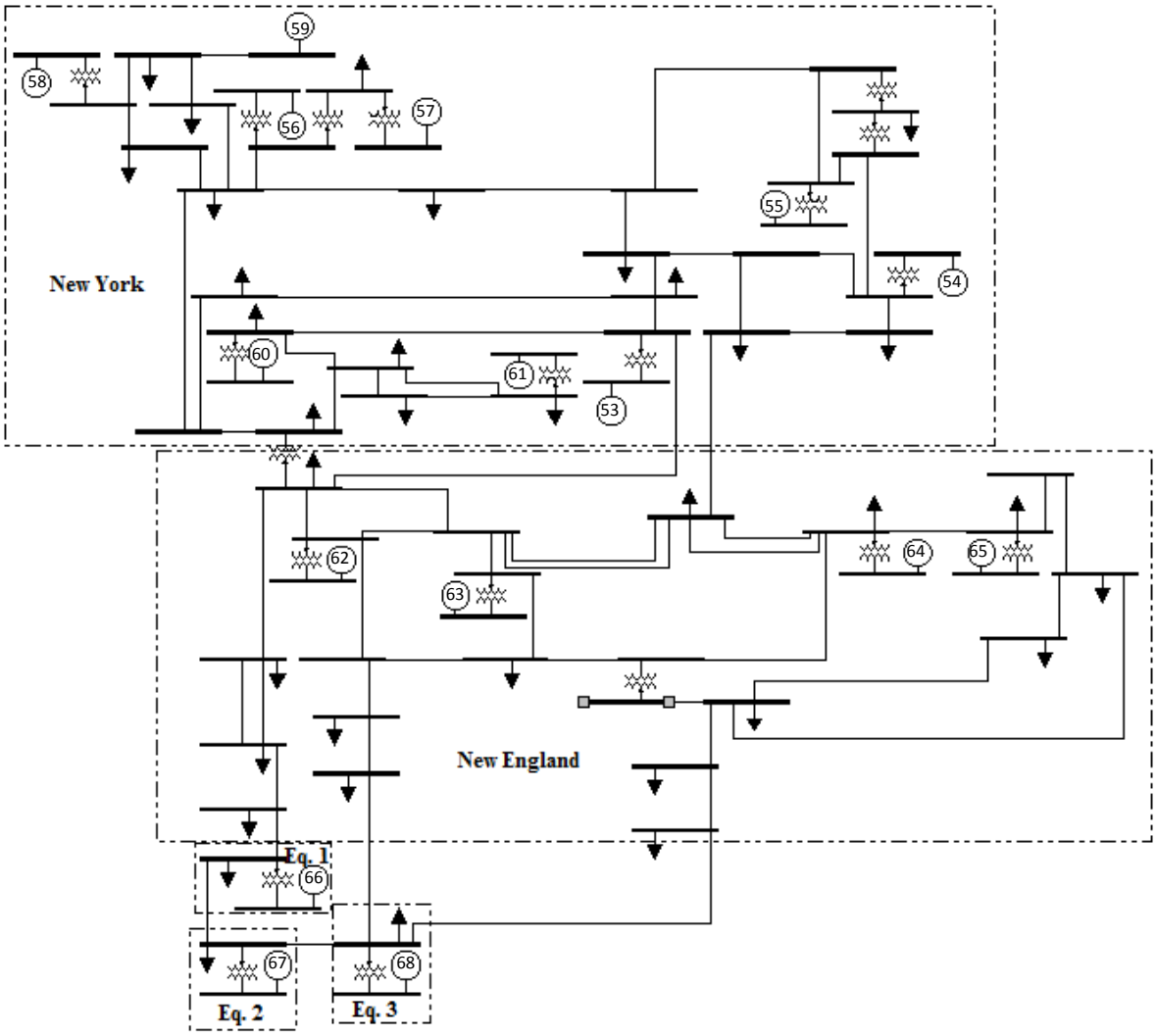

Figure 3.11 New England – New York reduced model. 68 buses and 16 generators

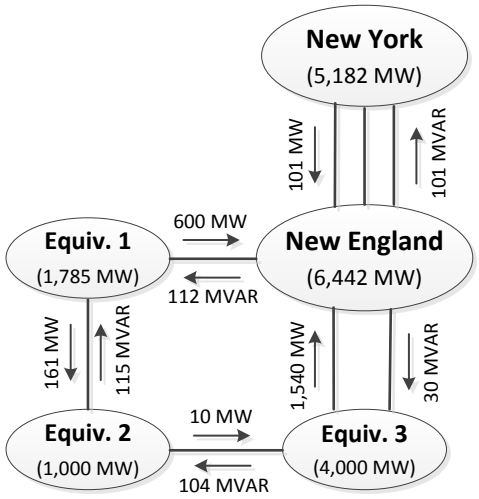

Figure 3.12 Balance of active and reactive power in the New England – New York model. Current scenario

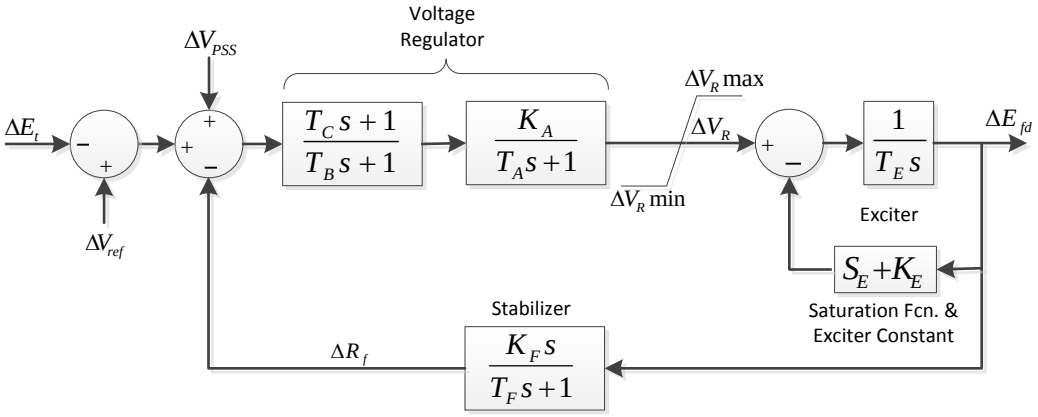

Figure 3.13 IEEE DC1 exciter model

The same machines include PSSs with the model shown in Figure 2.2. The remaining four generators (65 to 68) do not have a PSS and their exciters are not included in the model. The model was built such that the state vector for each machine is given by:

$$\boldsymbol{x}_{mi}^{T} = \begin{cases} \left[\Delta\delta_i \quad \Delta\omega_{ri} \quad \Delta e'_{qi} \quad \Delta\psi''_{di} \quad \Delta e'_{di} \quad \Delta\psi''_{qi} \quad \Delta V_{Ri} \quad \Delta E_{fdi} \quad \Delta R_{fi} \quad \Delta \mathrm{v}_{2\mathrm{i}} \quad \Delta \mathrm{v}_{1\mathrm{i}} \quad \Delta V_{PSSi}\right] & \text{for } i = 53, \ldots, 64 \\ \left[\Delta\delta_i \quad \Delta\omega_{ri} \quad \Delta e'_{qi} \quad \Delta\psi''_{di} \quad \Delta e'_{di} \quad \Delta\psi''_{qi}\right], & \text{for } i = 65, \ldots, 68 \end{cases} \tag{3.17}$$

For generators with excitation control, the first six states of each generator are machine variables, the next three are exciter variables as in Figure 3.13, and the last three are PSS variables according to Figure 2.2. Generators 65 to 68 are represented only by the machine state variables. The full state vector resulted from putting together all individual machine vectors, giving by:

$$\boldsymbol{x} = [\boldsymbol{x}_{m53} \quad \dots \quad \boldsymbol{x}_{m64} \quad \boldsymbol{x}_{m65} \quad \dots \quad \boldsymbol{x}_{m68}]^T \tag{3.18}$$

On the process of finding the parameters of the state equation $\dot{\mathrm{x}}(\mathrm{t}) = \mathrm{Ax}(\mathrm{t}) + \mathrm{Bu}(\mathrm{t})$, the complete state matrix A was computed in PST following the methodology explained in Section 3 resulting in a (168×168) matrix. A change of variables was not necessary in this case since the model was built using the internal states of the PSSs, however, slight differences in the definition of the internal variables assumed by the PST built-in models made it necessary to reformulate the dynamic equations. The difference consisted in the application of the pre-multiplying factors, $(\mathrm{T_{d2}} - \mathrm{T_{n2}})/\mathrm{T_{d2}}$ to compute $\Delta \mathrm{V_{PSS}}$, $(\mathrm{T_{d1}} - \mathrm{T_{n1}})/\mathrm{T_{d1}}$ to compute $\Delta \mathrm{v_{i1}}$, and $1/\mathrm{K_{PSS}}$ to compute $\Delta \mathrm{v_{i2}}$.

The same logic for deducting (3.10), (3.13) and (3.15) was followed to determine the terms of the input matrix B, evaluating at $\mathrm{x_i} = 0, \text{for i} = 53, \dots, 64$. The result of this process for the $\mathrm{k^{th}}$ $(\mathrm{k} = 53, \dots, 64)$ generator is:

$$\Delta \dot{v}_{i2k}(t)|_{\boldsymbol{x_i}=\boldsymbol{0}} = \frac{1}{T_{Wk}} u(t)$$

$$\Delta \dot{v}_{i1k}(t)|_{\boldsymbol{x_i}=\boldsymbol{0}} = \frac{K_{PSSk}(T_{d1k} - T_{n1k})}{T_{d1k}^2 T_{Wk}} u(t)$$

$$\Delta \dot{V}_{iPSSk}(t)\big|_{\boldsymbol{x_i}=\boldsymbol{0}} = \frac{K_{PSSk} T_{n1k}(T_{d2k} - T_{n2k})}{T_{d1k}^2 T_{Wk}} u(t)$$

All the parameter values of the generators and their controls can be found in Appendix A.
The resulting input matrix associated only with the external input has a dimension of (168×16):

$$\boldsymbol{B} = \begin{bmatrix} \boldsymbol{B}_{53} & \boldsymbol{0} & \boldsymbol{0} & \boldsymbol{0} \\ \boldsymbol{0} & \boldsymbol{B}_{54} & \boldsymbol{0} & \boldsymbol{0} \\ \boldsymbol{0} & \boldsymbol{0} & \ddots & \boldsymbol{0} \\ \boldsymbol{0} & \boldsymbol{0} & \boldsymbol{0} & \boldsymbol{B}_{68} \end{bmatrix} \tag{3.19}$$

where,

$$\boldsymbol{B}_k^T = \begin{cases} \left[0 \quad 0 \quad 0 \quad 0 \quad 0 \quad 0 \quad 0 \quad 0 \quad 0 \quad \frac{1}{T_{Wk}} \quad \frac{K_{PSSk}(T_{d1k} - T_{n1k})}{T_{d1k}^2 T_{Wk}} \quad \frac{K_{PSSk} T_{n1k}(T_{d2k} - T_{n2k})}{T_{d1k}^2 T_{Wk}}\right], & \text{for } k = 53, \dots, 64 \\ [0 \quad 0 \quad 0 \quad 0 \quad 0 \quad 0], & \text{for } k = 65, \dots, 68 \end{cases} \tag{3.20}$$

Ultimately, in the proposed scheme wide area measurements will be used to make possible a centralized controller. The system will be devised to rely on PMU measurements, thus at this stage it is reasonable to assume that rotor speed deviation of all machines will be available. This allows the definition of the output vector as,

$$\boldsymbol{y} = [\Delta\omega_{53} \quad \Delta\omega_{54} \quad \dots \quad \Delta\omega_{68}]^T \tag{3.21}$$

The sizes of x and y are (168×1) and (16×1) respectively. This leads to the definition of the output matrix in $\boldsymbol{y} = \boldsymbol{Cx} + \boldsymbol{Du}$ as,

$$\boldsymbol{C} = \begin{bmatrix} \boldsymbol{C}_{53} & \boldsymbol{0} & \boldsymbol{0} & \boldsymbol{0} \\ \boldsymbol{0} & \boldsymbol{C}_{54} & \boldsymbol{0} & \boldsymbol{0} \\ \boldsymbol{0} & \boldsymbol{0} & \ddots & \boldsymbol{0} \\ \boldsymbol{0} & \boldsymbol{0} & \boldsymbol{0} & \boldsymbol{C}_{68} \end{bmatrix} \tag{3.22}$$

with a dimension of (16×168), where,

$$\mathrm{C_k} = \begin{cases} [0 \quad 1 \quad 0 \quad 0 \quad 0 \quad 0 \quad 0 \quad 0 \quad 0 \quad 0 \quad 0 \quad 0], \text{for } \mathrm{k} = 53, \dots, 64 \\ [0 \quad 1 \quad 0 \quad 0 \quad 0 \quad 0], \qquad\qquad\qquad\qquad \text{for } \mathrm{k} = 65, \dots, 68 \end{cases}$$

No direct effect of the input is present in the output, then the feed forward matrix $\boldsymbol{D}$ in the output equation equals zero.

3.2.2 Small Signal Analysis

The linearized model of the system allows determining the oscillation modes through the computation of the eigenvalues of $\mathbf{A}$. The result reveals that all 122 eigenvalues have a negative real part, and therefore are stable. 46 oscillatory modes are present for rotor modes as well as for damper windings, AVRs, and PSSs; the remaining 76 eigenvalues are non-oscillatory stable modes. Figure 3.14 shows the oscillatory eigenvalues represented by their frequency and damping ratio. The figure also shows that three modes are have damping ratio less than 5%; these modes are considered to be insufficiently damped according to engineering practice [95], and therefore reveal the need to take measures such as retuning involved PSSs or adding other control mechanisms in order to increase damping of these frequencies, as described in the next section.

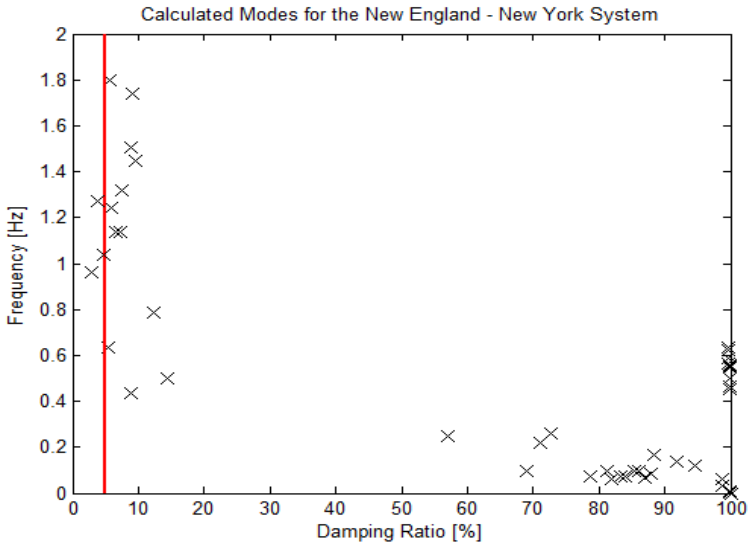

Figure 3.14 Oscillatory modes of the current scenario of the NE –NY system

Right and left eigenvectors of $\mathbf{A}$, respectively $\boldsymbol{\phi}_i$ and $\boldsymbol{\psi}_i$ $(i = 1, \dots, n)$, are used to compute the participation matrix [74]:

$$\mathbf{P} = [\boldsymbol{p}_1 \quad \boldsymbol{p}_2 \quad \cdots \quad \boldsymbol{p}_n], \quad \boldsymbol{p}_i = \begin{bmatrix} p_{1i} \\ p_{2i} \\ \vdots \\ p_{ni} \end{bmatrix} = \begin{bmatrix} \phi_{1i}\psi_{i1} \\ \phi_{2i}\psi_{i2} \\ \vdots \\ \phi_{ni}\psi_{in} \end{bmatrix} \tag{3.23}$$

where,

ϕ_{ki} is the element of the k^{th} row and the i^{th} column of the modal matrix $\Phi = [\phi_1 \quad \cdots \quad \phi_{\mathrm{n}}]$

ψ_{ki} is the element of the k^{th} row and the i^{th} column of the modal matrix $\Psi = [\psi_1 \quad \cdots \quad \psi_{\mathrm{n}}]$

In this case, n in (3.23) equals 168 and the size of the participation matrix is (168×168). Every column of P is associated to one eigenvalue and every row corresponds to a particular state. The entries of the participation matrix are complex numbers whose magnitude denotes the size of the contribution or participation of a given state in a specific mode. Table 3-1 details a part of the participation matrix, only including oscillating modes with a damping ratio inferior to 20%, and the states that contribute with a magnitude greater than 0.1. This matrix is normalized such that the state with the highest participation in certain mode has unitary magnitude.

Table 3-1 Oscillation modes with damping < 20% for the New England – New York system

		λ_{67}	λ_{70}	λ_{72}	λ_{74}	λ_{77}	λ_{80}	λ_{83}	λ_{85}	λ_{87}	λ_{89}	λ_{91}	λ_{93}	λ_{95}	λ_{97}	λ_{99}
Damping [%]		8.9%	14.3%	5.5%	12.4%	2.9%	4.6%	7.2%	6.5%	5.9%	3.9%	7.5%	9.5%	8.9%	9.1%	5.6%
Frequency [Hz]		0.43	0.50	0.63	0.79	0.96	1.04	1.14	1.14	1.24	1.27	1.32	1.45	1.51	1.74	1.80
G53	**Δδ**	0	0	0	0	0	0	0	0	0	0	0	0	0	0.99	0
	Δω	0	0	0	0	0	0	0	0	0	0	0	0	0	1.00	0
	ed'	0	0	0	0	0	0	0	0	0	0	0	0	0	0.15	0
G54	**Δδ**	0	0	0	0	0	0.98	0	0	0.82	0	0	0	0	0	0
	Δω	0.11	0	0	0	0	1.00	0	0	0.83	0	0	0	0	0	0
G55	**Δδ**	0	0	0	0	0	0.69	0	0	0.98	0	0	0	0	0	0
	Δω	0.11	0	0.10	0	0	0.71	0	0	1.00	0	0	0	0	0	0
G56	**Δδ**	0	0	0.14	0	0	0	0.16	0	0	0	0	0	0.98	0	0
	Δω	0	0	0.16	0	0	0	0.17	0	0	0	0	0	1.00	0	0
G57	**Δδ**	0	0	0.17	0	0	0.22	0.98	0	0	0	0	0	0.35	0	0
	Δω	0	0	0.19	0	0	0.23	1.00	0	0	0	0	0	0.35	0	0
	ed'	0	0	0	0	0	0	0.11	0	0	0	0	0	0	0	0
G58	**Δδ**	0	0	0.23	0	0	0.13	0.67	0	0	0	0	0.64	0	0	0
	Δω	0.12	0	0.25	0	0	0.14	0.69	0	0	0	0	0.65	0	0	0
	ed'	0	0	0	0	0	0	0	0	0	0	0	0.15	0	0	0
G59	**Δδ**	0	0	0.18	0	0	0	0.32	0	0	0	0	0.98	0	0	0
	Δω	0.10	0	0.20	0	0	0	0.32	0	0	0	0	1.00	0	0	0
G60	**Δδ**	0	0	0	0	0	0	0	0	0	0.16	0.98	0	0	0	0
	Δω	0	0	0	0	0	0	0	0	0	0.16	1.00	0	0	0	0
	ed'	0	0	0	0	0	0	0	0	0	0	0.11	0	0	0	0
G61	**Δδ**	0	0	0.24	0	0.96	0	0	0	0	0	0	0	0	0	0
	Δω	0.14	0	0.28	0	1.00	0	0	0	0	0	0	0	0	0	0
	eq'	0.17	0	0	0	0	0	0	0	0	0	0	0	0	0	0
	Efd	0.13	0	0	0	0	0	0	0	0	0	0	0	0	0	0
G62	**Δδ**	0	0	0	0	0	0	0	0	0	0.99	0.18	0	0	0	0
	Δω	0	0	0	0	0	0	0	0	0	1.00	0.19	0	0	0	0
G63	**Δδ**	0	0	0	0	0	0	0	0	0	0	0	0	0	0	0.99
	Δω	0	0	0	0	0	0	0	0	0	0	0	0	0	0	1.00
G64	**Δδ**	0.17	0	0.14	0	0	0	0	0.98	0	0	0	0	0	0	0
	Δω	0.21	0	0.14	0	0	0	0	1.00	0	0	0	0	0	0	0
G65	**Δδ**	1.00	0	1.00	0	0	0	0	0.20	0	0	0	0	0	0	0
	Δω	0.97	0	0.98	0	0	0	0	0.20	0	0	0	0	0	0	0
G66	**Δδ**	0.19	0.87	0	0.42	0	0	0	0	0	0	0	0	0	0	0
	Δω	0.19	0.88	0	0.42	0	0	0	0	0	0	0	0	0	0	0
G67	**Δδ**	0.25	0	0	1.00	0	0	0	0	0	0	0	0	0	0	0
	Δω	0.25	0	0	1.00	0	0	0	0	0	0	0	0	0	0	0
G68	**Δδ**	0.10	1.00	0	0.11	0	0	0	0	0	0	0	0	0	0	0
	Δω	0	1.00	0	0.12	0	0	0	0	0	0	0	0	0	0	0
		IA	IA	IA	IA	L	L	L	L	L	IA	IA	L	L	L	L

From Table 3-1, there are six inter-area modes, denoted by IA, and other nine local modes marked as L. In inter-area modes the frequency is close to or below 1 Hz, while in local modes it is higher than 1 Hz. Phase angles of the elements in the participation matrix are useful to visualize the mode shape, namely, the relative distribution in phase of state contributions. Figure 3.15 to Figure 3.17 represent the rotor angle participation factors for the inter-area modes, and Figure 3.18 does the same for two local modes that exhibit low damping. The modes represented in Figure 3.16(a), Figure 3.17(a) and Figure 3.18(a) and (b) are poorly damped, and therefore will be subjected to further control actions as described in the next section.

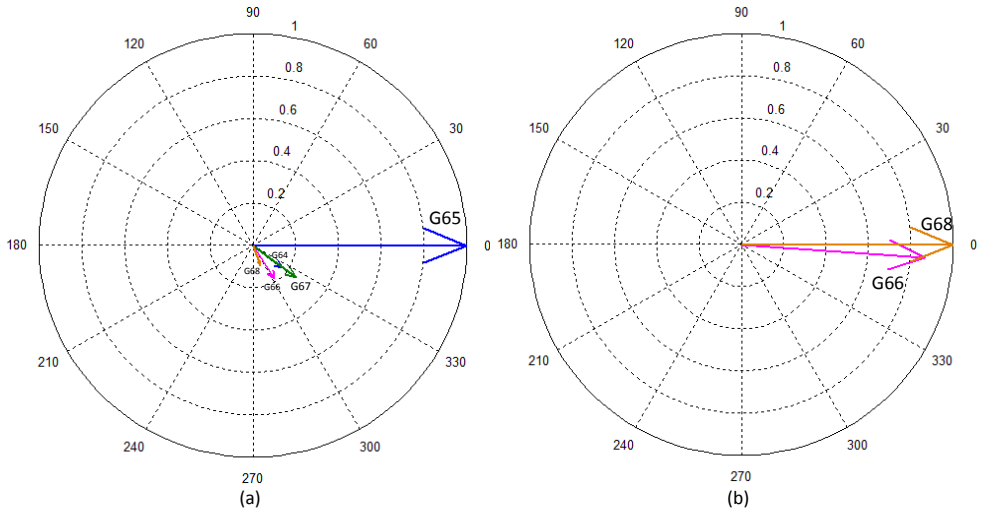

Figure 3.15 Inter-area modes in the New England – New York system. (a) λ_{67}: 0.43 Hz, 8.9%. (b) λ_{70}: 0.5 Hz, 14.3%

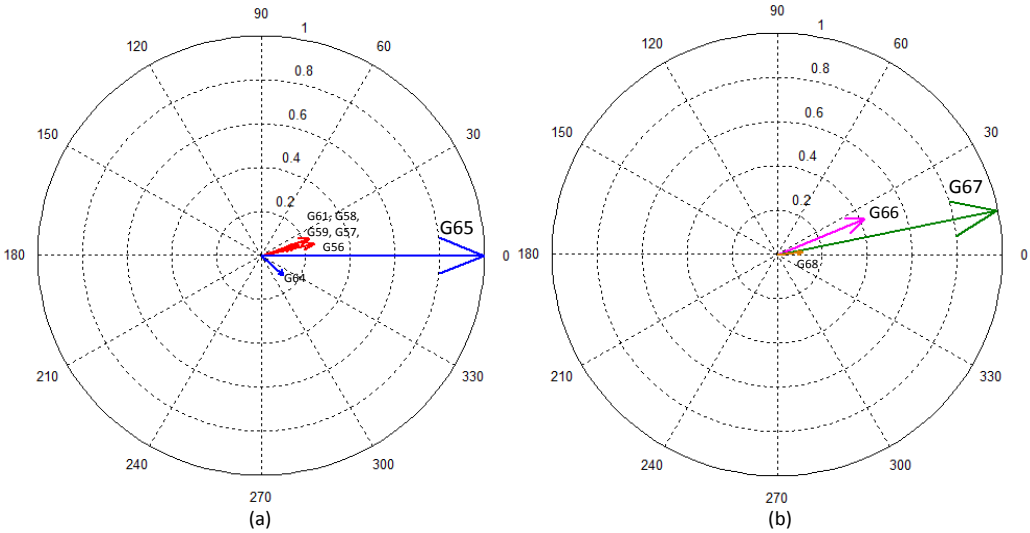

Figure 3.16 Modes 72 and 74 of the New England – New York Syst. (a) λ_{72}: 0.63 Hz, 5.5%. (b) λ_{74}: 0.79 Hz, 12.4%

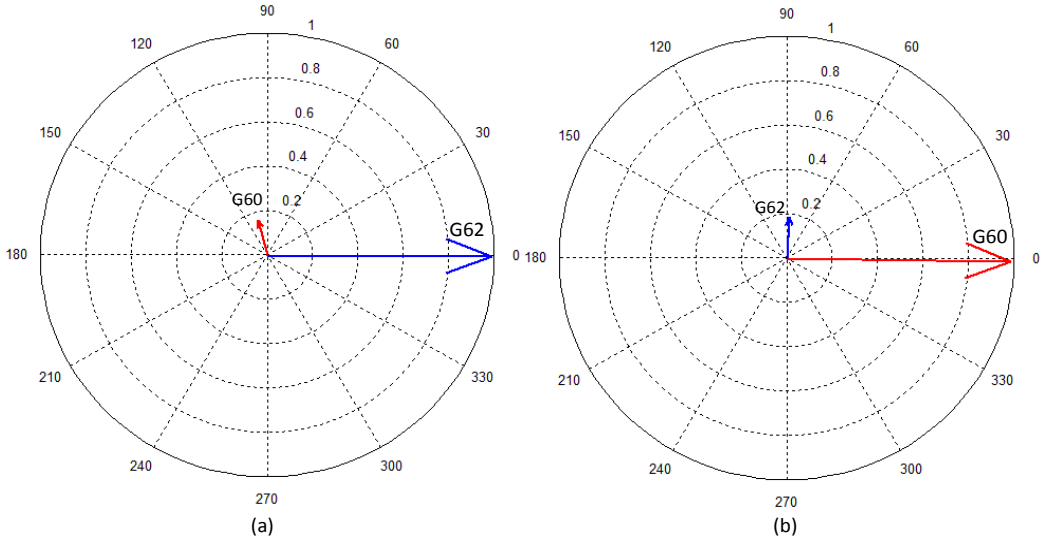

Figure 3.17 Modes 89 and 91 of the New England – New York Syst.
(a) λ_{89}: 1.27 Hz, 3.9%. (b) λ_{91}: 1.32 Hz, 7.5%

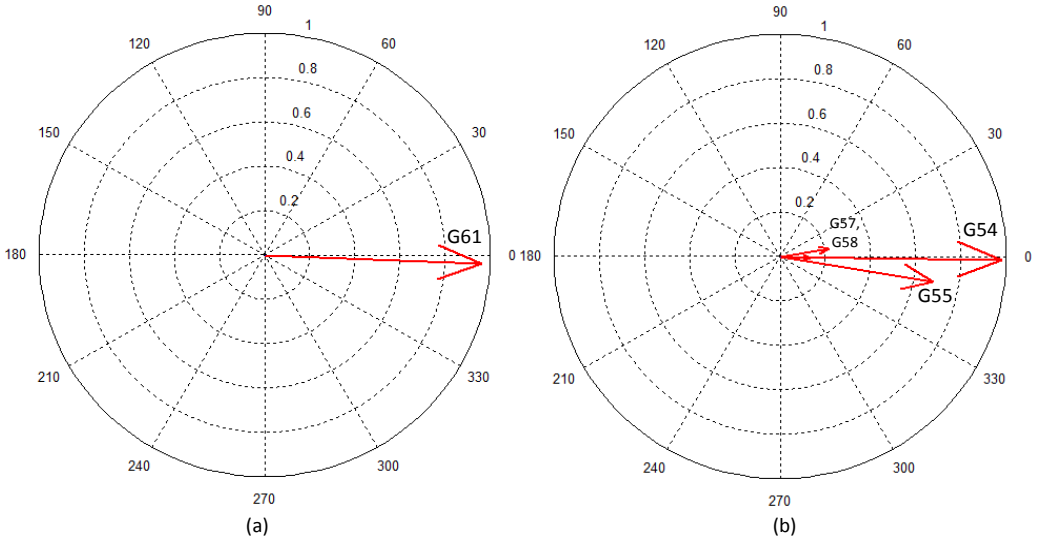

Figure 3.18 Local modes in the New England – New York system.
(a) λ_{77}: 0.96 Hz, 2.9%. (b) λ_{80}: 1.04 Hz, 4.6%

3.2.3 Centralized Control for Increased Damping

Before attempting to design a centralized controller to damp oscillations in the system under study, it is worthwhile to assess the ability of the input signals (located at each available stabilizer) to affect the dynamic behavior of the system, namely, controllability. This verification can be done by simple inspection of the input matrix once the state-space model is converted to the Jordan canonical form as it is discussed in [74]. For the present case of study using the input matrix **B** defined in (3.19) and the concepts of controllability described in Section 2.2.1, it was determined

that all the modes of the state equation $\dot{\boldsymbol{x}} = \mathbf{A}\boldsymbol{x} + \mathbf{B}\boldsymbol{u}$ for the New England – New York system are controllable through the input $\boldsymbol{u}$.

The state feedback method reviewed in Section 2.2.2 was used to accomplish the pole placement task. According to that exposition and to Table 3-1 there are three modes ($\lambda_{77}, \lambda_{80}$ and λ_{89}) that are insufficiently damped (less than 5%), and are the perfect candidates to be added to the set $\mathcal{L} = \{\lambda_{c1}, \lambda_{c2}, \dots, \lambda_{cn}\}$ of desired eigenvalues for the closed loop system. Other choices might be ($\lambda_{72}, \lambda_{87}$ and λ_{99}) that are damped slightly above 5%. For the sake of illustration, an arbitrary damping coefficient of 6.5% for these six modes is chosen as the control objective. Then the set $\mathcal{L}$ will contain all the original eigenvalues, except for the modifications listed in Table 3-2.

Table 3-2 Eig. to modify with control of stabilizers

Eigenvalue	Original Value	Desired Value
λ_{72}	-0.2189 ± 3.9822i 5.5% 0.63	-0.2583 ± 3.9823i 6.5% 0.63
λ_{77}	-0.1726 ± 6.0322i 2.9% 0.96	-0.3912 ± 6.0319i 6.5% 0.96
λ_{80}	-0.3038 ± 6.5363i 4.6% 1.04	-0.4240 ± 6.5364i 6.5% 1.04
λ_{87}	-0.4597 ± 7.8216i 5.9% 1.24	-0.5073 ± 7.8213i 6.5% 1.24
λ_{89}	-0.3132 ± 7.9970i 3.9% 1.27	-0.5187 ± 7.9972i 6.5% 1.27
λ_{99}	-0.6276 ± 11.2967i 5.6% 1.80	-0.7327 ± 11.2965i 6.5% 1.80

The function ***place*** in the Control System Toolbox of Matlab® is designed according to the algorithm presented in [79]. The application of this function to the New England – New York linearized system, considering the set $\mathcal{L}$ previously described, produces the desired constant feedback matrix $\mathbf{F}$, achieving an allocation percentage of 99.9994%. Figure 3.19 shows the original pole locations of the system without centralized control of PSSs, and their migration to the assigned positions in the closed loop system.

Even though a linearized model was used in the design task, the feedback matrix $\boldsymbol{F}$ also acts to some extent when the system is subject to transient conditions. To observe this behavior a three phase fault was applied at bus 53 for three cycles (0.05 s). The response will be most appreciated in modes λ_{77} (0.96 Hz) and λ_{89} (1.27 Hz), because they are the ones that experienced greater damping increase. These oscillation modes are mostly affected by machines 61 and 54 respectively ass can be seen in Table 3-1. The results are presented in Figure 3.20 for generator 61, and in Figure 3.21 for generator 54; a positive effect of the feedback control implementation is observed.

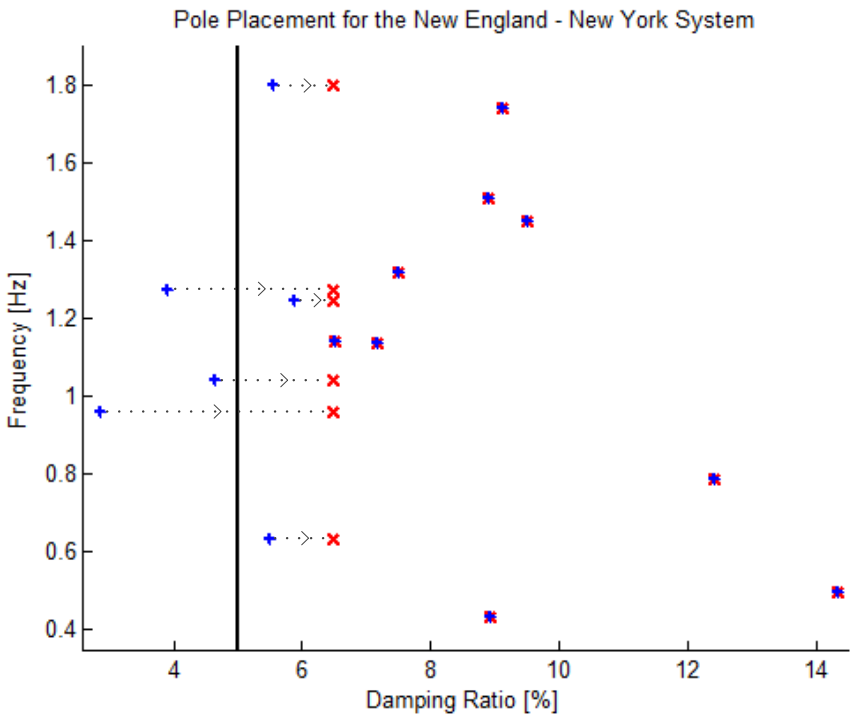

Figure 3.19 Original pole locations (+) and attained locations (×) by state feedback

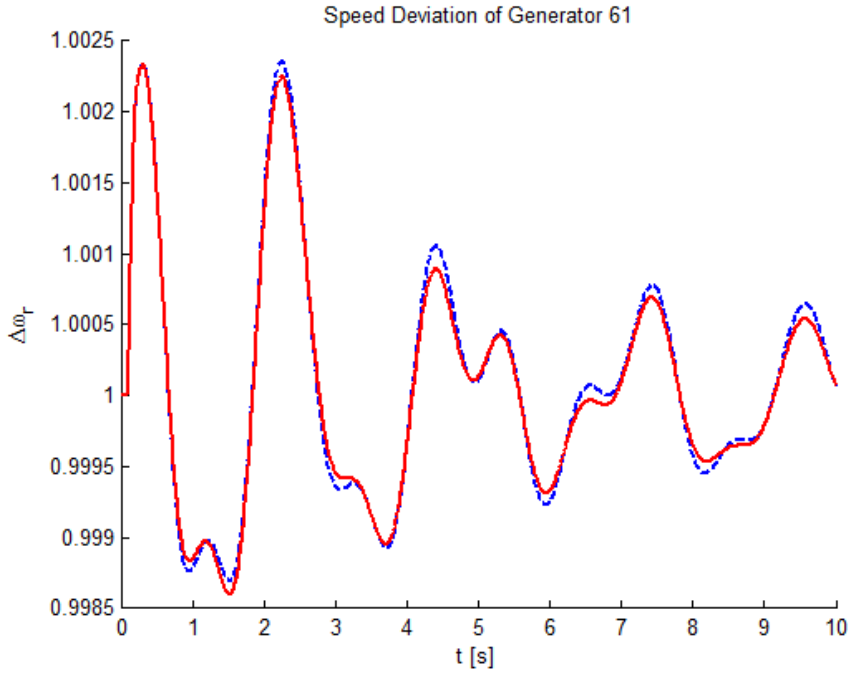

Figure 3.20 Comparison of the speed deviation of generator 61 with (continuous line) and without (dashed line) centralized control of PSSs

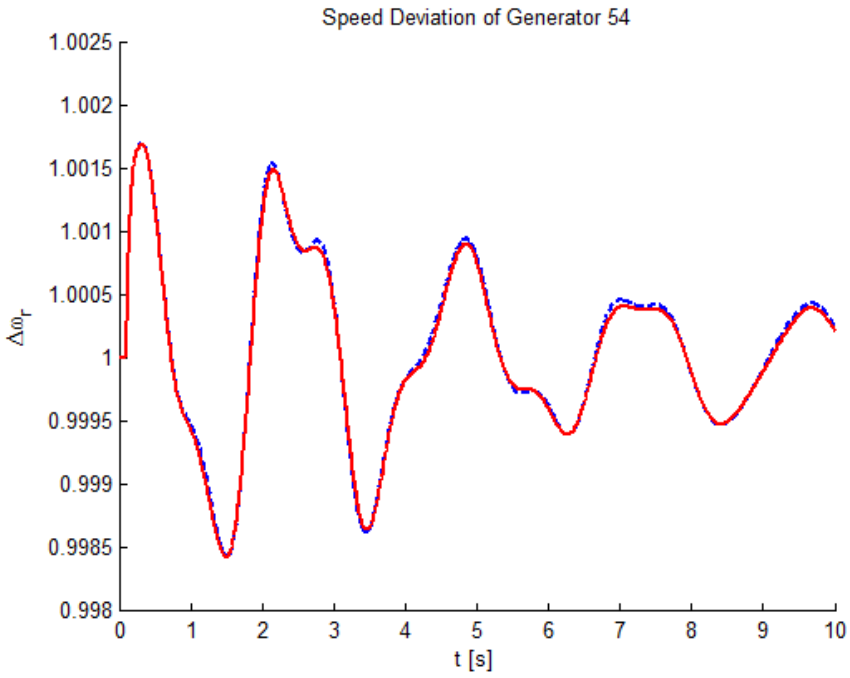

Figure 3.21 Comparison of the speed deviation of generator 54 with (continuous line) and without (dashed line) centralized control of PSSs

CHAPTER 4 Development of a Robust Controller and its Implementation

The centralized controller proposed in the previous chapter, when applied to the reduced New England-New York system, is capable of increasing the damping of oscillation modes by taking advantage of all available PSSs simultaneously. This design does not require any modification to the parameters of the existing stabilizers, and it exerts correcting actions on possible tuning deficiencies of local controllers. However, the applicability of this scheme is limited since it was designed for a specific configuration of the system, corresponding to a single operation scenario with a particular system topology. In this chapter, robustness is added to the proposed scheme to make it applicable to a variety of system configurations, load-generation schedules, and future planned expansions.

The model used to demonstrate the proposed enhancement is a dynamic equivalent of an academic version of the Central American system, which represents the major electromechanical characteristics of the interconnected transmission networks of six countries in Central America. A methodology for dynamic reduction of a power system is presented and applied to this system. Availability of wide area measurements is assumed to design the gain scheduling strategy with the use of decision trees. The final section is devoted to account for the effect of latency on the centralized controller.

4.1 Dynamic Reduction of the Central American System

The Central American region has an interconnected transmission system that links the grids of Guatemala, El Salvador, Honduras, Nicaragua, Costa Rica and Panama, as Figure 4.1 sows. In the rest of this text these areas will be denominated as areas 1 to 6 respectively. The transmission corridor through these countries operates at a voltage level of 230 kV with a 400 kV line between Guatemala and Mexico.

Figure 4.1 Central American System Interconnections [98]

Figure 4.2 shows the backbone of the 230 kV transmission system [97]. This network consists of 1,248 nodes, 130 generation plants, and about 6,400 MW in a deregulated regional energy market, coordinated by the Regional Operating Entity (EOR). The geography of the Central American isthmus forces the regional transmission grid to have an inherently radial topology, comprising approximately 1,900 km in a single transmission line trajectory from North to South. The topology of the Central American System makes it prone to develop North-South inter-area small signal oscillations this fact has stimulated the installation of power system stabilizers at sixteen generation plants all over the system.

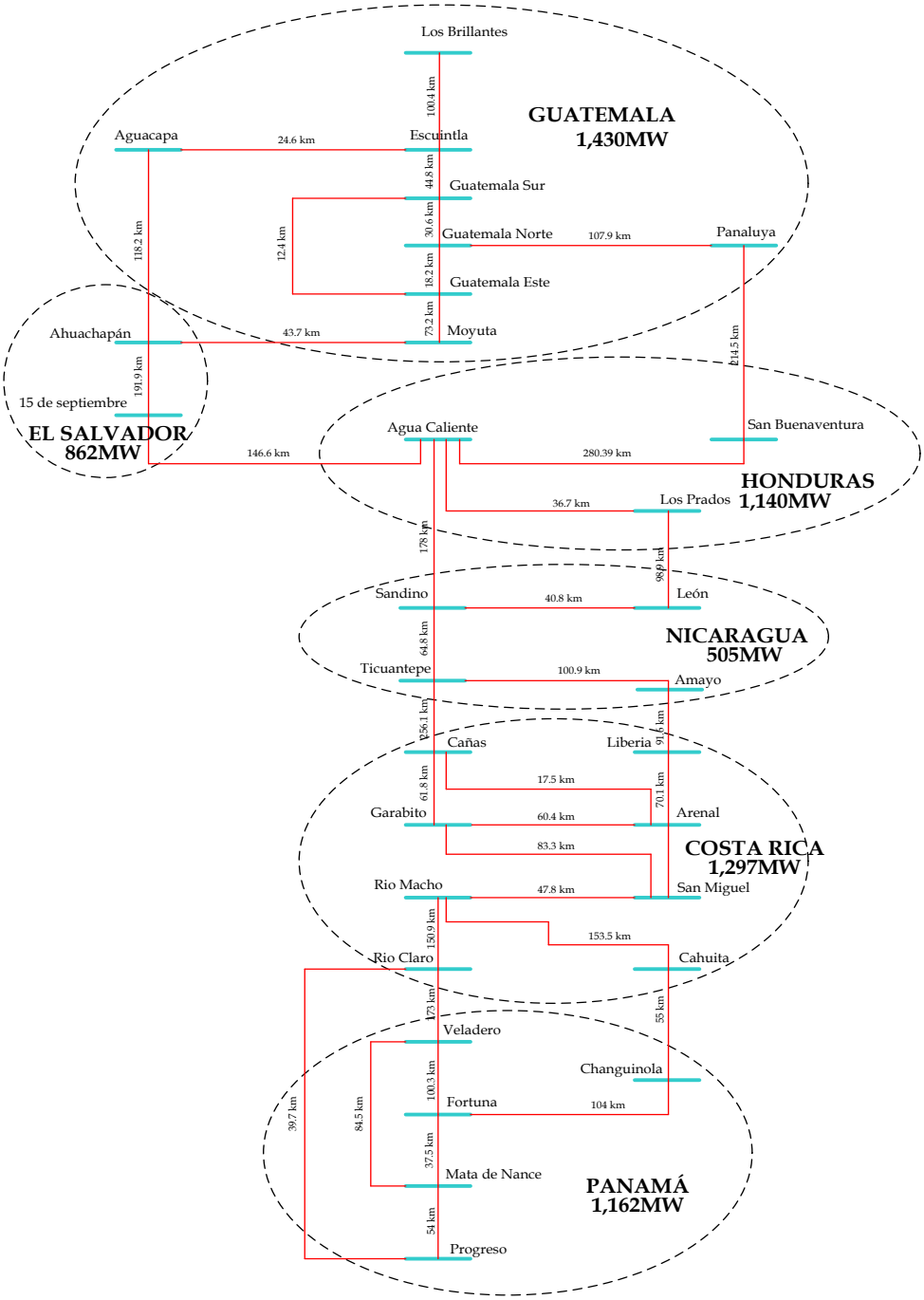

Figure 4.2 Backbone of the Central American Power System

Small signal characteristics of the Central American System make it an excellent subject to test the centralized controller proposed in this dissertation; nonetheless the size of the system poses a heavy burden for the computational tasks encompassed in this study. A reduced version of this system, that exhibits the same physical features as the original, is preferred to facilitate the design process which at this level is intended to be illustrative.

The reduction of the Central American System is intended to have a physical model as a product. This would allow the creation of a reduced database that would be of easy implementation in any commercial power system's analysis tool, a result that would be of practical use for players in the power industry. For this reason, reduction methods that rely on purely mathematical equivalents are not to be considered. Instead, the approach taken here consists in an elimination process, where initially the generators that do not cause an important impact on system's dynamics are neglected. In a subsequent stage the parameters of some selected remaining machines are optimized, in order to obtain a better approximation to the original dynamic behavior.

4.1.1 Reduction Stage 1: Elimination of Generators

Since the greatest interest of this project is on the small signal behavior of the system, the elimination process was aimed to produce a reduced model that primarily resembles the small signal characteristics of the complete model. This implies that the most important oscillation modes, and the generation plants participating on them should be kept as unaltered as possible. Furthermore, on the elimination process all generators with PSSs in the original model are left unaltered. This is to use these stabilizers in the centralized control and receive the external control signals that act on the oscillations.

Under these considerations, if the number of machines is to be reduced with little sacrifice on the modes with the lowest damping factors, then limits had to be set on the threshold of participation factors. The original model is described by 1,173 states; hence the same number of eigenvalues, that come from 130 generators with six states each, 118 automatic voltage regulators with three states each, and 13 power system stabilizers with three states each. Stage 1 of the reduction strategy consists in making a judicious selection of what eigenvalues are considered more important, and discriminating the generators and their respective models that do not participate importantly in the selected modes.

In an iterative process, different thresholds on damping and participation factors were tested to verify the number of plants that would come out in each case, while trying to keep a low total error. The total error was computed as the total absolute sum of individual eigenvalue discrepancies. Table 4-1 compiles the results of several iterations that considered different sets of eigenvalues as important, depending on how much damping factor they presented. In addition, several limits were rehearsed since this caused the biggest impact on the number of neglected generators. The last row of this table registers the adopted limits of reduction: 64 generators and their controls are required when only machines with a participation factor greater than 5% are considered in the modes having damping factors lower than 14%.

Table 4-1 Number of generators resulting from the selection of different thresholds on participation factors and eigenvalues considered

Important Damping [%]	Participation Factor [%]	Resulting Generators
<100	>0	130
<15	>1	96
<15	>2	91
<15	>1	85
<14	>5	64

Figure 4.3 shows the results obtained at the end of Stage 1 in the form of eigenvalue location. It can be seen in Figure 4.3 that the reduction process at this stage only caused a slight difference on the oscillation frequency, and a more noticeable contrast on damping factor of some modes. The largest error is in the eigenvalue with the lowest damping factor, which is precisely the most important one for stability analysis. This frailty of the reduced model is improved in the next stage of reduction.

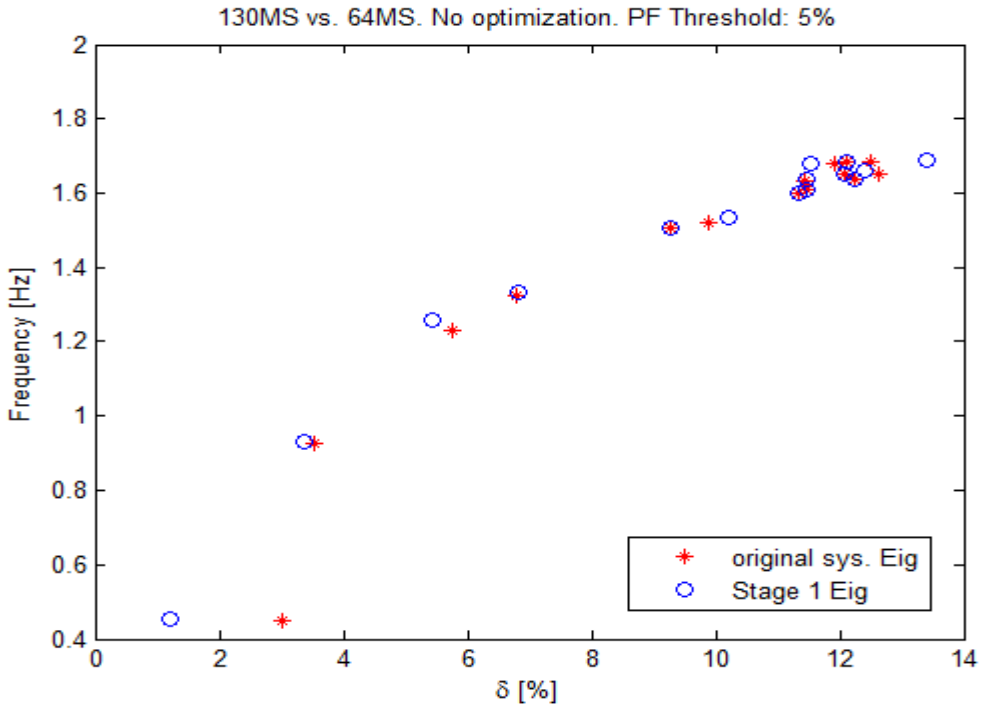

Figure 4.3 Location of eigenvalues in the original model vs. the reduced model at Stage 1.

4.1.2 Reduction Stage 2: Optimization of Selected Parameters

The most important discrepancies between the eigenvalues of the pre and post reduction models are associated with damping factors more than with frequencies of oscillation. Since PSSs are capable of producing damping torque components, it is reasonable to assume that stabilizers are suitable to correct the errors in damping shown in Figure 4.3.

Three PSSs were added to the reduced model at generators 3204, 50820 and 53854. Details on the reduced model of the Central American System can be found in Appendix A. These generators were selected for added PSSs based on their participation factors on the modes targeted for correction. Emphasis was made on generators that affected the modes with biggest damping discrepancies on Figure 4.3, and simultaneously caused little effect on other modes.

The parameters of the three added PSSs were assigned by an optimization process that minimized the objective function,

$$g = \sum_{k=1}^{N} |\lambda_{0k} - \lambda_k| \tag{4.1}$$

The Genetic Algorithm presented in Chapter 2 was used for this task. The process involved an interaction between the optimization routine executed in a Matlab environment, and the small signal analysis performed with SSAT of DSA Tools.

Figure 4.4 presents the block diagram of the optimization process, starting with the previous knowledge of the dynamic files representing the original and the reduced model obtained on Stage 1. The initial parameters for the added PSSs are set as typical values for machines of similar sizes. The algorithm continues by assigning a new set of parameters to the PSSs according to the genetic strategy, and writing these values in the dynamic file.

The created dynamic file is used in SSAT to perform small signal analysis, from which a respective set of eigenvalues is obtained. Using this update, the objective function *g* is computed in Matlab, and the optimization loop is closed by checking if *g* is at a minimum. The routine that was developed for this purpose is detailed in Appendix B.

The results of the optimization stage are evaluated by small signal analysis, frequency response and transient behavior. Figure 4.5 shows the location of the eigenvalues of the reduced model vs. the original model. The success of the optimization procedure can be measured when comparing to the results on Figure 4.3, at the end of Stage 1.

Another way of evaluating the reduced model is by the frequency response of two generators, using shaft angle deviations in remote generators as inputs, and using frequency deviations in other generators as outputs. Figure 4.6 and Figure 4.7 show respectively the magnitude and angle responses when the rotor angle of Gen 6124 is used as an input, and the output is the frequency deviation of Gen 3032. Figure 4.8 and Figure 4.9 show the response when the input is the shaft angle deviation at Gen 4405, and the output is the frequency deviation at Gen 6060.

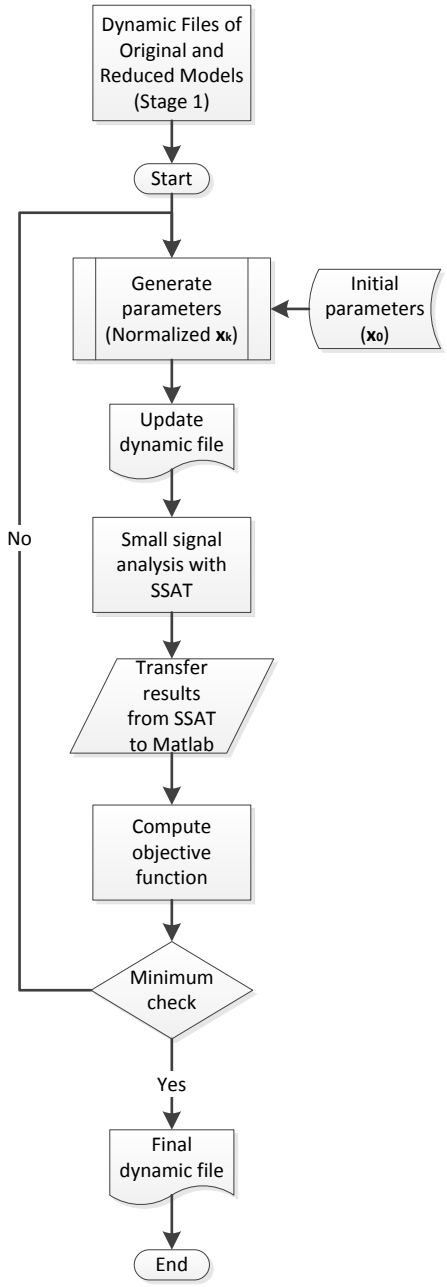

Figure 4.4 Block diagram representation of the optimization process for Stage 2 of reduction.

From a transient standpoint, a single-phase to ground short circuit at line 1125-28161 was simulated, and the voltage magnitude was recorded at Bus 1101; this result is shown in Figure 4.10. Voltage measurements at Bus 3032 and 6096 are plotted in Figure 4.12 and Figure 4.14 respectively. A two-phase to ground short circuit at line 4408-50000 was also simulated, and the rotor angles at Gen 1101, Gen 3032, and Gen 6096 were plotted in Figure 4.11, Figure 4.13, and Figure 4.15 respectively.

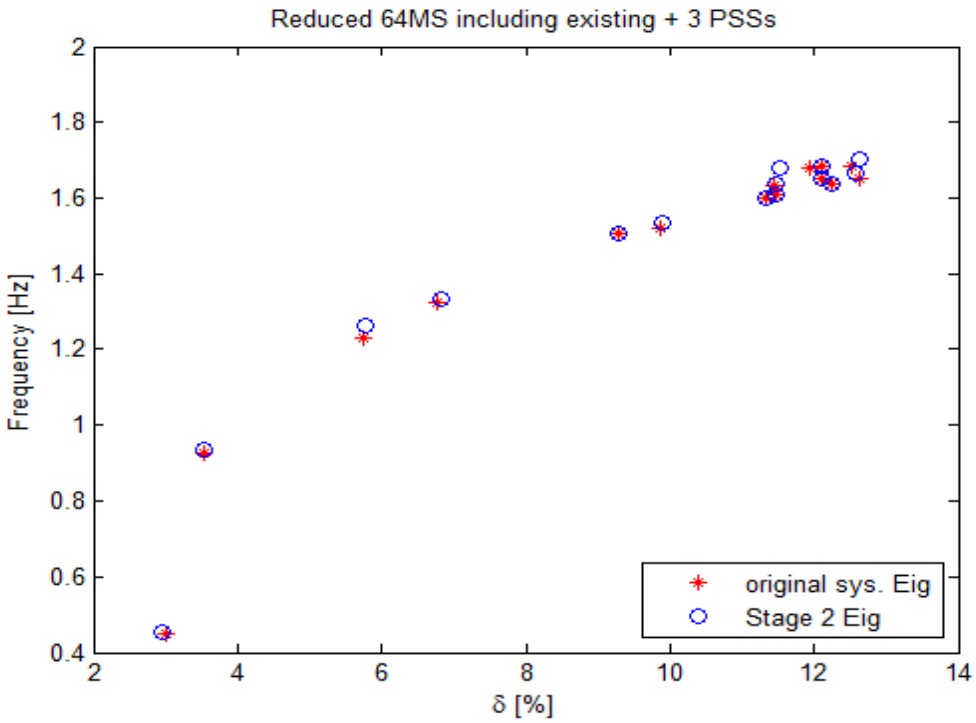

Figure 4.5 Location of eigenvalues in the original model vs. the reduced model at Stage 2.

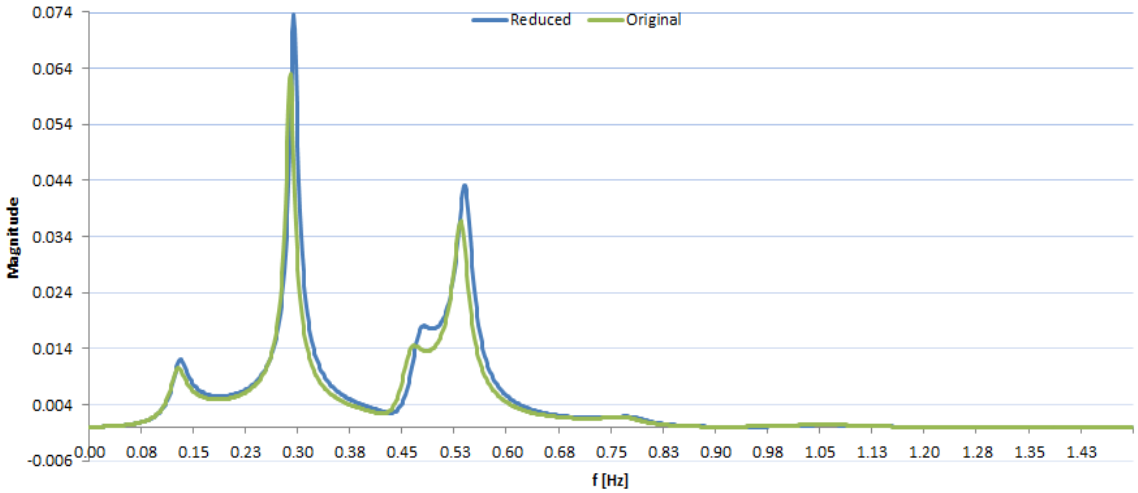

Figure 4.6 Magnitude response. Input: rotor angle of Gen 6124. Output: frequency deviation of Gen 3032

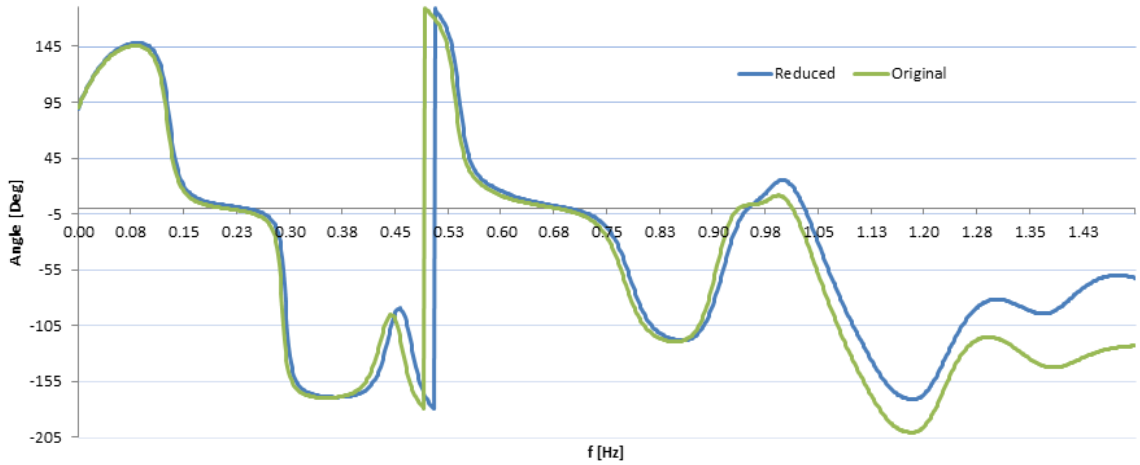

Figure 4.7 Angle response. Input: rotor angle of Gen 6124. Output: frequency deviation of Gen 3032

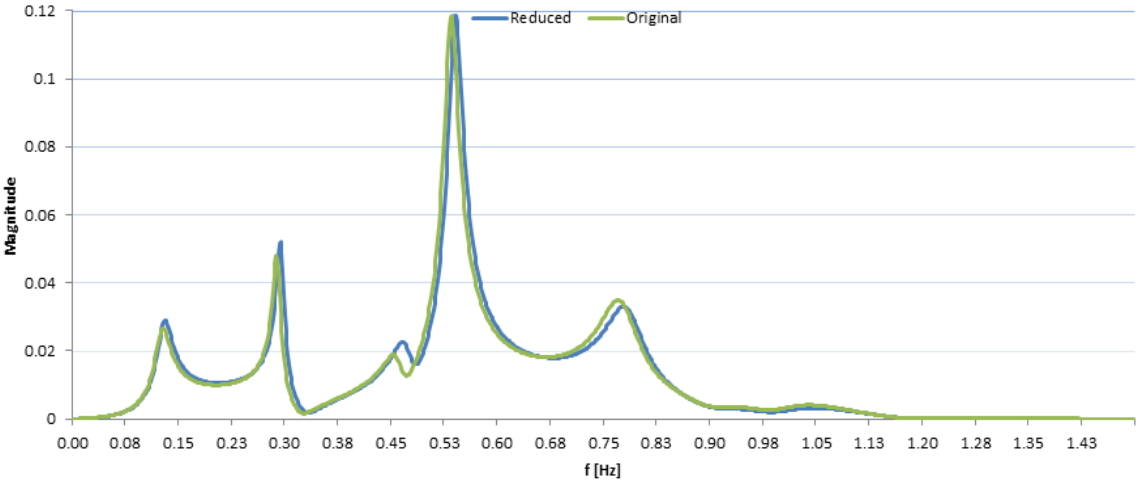

Figure 4.8 Magnitude response. Input: rotor angle of Gen 4405. Output: frequency deviation of Gen 6060

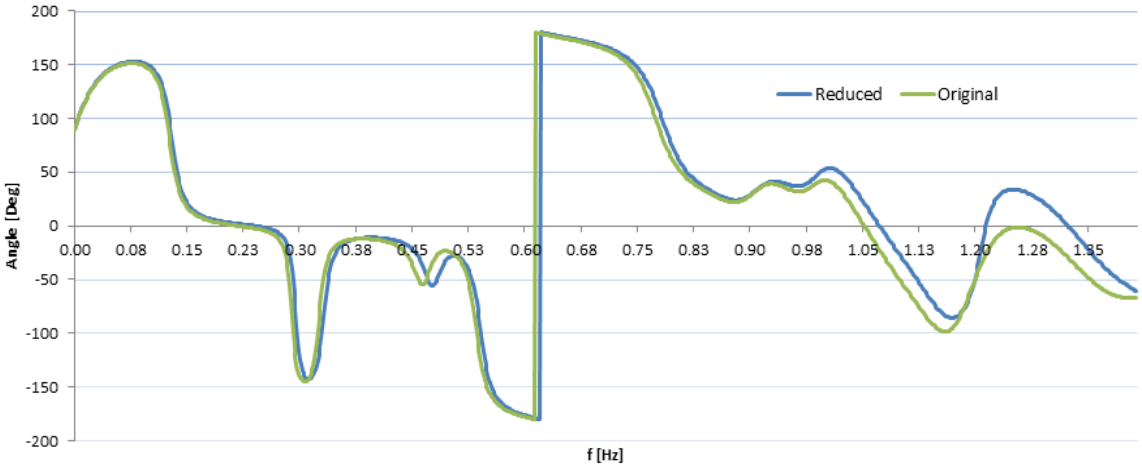

Figure 4.9 Angle response. Input: rotor angle of Gen 4405. Output: frequency deviation of Gen 6060

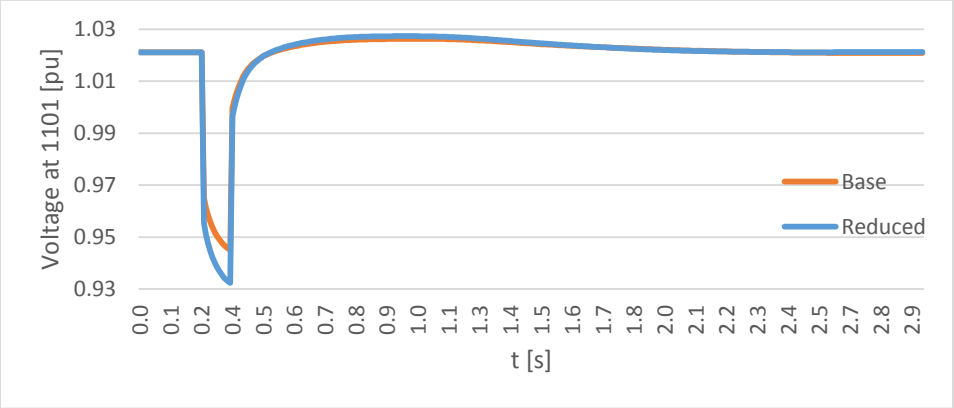

Figure 4.10 Voltage magnitude at Bus 1101 after a single phase to ground short circuit at line 1125-28161

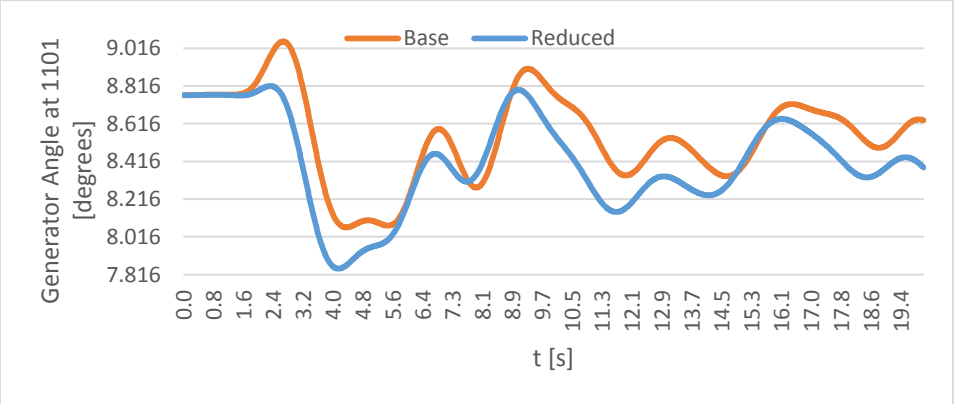

Figure 4.11 Rotor angle at Gen 1101 after a two phase to ground short circuit at line 4408-50000

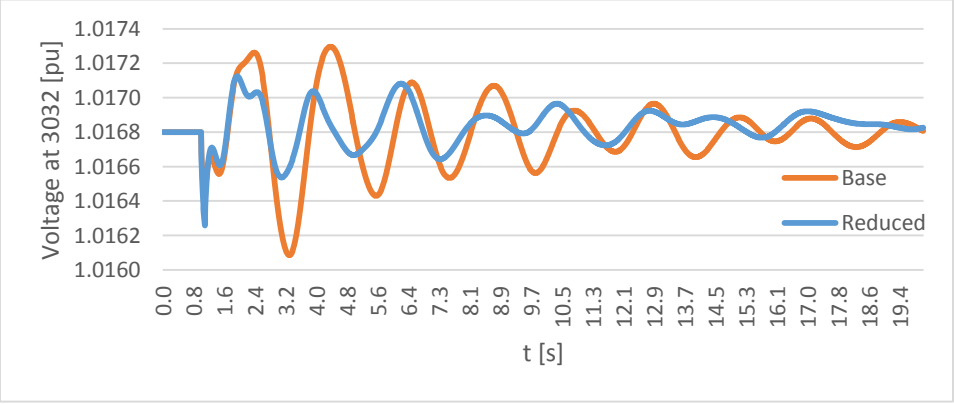

Figure 4.12 Voltage magnitude at Bus 3032 after a single phase to ground short circuit at line 1125-28161

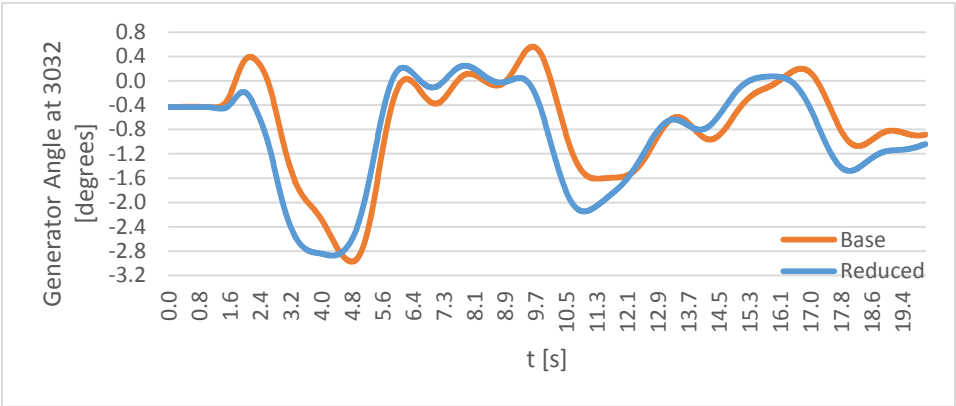

Figure 4.13 Rotor angle at Gen 3032 after a two phase to ground short circuit at line 4408-50000

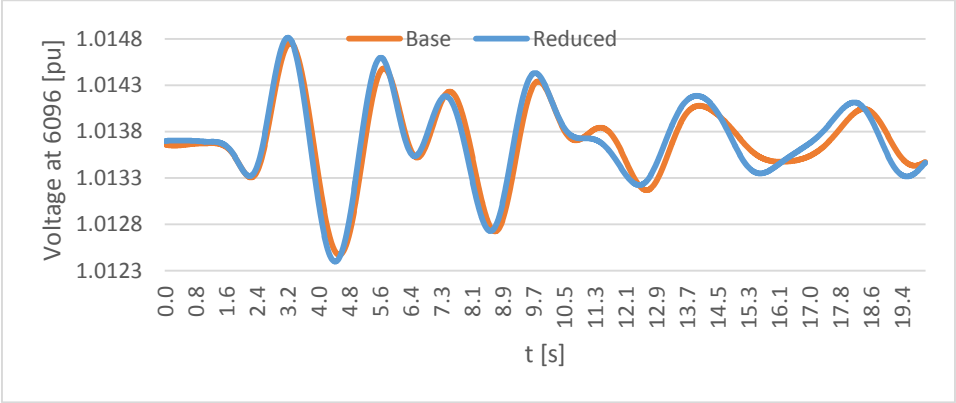

Figure 4.14 Voltage magnitude at Bus 6096 after a single phase to ground short circuit at line 1125-28161

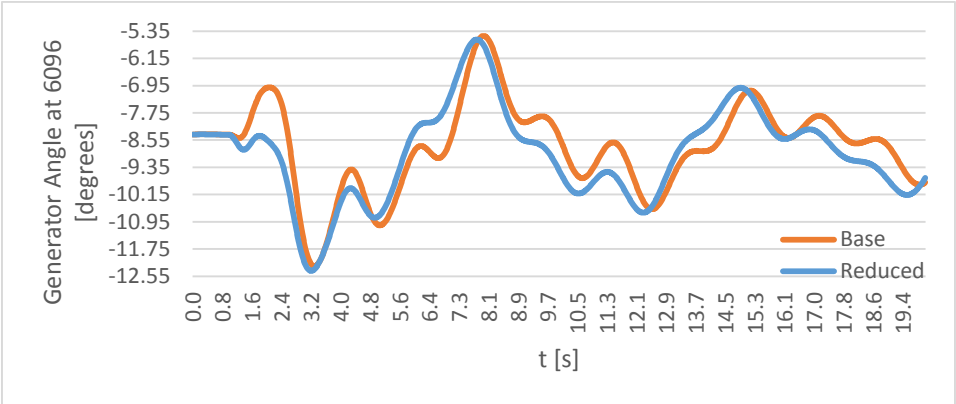

Figure 4.15 Rotor angle at Gen 6096 after a two phase to ground short circuit at line 4408-50000

The transient responses show their biggest magnitude discrepancies in the first or second swing. The largest discrepancies between original and reduced models were 0.016pu for voltage (Figure 4.10), and 0.6 degrees for angle (Figure 4.13). The frequency content and relative phase of the responses of original and reduced systems does not show important deviations.

From Figure 4.5, it is obtained that the maximum error in damping between the original and the reduced systems is 0.5% for an eigenvalue with close to 12% damping, and those eigenvalues with damping less than 10% the reduced system deviates 0.1% at most. Frequency deviations are of 0.03Hz at most. The magnitudes of the observed differences between these two models are not significant for the design of the small signal controller, nor for practical power system analysis; hence the reduced model is considered to be appropriate for these purposes. The reduced model obtained by the proposed methodology consisted of 64 generators, 55 automatic voltage regulators, and 16 power system stabilizers. This represents a reduction of 50% from the original model, and allows a more manageable model for upcoming studies, with no important detriment to the original behavior.

4.2 Range of Operational Conditions

A power system in normal operating conditions experiences a wide range of variations of load, generation, and configuration that ultimately respond to the demand of electric energy shaped by human activity. The diverse nature of energy sources, their geographical distribution and availability, and the transmission and distribution infrastructure capable of transporting and delivering energy, all play an important role in defining the power flow distributions and energy markets' behavior.

The combination of all these factors at a given point in time, defines a snapshot of the system that shows the current operation point characterized by the set consisting of voltages at all buses, and active and reactive power flows through all transmission and distribution links. A continuous monitoring of the system state is performed by Supervisory Control and Data Acquisition (SCADA) systems for purposes of operation and remote control, however, analysis and design tasks are usually performed only for a number of operation points that describe circumstances in which the system is either stressed, at some kind of extreme situations, or other representative conditions during the expected operation range. These conditions include combinations of minimum, medium and maximum load, winter and summer load-generation arrangements, energy transactions between areas, and specific transmission configurations.

It is intended that the proposed centralized controller will be effective to increase damping of targeted oscillation modes that may appear in a wide range of operating conditions, hence the definition of cases to be used during the design process should be done carefully and based on an expert knowledge of the system. For this study, the span of operating conditions was generated from a combination of load variations, energy transfers between areas, and generation and transmission configurations as it was done in [99]. According to [99], the demand scenarios considered are the maximum, medium, and minimum load, which in terms of active power correspond to approximately 100%, 80% and 50% respectively of the maximum load conditions.

The 230kV transmission corridor that interconnects the control areas of the system is designed to withstand 300MW transfers between any pair of areas. Furthermore, energy transactions are more likely to originate from areas with excess of generation to areas with generation deficit. In accordance with this fact, the cases shown in Table 4-2 were considered to have among others a reasonable probability of occurrence.

Table 4-2 Combination of Demand Scenarios and Transaction Pairs to Generate the Complete Range of Cases

DEMAND SCENARIO	TRANSAC. MW	AREA	
		FROM	TO
MAX/MED/MIN	0	NA	NA
	300	1	2
	300	1	3
	300	1	4
	300	1	5
	300	1	6
	300	5	2
	300	5	3
	300	5	4
	300	6	2
	300	6	3
	300	6	4
	300	6	5

In addition to the 39 cases resulting from the combinations of demand and transaction cases, a list of contingencies was considered as defined in [99]. These contingencies are such that they induce important load-generation unbalances and in most cases entail distinct system configurations that could be sustained for prolonged periods of post-disturbance. The variability of scenarios that results from a combination of demand-transaction-contingency cases is wide and considered to contribute with sufficient modal shifts to be acceptable for the design purposes of this study. The list of contingencies includes loss of generation and loss of transmission links at specified buses as detailed in Table 4-3.

If every one of the 39 contingencies enumerated in Table 4-3 is applied to the 39 Demand-Transaction cases, then the span of operating conditions that will be used to add robustness to the centralized controller design will contain $39^2 = 1521$ cases.

4.3 Computation of Gains for Feedback Control

From Table 4-3, contingencies 20, and 33 to 39 are capable of provoking the formation of islands in the system. When this happens, one of the formed islands remains supported by one single generation plant and only in very few circumstances can this condition be sustained and stability regained. Because of these circumstances cannot be adopted for long periods of time these considerations leave 32 events[4] that can remain in place for regular operation in a post-contingency scenario after the transient period. The combination of 39 operation points with 32 contingencies, considered as reconfiguration events, leads to 1248 cases that can be representative of sustainable steady state operating conditions. This method of generating operation points is appropriate to observe the diversity of conditions that can be encountered in a real system, although for a practical implementation it would be proper to

[4] This list of 32 events now includes the no-contingency case, which certainly leads to a configuration that can be sustained in normal operation.

aggregate to this list other reconfiguration events that could originate from maintenance schedules, and/or from short or long term transmission planning.

Table 4-3 Contingencies with Important Load-Generation Unbalances

TYPE OF CONTINGENCY	CONT. NUMBER	BUS	
		FROM	TO
Loss of generation	1	237	N/A
	2	4	N/A
	3	917	N/A
	4	924	N/A
	5	295	N/A
	6	605	N/A
	7	611	N/A
	8	615	N/A
	9	1218	N/A
	10	1102	N/A
	11	711	N/A
	12	744	N/A
	13	714	N/A
single line outage	14	929	931
	15	914	931
	16	915	922
	17	915	928
	18	924	925
	19	917	930
	20	297	343
	21	603	605
	22	602	606
	23	604	606
	24	563	573
	25	563	583
	26	602	605
	27	2	5
	28	5	8
	29	917	930
	30	411	423
	31	358	301
	32	650	711
	33	23	937
	34	423	938
	35	424	603
	36	607	939
	37	639	1196
	38	784	9
	39	784	882

A linearization of the Central American system at every operation point is performed to analyze possible variations on its small signal behavior, where the effect on damping factors of existing oscillation modes is of special interest. After computing the state matrices corresponding to all operation scenarios, wide

variations of eigenvalues were found. Figure 4.16 shows the location of eigenvalues when the system is in the very particular condition of maximum demand, with no transactions between areas, and with generator 237 out of line. Figure 4.17 shows the mode shapes of the two rotor angle modes with less damping factor, demonstrating that they correspond to inter-area oscillations. In mode 208, the six areas oscillate at a frequency of 0.44 Hz with a damping factor of 3%. The second mode, numbered 259 shows oscillations between the North block and the South block at 0.92 Hz, with a damping factor of 3.53%. Both modes have insufficient damping.

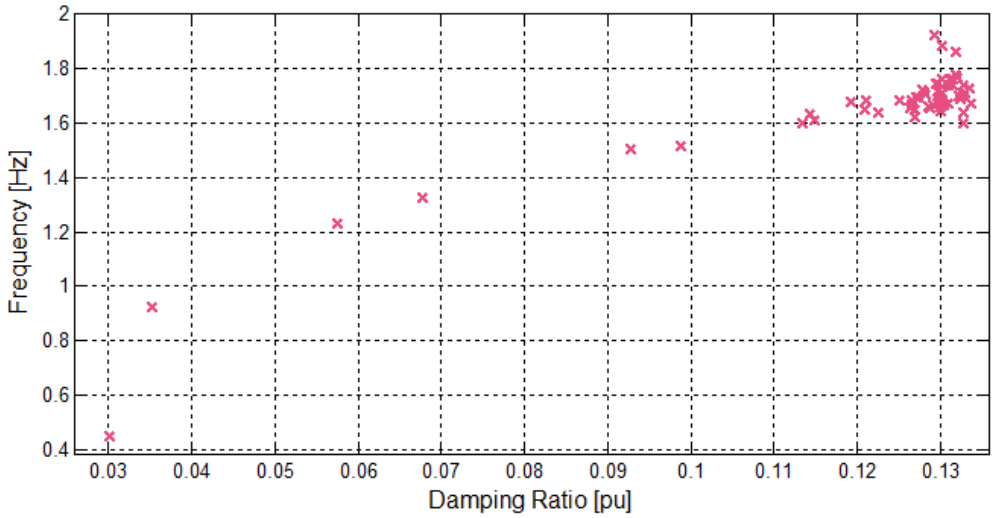

Figure 4.16 Eigenvalue locations for the Central American System with no transactions in maximum demand, and generator 237 out of line

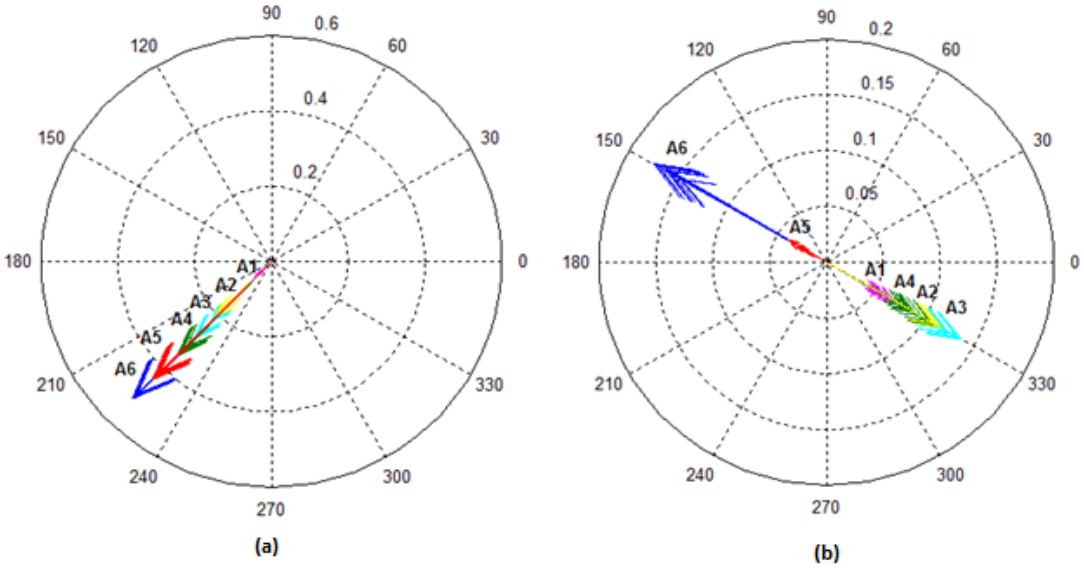

Figure 4.17 Mode shapes of the rotor angle modes with the lowest damping factor in the Central American System. (a) λ_1: 0.44 Hz, 3%. (b) λ_3: 0.92 Hz, 3.53%

In contrast to the single operation point analyzed previously, Figure 4.18 depicts the eigenvalue exhibiting the lowest damping factor of the system under study for the 1248 linearizations about the respective operation points. The cases corresponding to maximum demand are shown with ***x***, while those for medium and for minimum demand are plotted with ***o*** and with ***+*** symbols, respectively.

As shown in Figure 4.18, important frequency and damping factor variations were registered for the defined range of cases. For this particular oscillation mode between areas 1 and 6, high demand cases have a major impact, experiencing variations in frequency from 0.359Hz to 0.538Hz, and from 0.3% to 3.6% in damping.

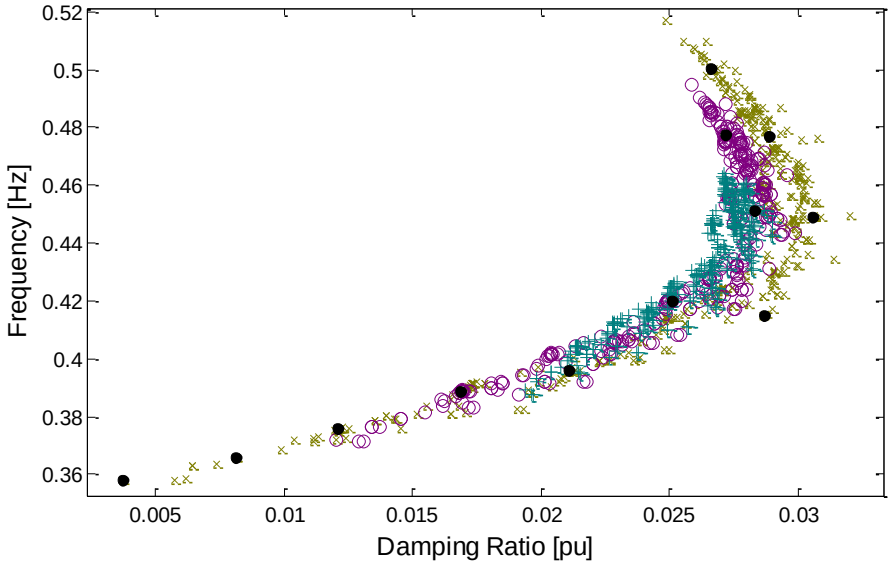

Figure 4.18 Location of the eigenvalue exhibiting the lowest damping factor for the complete span of operation points. *x*: Maximum demand cases. *o*: Medium demand cases. *+*: Minimum demand cases

In an attempt to define a number of operation points that represent remarkable areas of the complete span of system variations, and yet it is limited to the extent of the design effort for the demonstrative nature of this study, an arbitrary number of 12 points is adopted as representative operation points for which control gains are designed. The black filled circles in Figure 4.18 show the location of the eigenvalues with the lowest damping factor, on which the graphical selection of the 12 representative operation points was based.

After the representative eigenvalues were selected graphically, the respective operation points were mapped back to find the exact system conditions that originated such small signal behavior. This result is summarized in Table 4-4, where each case is defined by the load amount present in the system, the type of transaction that was taking place, and the particular configuration event, or the single element that was out of service according to the definitions of Table 4-3.

Table 4-4 Reference Operation Points used for Gain Design

OP. POINT	CASE NUM.	DEMAND	TRANSACTIONS		CONFIG. EVENT
			FROM	TO	
1	340	Max	6	2	21
2	50	Max	1	3	18
3	120	Max	1	6	25
4	352	Max	6	3	39
5	401	Max	6	5	17
6	339	Max	6	3	19
7	167	Max	5	3	8
8	730	Med	6	4	27
9	505	Med	1	6	26
10	848	Min	1	5	16
11	641	Med	5	3	1
12	376	Max	6	3	25

Figure 4.19 shows how the 12 points selected for the eigenvalue with the lowest damping factor are reflected in the second lowest damped eigenvalue. Once again in this case, topological and transaction variations that take place at high load conditions are the ones that induce larger variations in damping factor an frequency, where the first one ranges between 3.3% and 3.8%, and the second one oscillates between 0.87Hz and 0.93Hz.

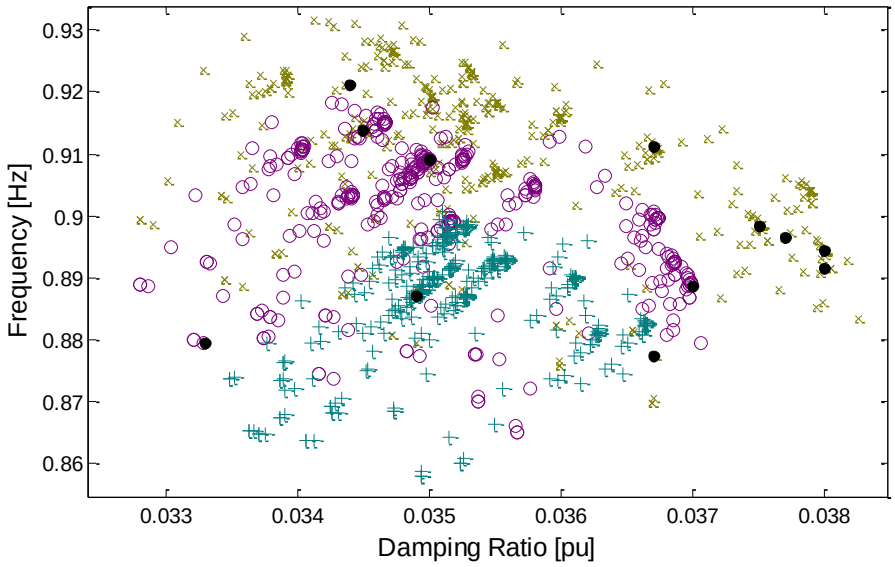

Figure 4.19 Location of the eigenvalue exhibiting the second lowest damping factor for the complete span of operation points. *x*: Maximum demand cases. *o*: Medium demand cases. *+*: Minimum demand cases

The state matrices representing the linearization of the system at every operation point in Table 4-4 are characterized by their own eigenvalues. Figure 4.20 shows the five first eigenvalues sorted by increasing

damping factor. As it can be seen in this figure, eigenvalues λ_1 and λ_3 (and their complex conjugates λ_2 and λ_4, respectively) are below the generally accepted threshold of 5% damping. The state feedback method used in subsection 3.2.3 for the control of the New England – New York system, is applied here to every case of Table 4-4 in order to displace the poorly damped eigenvalues to the acceptable value of 5%. In all the cases in the referred table this implies the design of the feedback gains $\boldsymbol{F}$ shown in Figure 4.21, so that the state vector is used to generate external input signals to all available PSSs, using them as vehicles to transfer the control signals to the exciters of these machines. Of the 597 eigenvalues the system exhibits, the feedback gains will correct only two, and will leave the remaining 595 at their original values.

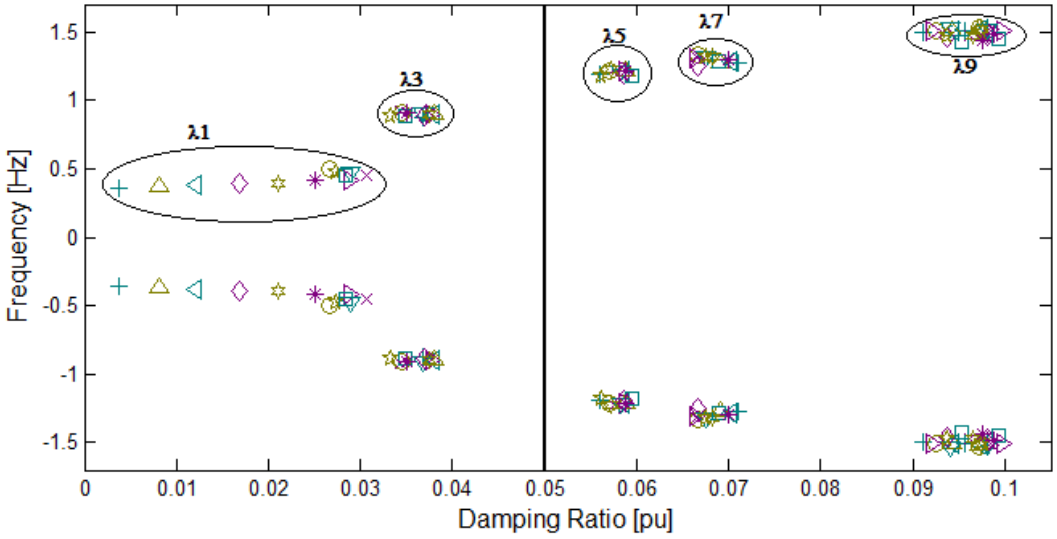

Figure 4.20 Five eigenvalues with the lowest damping factor for the 12 representative cases of the operation span of the Central American System. The eigenvalues for cases 1 to 12 are represented with the symbols +, x, o, ◁, ▷, Δ, ▽, ◊, ☆, □, ✳, and ✶ respectively.

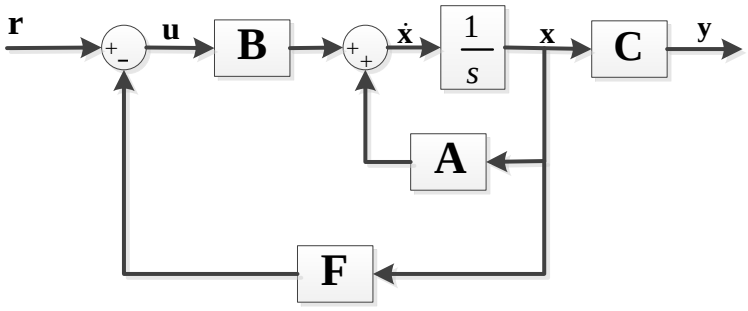

Figure 4.21 State feedback method to be applied to the 12 system configurations to correct the poorly damped oscillation modes

The reduced model of the Central American System that is being used in this study has 64 generators, where 55 of them have automatic voltage regulators, and 16 of them have PSSs, although only 13

stabilizers can be used in the control loop. Each generator is represented by six states, while the voltage regulators and the stabilizers each have three states, as follows:

Generator States:

$\boldsymbol{\Delta\delta}$: Machine angle

$\boldsymbol{\Delta\omega_r}$: Machine speed

$\boldsymbol{\Delta\psi_{fd}}$: Field flux

$\boldsymbol{\Delta\psi_{1d}}$: Damper 1 d-flux

$\boldsymbol{\Delta\psi_{1q}}$: Damper 1 q-flux

$\boldsymbol{\Delta\psi_{2q}}$: Damper 2 q-flux

AVR States:

$\boldsymbol{V_r}$: Regulator output

$\boldsymbol{E_{fd}}$: Exciter output

$\boldsymbol{R_f}$: Stabilizing transf.

PSS States:

$\boldsymbol{pss_1}$: Washout variable

$\boldsymbol{pss_2}$: First lead-lag variable

$\boldsymbol{pss_3}$: Second lead-lag var.

With regard to the state space equations (4.2) the results is a (597x1) state vector $\boldsymbol{x}$. The number of inputs to this system would be equivalent to 13 external inputs to PSSs, 55 voltage references to AVRs, and 64 torque references to every generator. However in this case only 13 entries of $\boldsymbol{u}$ will be nonzero, since voltage reference deviations as well as torque references are kept null. It is understood that the feedback control task demands the availability of the complete state vector, either by direct measurement or computation, or as a result of an observation stage. Although in a real-life power system implementation a state observer would be indispensable, for this study the availability of all states is assumed and the output vector $\boldsymbol{y}$ equals the state vector $\boldsymbol{x}$, making $\mathbf{C}$ an identity matrix of order 597.

$$\dot{\boldsymbol{x}} = \mathbf{A}\boldsymbol{x} + \mathbf{B}\boldsymbol{u} \qquad (4.2)$$
$$\boldsymbol{y} = \mathbf{C}\boldsymbol{x}$$

When feedback control is applied the input signal $\boldsymbol{u}$ must be replaced by the difference of the reference signal and the transformed state as in (4.3). In this equation, the reference signal $\boldsymbol{r}$ is disregarded as it is expected in a regulator problem, leaving $\boldsymbol{u} = -\mathbf{F}\boldsymbol{x}$ as the input signal that will proceed from the centralized controller. The dimension of the feedback matrix $\mathbf{F}$ corresponds to the number of PSSs and to the number of available measurements, giving a size of (13x597).

$$\boldsymbol{u} = \boldsymbol{r} - \mathbf{F}\boldsymbol{x} \qquad (4.3)$$

The result of aggregating the external signal $\boldsymbol{u}$ to the linearized model is presented in subsection 3.1.4, concluding that the terms given by (3.10), (3.13), and (3.15) account for the necessary modifications to the state and input matrices $\mathbf{A}$ and $\mathbf{B}$ in (4.2) so that the controller input can be handled.

Once the controllability requirements have been verified for the cases in Table 4-4, the same design procedure that was introduced in Subsection 3.2.3 for a single feedback gain can be extended to the twelve cases of interest. The design task was developed in Matlab by means of the `place` function, resulting in twelve gain matrices ($\mathbf{F}_1$ to $\mathbf{F}_{12}$), each one capable of relocating poles λ_1 and λ_3 (Figure 4.20) on top of the 5% damping line in the same figure.

Figure 4.22 plots the action of gain 11 on the system when it is precisely at the same operation point for which it was designed: a medium demand scenario with 300MW being sent from area 5 to area 3, and with the generator at bus 237 in area 1 out of line. Here the poles with a damping factor of less than 5%

are effectively displaced in the complex plane to the points with the same frequency of oscillation, but with 5% damping. The rest of the poles are kept in the original locations in an effort to minimize the required control actions.

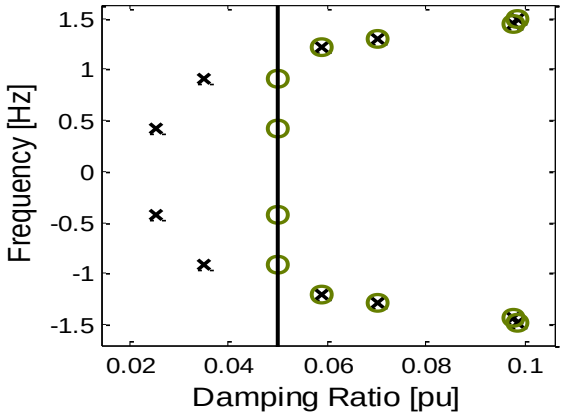

Figure 4.22 Operation point 11, before (x) and after (o) the respective gain has been applied

If during normal behavior of the system the operation point drifts to another location, the feedback gain being applied may or may not continue to be suitable to provide sufficient damping. This is illustrated in Figure 4.23, where the action of the gain designed for the same operation point as before, $\mathbf{F}_{11}$, is applied to the same circumstances of the previous case, except that here the system has moved to maximum demand. It can be observed that in this case the feedback gain provides more damping than required, which is a welcome effect. Conversely, if gain $\mathbf{F}_{11}$ continues to be applied when the system drifts from medium to minimum demand scenarios, with identical energy transactions as well as selfsame topological configuration, the feedback control becomes ineffective to secure all the oscillation modes with a damping of at least 5%, as shown in Figure 4.24.

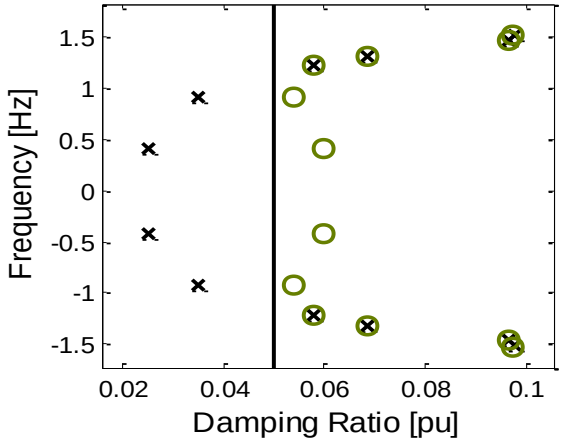

Figure 4.23 Action of F_{11} when the operation point has changed from medium to maximum demand. case 1. Without feedback: x. With feedback: o

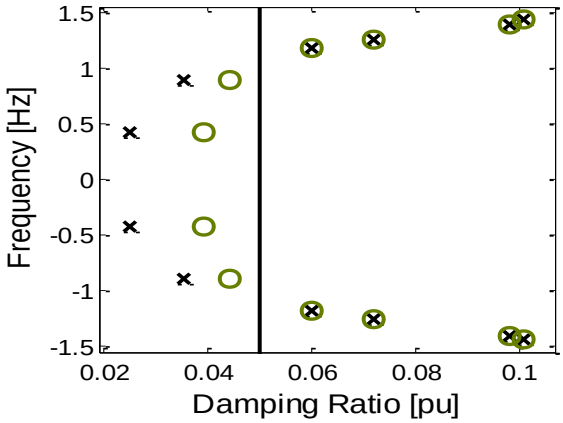

Figure 4.24 Action of F_{11} when the operation point has changed from medium to minimum demand, case 2. Without feedback: x. With feedback: o

4.4 Gain Scheduling

In the previous section it was explained that the application of a specific feedback gain when the system is not precisely operating at the point for which it was designed, may result in either insufficient or extra damping of the targeted modes. In the case where damping of all poles is adequate (greater than 5%) there is no inconvenience in operating with this disparity between gain and operation point, nevertheless if the amount of damping provided by the feedback loop is less than 5%, the consequences may be devastating for the power grid and may lead to partial or widespread blackouts. The prevention of this situation is an essential goal in the design of the centralized controller.

Gain scheduling is a technique adopted for this type of problems and has been perfected in flight control applications where all the gains are combined in a proportion dictated by a set of scheduling variables, generating an equivalent gain that modifies, as designed, the dynamics of the system [100]. In this study another gain scheduling strategy is harnessed, where the controller is in charge of commuting between feedback gains as a function of the scheduling variables, in such a manner that every system condition, either stationary or transient, is warranted enough amount of damping to all oscillation modes. Carrying out this gain scheduling design is contingent on the system being in steady state, or passing through transient conditions; these variations are addressed in the following sections.

4.4.1 Gain Scheduling in Steady State

When the system is operating in steady state, changes from one operating point to another take place gradually, allowing the system to be represented at discrete time instants with linearized versions about the respective point of operation. The range of system conditions developed in Section 4.3 provides a 1521-point characterization of the Central American system that, at least for illustrative purposes, can be considered to be a sufficient representation of the scenarios most likely to occur at any time.

It is assumed that at a given point in time the system is in steady state, in the conditions of the k^{th} linearization as in (4.4), where $\mathbf{A}_k$ has the respective set of eigenvalues $\mathbf{\Lambda}_k$, and where k can be any integer from 1 to 1521.

$$\dot{\mathbf{x}} = \mathbf{A}_k\mathbf{x} + \mathbf{Bu} \qquad (4.4)$$

The problem to solve is to determine the gain that should be applied in these conditions such that the damping of all poles in $\mathbf{\Lambda}_k$ are on or above the 5% threshold, and to identify an appropriate scheduling variable that is sensitive enough to the topological and operational changes that affect the modes of oscillation of the system.

At point k, as well as at any other steady state point, a power system can be completely described by its admittance matrix $\mathbf{Y}$ [101], which is a function of the system's topology and its electrical parameters, and by the set of all voltages at all buses, denoted by $\mathbf{V}$, typically regarded as the Load Flow solution. In fact, the currents or power flows at all branches can be found by (4.5), giving all the information necessary for static conditions.

$$\mathbf{I} = \mathbf{VY} \qquad (4.5)$$

In a practical power system, even without the knowledge of the currents through transmission links, in many cases a trained operator can discern an approximate status of the system or its current transmission configuration, by only examining voltage magnitudes and angles at relevant buses, i.e. by observing voltages at adjacent nodes a trained eye can have a glimpse of the system's topology and current flows. Based on previous knowledge of how the system behaves, voltage magnitudes and angles can indicate if a transmission line or a transformer is open or closed, if a transaction of importance is taking place, or if certain generation plant or load is in service or not.

The previous argument leads to the believe that it would be reasonable to assume that the set of voltages at all buses would be a good candidate for a scheduling variable; this variable would be a good selection to utilize in a classification tool for data mining with decision trees. That is precisely what has been done in this study: Define the time synchronized voltage measurements throughout the system as a scheduling variable, and use it to yield a decision on what gain should be applied at a given operating point. Decision trees have been used to classify the data because of their robustness and the convenience of a graphical interpretation of the results.

Every operating point k, characterized by its respective state matrix $\mathbf{A}_k$ and its associated set of eigenvalues, is presented with every feedback gain j. The resulting state matrix is modified to $\mathbf{A}_k - \mathbf{BF}_j$ with a new set of eigenvalues that may or may not have all its elements with a damping greater than 5%. The application of a gain j will result in an outcome for case k that would translate to one of two possibilities: Either the damping factor of all eigenvalues resulted greater than 5%, or not. This implies that there would be 12 decision trees, each one with 1521 instances.

Nonetheless, not all the cases need to be considered from a steady state perspective since some of them lead to situations that cannot be sustained in long term scenarios. When performing dynamic simulations of all combinations of case-contingency and an applied gain, in 273 cases the occurrence of a contingency in a specific system configuration resulted in unstable behavior that ended in the formation of islands. In these instances, regardless of the applied gain the system continued to be unstable, therefore the consideration of these cases was not necessary and only 1248 instances were used to train decision trees.

Decision trees are capable of classifying any new instance, in the form of a new value of the scheduling variable, and predict up to a certain accuracy level what the outcome would be. The structure of the training data for the j^{th} decision tree is shown in Table 4-5.

The initial step to design the decision trees is to compute the eigenvalue sets for all combinations of instance and gain applied, where every instance is the set of bus voltages that takes place when a contingency from Table 4-3 occurs in a scenario of Table 4-2. This basically consists in the computation of the 1248 state matrices by linearizing the system about every operation point, and the subsequent computation of eigenvalues of the same state matrices after being altered by the feedback gain under consideration. This constitutes 14976 entries organized in 12 groups, as the training data for the decision trees.

Table 4-5 Training data for the j^{th} decision tree obtained after applying the j^{th} gain.

GAIN APPLIED: Fj	
Instance (case)	**Outcome δ>5%**
1	Yes or No
2	Yes or No
⋮	⋮
1248	Yes or No

The design of each decision tree is accomplished in Matlab by the use of the function `classregtree(X,Y)`, where X is an *n*x*m* matrix of predictors with *n* being the number of system configurations (1248), and *m* is the number of voltage measurements throughout the system; since the Central American system comprehends 1247 buses, and every voltage in steady state is represented entirely by its magnitude and angle, then *m*=2494. `Y` is the vector of *n* response values with information if a given gain connected in a specific case would result in damping greater than 5% for all modes, or not. The function `classregtree` then performs a classification if Y is a categorical variable, yielding a binary tree where each non-terminal node is split based on the values of a column of `X` [102].

In order to determine how the results of every decision tree will generalize to an independent instance, a 10-fold cross validation technique was conducted. In this process the complete data set was randomly partitioned in ten fractions. Nine of them were used to train the decision tree, whilst the remaining tenth was used to assess the effectiveness of the tree and the quality of its

results. This process was repeated in such a way that all the partitions were used in turns for validation. At every validation round the percentage of right guesses was recorded and used to average the expected accuracy of a given decision tree.

The accuracy of the decision trees after 10-fold cross validation is summarized in Table 4-6. It shows that the predictions each tree is capable of performing ranges between 93.76% and 99.68%. The smaller trees, identified by smaller numbers of pruning levels, are the ones that provide higher accuracy levels, while the opposite can be said about trees with large numbers of pruning levels.

Table 4-6 Results of the 10-Fold cross validation of the 12 decision trees.

	DECISION TREE NUMBER											
	1	**2**	**3**	**4**	**5**	**6**	**7**	**8**	**9**	**10**	**11**	**12**
PRUNING LEVELS	3	11	13	3	1	2	5	9	9	11	9	6
ACCURACY	0.9904	0.9376	0.9608	0.9904	0.9952	0.9968	0.9872	0.9523	0.9722	0.9632	0.94	0.9769

Based on voltage measurements every decision tree estimates the sufficiency of damping in the case a given gain is connected in the feedback loop. The decision trees obtained went from simple and concise forms like the one shown in Figure 4.25, which is the tree with the highest attained accuracy, to remarkably complex and slightly less accurate structures like the one in Figure 4.26. In these figures each branch is labeled with its decision rule, where for example M(885) indicates the voltage magnitude of Bus 885 (Figure 4.25), and A(708) refers to the angle of the voltage at Bus 708 (Figure 4.26). Each terminal node is labeled with the predicted value for that node, either the damping factor of all modes would be greater than 5% (d>5%), or at least one mode will have insufficient damping (d<5%).

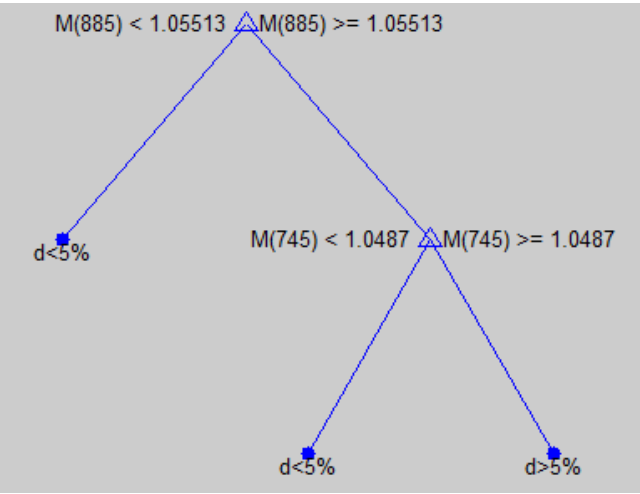

Figure 4.25 Decision tree 6 for steady state conditions. Accuracy: 99.68%. Decision node (Δ), Terminal node (•).

Details on the decision trees for steady state conditions can be found in Appendix C. From these results it can be inferred that mostly voltage magnitudes are the ones needed to make the decisions, but also some voltage angles are required. In addition, from the 2494 measurements that were used to train the trees, only 115 are necessary, from which 99 are magnitudes (86%)

and 16 are angles (14%). A Phasor Measurement Unit receiving voltage measurements from a bus will register both, magnitude and angle; considering this, it was determined that a number of 109 buses require PMU measurement, which is about 9% of the total number of buses in the system. Table 4-7 summarizes the needs for measurement to feed the decision trees for the centralized controller.

The centralized controller consists of twelve decision trees running in parallel and receiving periodic time synchronized voltage measurements from the 109 buses in Table 4-7. The period of the incoming measurements should be reasonably fixed such that it complies with regular power system operation in steady state, for instance a period of five minutes could be appropriate for this application.

Table 4-7 Buses that require voltage measurement through Phasor Measurement Units.

BUS NUMBER	DECISION TREE NUMBER											
	1	2	3	4	5	6	7	8	9	10	11	12
2			■	■						■	■	
3								■				■
5		■						■				
6		■		■				■				■
18								■				
19										■		
21								■				
23											■	
25	■			■						■		
36	■						■					
37		■										
49		■										
50												■
54											■	
55		■										
56							■					
74									■			
94									■			
107		■					■	■				
133											■	
137											■	
141											■	
142								■			■	
159												■
162	■											
183		■							■			
212		■									■	
253											■	
281			■								■	
282			■							■	■	
283			■	■			■		■	■		
284				■								
285												■
288		■	■						■		■	
290		■										
293												■

BUS NUMBER	DECISION TREE NUMBER											
	1	2	3	4	5	6	7	8	9	10	11	12
300		■										
302		■					■					
303		■										
304										■		
311		■					■	■				
312		■										
316					■							
333									■			
334										■		
346					■				■	■		
347									■			
366									■			
371										■		
372										■		
405		■										
423										■		
437			■									
433											■	
438										■		
437												■
439												■
442			■									
445											■	
447			■									
451										■		
452			■									
455	■							■				
460												■
504										■	■	
464								■				
601					■						■	
604		■										
639		■	■				■	■		■	■	■
640		■			■		■		■			
644		■										
651										■		

Table 4.7 Continued Buses that require PMU measurement t.

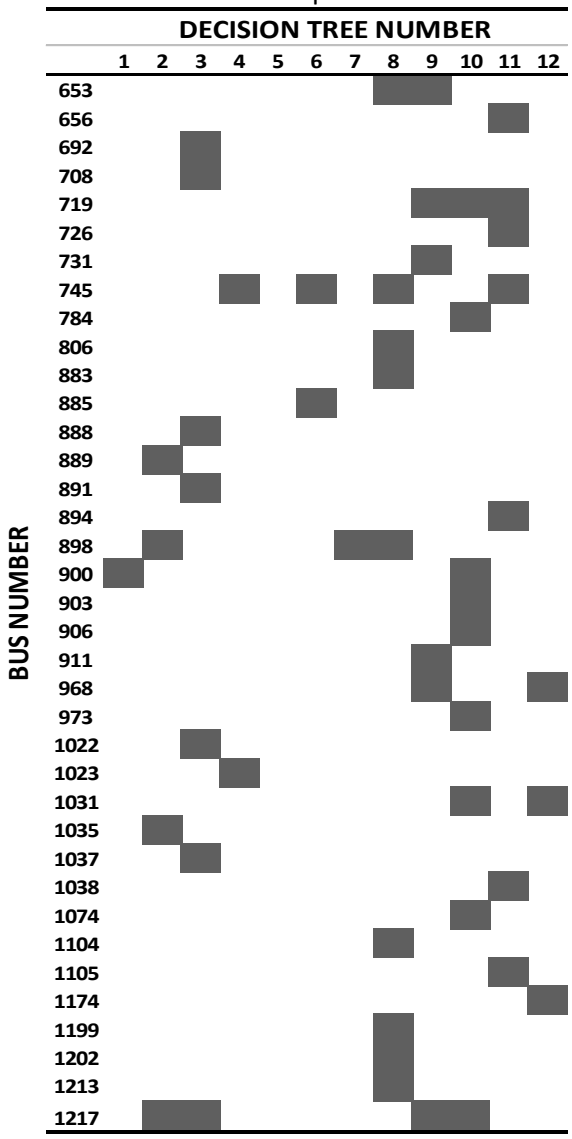

When a set of measurements (denominated as an instance) is received at the centralized controller, it is evaluated simultaneously in all the decision trees. The prediction of each tree associated to its respective feedback gain, indicates what gains would result in an appropriate or in an insufficient damping of the system. At this point it is possible that a number of apposite feedback gains could improve the small signal stability behavior of the system; in this situation the obvious question is what gain to use.

At first glance, since all the gains recommended by the decision trees are expected to work correctly, the answer to that question seems to be “anyone”. However, recalling Table 4-6 it is evident that although all the decision trees are fairly accurate, some of them are more trustworthy than others. This suggests that a better approach would be undertaken if Table 4-6 was used as an order of merit to help decide the best feedback gain among the ones suggested by the trees. The implementation of this decision logic can easily be programmed in the centralized controller and hence it is the recommended solution.

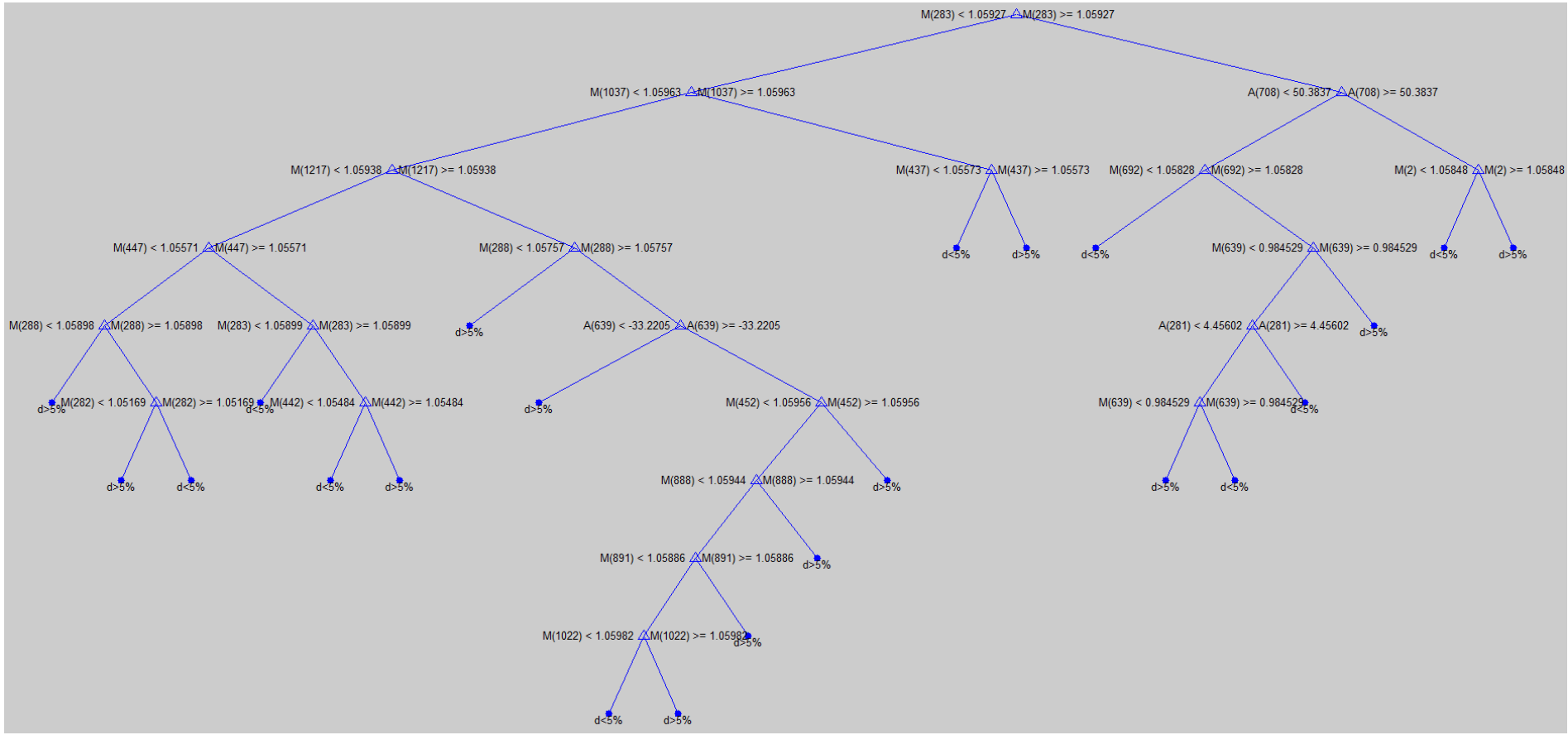

Figure 4.26 Decision tree 3 for steady state conditions. Accuracy: 96.08%. Decision node (Δ), Terminal node (•).

Figure 4.27 shows a typical load curve during a 24-hour period, without any contingency or reconfiguration in the system. For this profile, all decision trees were evaluated every 15 minutes with the result that all of them, except T08 and T10, contributed to a damping greater than 5% throughout the day. There were some periods when T08 and T10 produced insufficient damping, these periods are shown in Figure 4.27. According to Table 4-6, for this particular example, T06 should be employed during the 24-hour period.

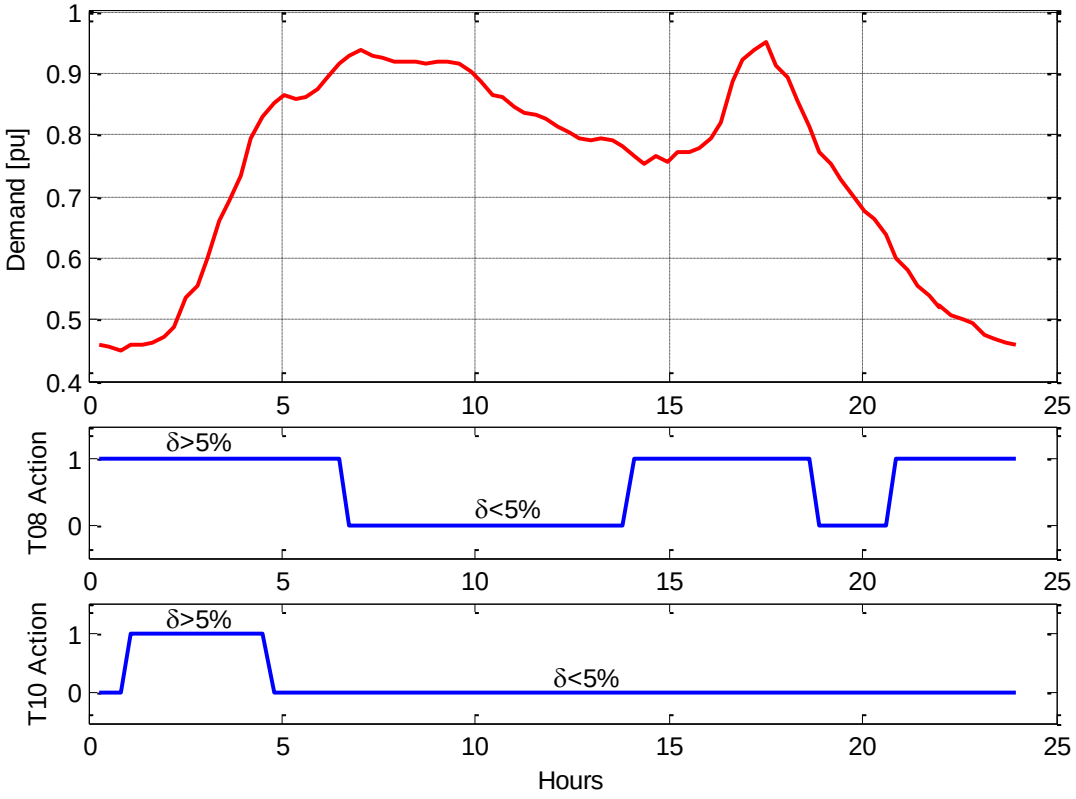

Figure 4.27 Action of decision trees when submitted to a typical day operation with no contingencies.

A transition of feedback gains taking place during steady state conditions is not likely to entail large disturbances. To illustrate this, consider a maximum demand case with 300MW flowing from Area 5 to Area 3, and with the generator at bus 237 (area 1) out of line. When Gain 5 is applied the system has insufficient damping, as shown in Figure 4.28, but when the gain is commuted to Gain 11 the poles are moved to a secure position with damping greater than 5%, as depicted in Figure 4.29 . Figure 4.30 illustrates what happens with the PSS output at Generator 3 during the transient period after the commutation of gains. To produce this plot, the system was subject to a slight disturbance in order to make the controller act. The disturbance was a slight variation in PSS reference at the generator at bus 1. It is expected that when the system is in steady state, any gain switching will not produce significant disturbances.

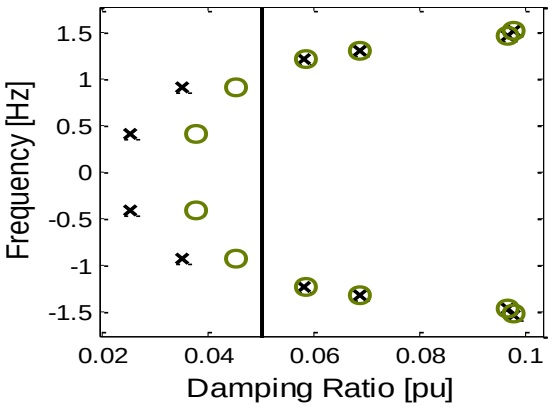

Figure 4.28 Gain F_{05} at maximum demand with 300MW sent from area 5 to area 3. Generator at bus 237 is off line. Without feedback: x. With feedback: o

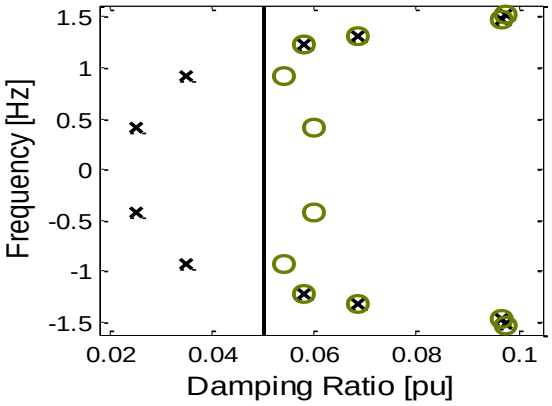

Figure 4.29 Gain F_{11} at maximum demand with 300MW sent from area 5 to area 3. Generator at bus 237 is off line. Without feedback: x. With feedback: o

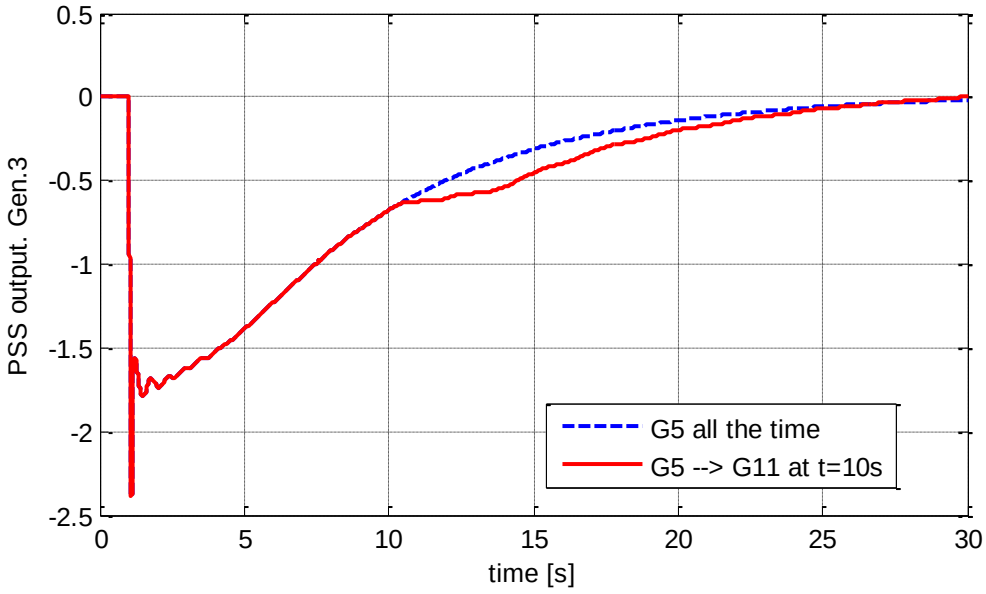

Figure 4.30 PSS output at generator 3 after a transition takes place from gain F_{05} to F_{11}.

Regarding the location of PMUs, it was stated previously that 109 buses required time synchronized voltage measurements in order to implement the decision trees embedded in the controller, and in charge of performing gain selection. In addition to those PMUs, every generation plant requires a PMU to provide measurements for feedback control, totalizing 173 PMUs to be placed in the system according to Table 4-7 and generator locations. Even though the number and location of phasor measurement units described here are sufficient to fulfill the needs of the centralized controller, neither the quantity nor the positioning are optimal from the perspective of power system operation.

Power system utilities and transmission operators usually seek PMU distributions that can achieve full observability of the network with the minimum number of devices, where full observability is understood as the capability of having time synchronized measurements at all buses in the grid, either by direct or by indirect measurement. Such methodologies to locate PMUs in the Central American System have been developed in [103] and [104].

[104] develops a gradual optimal PMU placement approach that guarantees minimum regional observability at the initial stage and full observability for the complete implementation. Organizational and regulatory characteristics of the system under study are considered to guarantee that the obtained result is not only effective, but also feasible for the region to implement.

So far, the proposed centralized controller will be able to improve the small signal stability behavior of the system under study during normal system operation, which is the vast majority of time. It remains unseen what can be done when the system experiences disturbances that lead to noticeable and potentially problematic transients; this is discussed in the following subsection.

4.4.2 Gain Scheduling Under Contingencies

After a fault, a generation outage or a loss of load, the power grid evolves to another operation point granted that stability is not lost; otherwise a system collapse may follow depending on the type of event and the system initial conditions. Once the centralized controller programming for normal system operation is determined, the remaining problem is the controller behavior under disturbance periods caused by contingencies.

To understand this problem, the system has to be analyzed during dynamic conditions while being subject to the effect of the previously designed feedback gains. The determination of how the Central American system reacts to the contingencies detailed in Table 4-3 was assessed by simulation using Power System Toolbox PST© Version 3.0, which runs in a Matlab environment.

1521 combinations of case-contingency that arise from Table 4-2 and Table 4-3 were tested thirteen times. The first twelve rounds of simulations corresponded to every feedback gain being applied two seconds after the contingency happened; the thirteenth round was run with no feedback gain applied. Every simulation of the 19773 that were performed was characterized as “stable” or “unstable”.

Every simulation was run for twelve seconds, leaving ten seconds after the application of the feedback gain for stability assessment. The determination of stability was performed by Prony analysis[5] on the rotor angle of all machines: if all rotor angle behaviors could be represented only by decaying sinusoids, the system was considered stable; otherwise the response was classified as unstable. The observations that resulted from this stage allow concluding that even though some of the gains have the capability of stabilizing the system, the result would be the same if the gain was removed at t = 2 seconds. In the rest of the cases the system being stable or unstable is not contingent on the feedback loop.

This makes the case that it would be unnecessary to take further steps attempting to design the centralized controller to operate in transients following contingencies, and in fact the best approach would be to disconnect the controller in such conditions. This task can be accomplished using built in characteristics of protection equipment. Since the occurrence of a contingency is registered by fault recorders or protection relays and marked with a flag, it is feasible to send a disabling signal to the centralized controller to prevent its operation during fault conditions.

4.5 Effect of Latency on the Centralized Controller

The implementation of the centralized controller requires data transmission from all PMU locations to a control center. In practice this is done by collecting the incoming data from all PMUs in one or more Phasor Data Concentrators (PDCs). Simultaneously, several PDCs can be interconnected in cascading layers until the data stream reaches the control center; this is illustrated in Figure 4.31. PMUs are generally capable of sending time tagged voltage and current data at reporting rates ranging from 10 frames per second (fps) to 60 fps. 30 fps is a commonly encountered value in 60 Hz power systems.

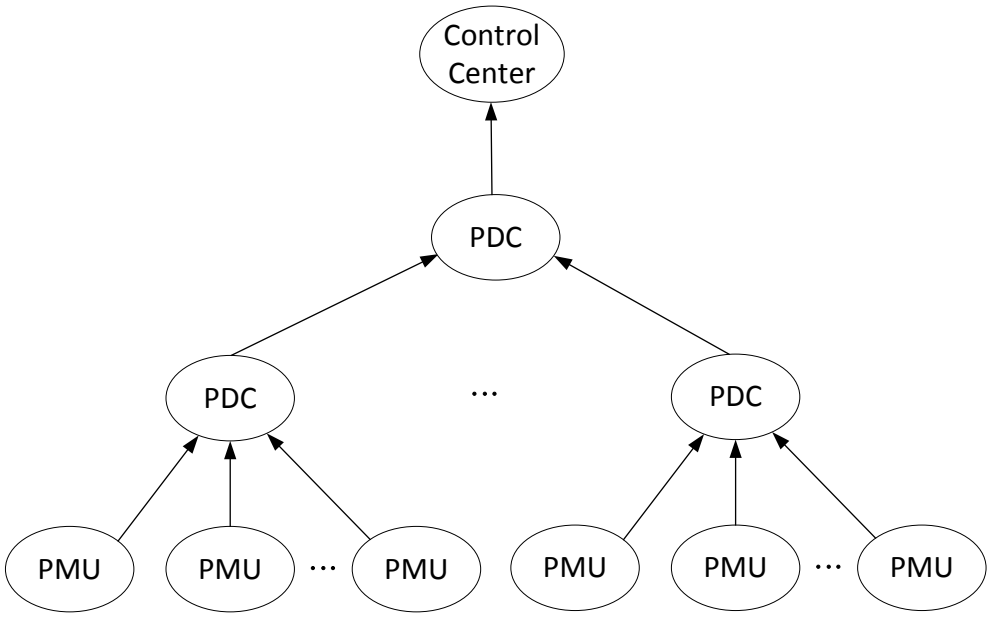

Figure 4.31 A structure of two layers of PDCs for data transmission in a WAMS.

[5] For details on the Prony Method refer to Section 2.4

As explained in [105], although data from all PMUs share the same time tags, it is not likely that all data traveling through different communication channels reaches the common destination at the same time; each channel is expected to show a different amount of latency. This discrepancy is caused by limitations in communications channels, different network configurations, and diverse PMU manufacturers. The function of PDCs is to aggregate, validate, and time-align incoming data from all associated PMUs, such that its output stream contains all available information marked with the same time tag. To perform this function, PDCs must count with buffering capabilities that allow waiting up to a set delay for the data from all PMUs before all the coincident data is streamed out to the upper level.

These delays lead to consider the PMU and PDC devices, along with the communications channels, an integral part of the control loop. In this study, these technical limitations have been accounted for by analyzing the effect of latency in the state feedback loop, assuming that all delays originating in the PMUs, communication channels, and PDCs, can be combined into one single latency value.

The evaluation of latency effects in the control system starts by discretizing the state model while introducing a delay in the measurements; this delay is illustrated in Figure 4.32 by the block e^{-sD}. The solution for the linear, time invariant system $\dot{\boldsymbol{x}} = \mathbf{A}\boldsymbol{x} + \mathbf{B}\boldsymbol{u}$ is [78],

$$\boldsymbol{x} = e^{\mathbf{A}t}\boldsymbol{x}(\mathbf{0}) + \int_0^t e^{\mathbf{A}(t-\tau)}\mathbf{B}\boldsymbol{u}(\tau)d\tau \qquad (4.6)$$

where $e^{\mathbf{A}t}$ is the state transition matrix in the special case of an LTI system.

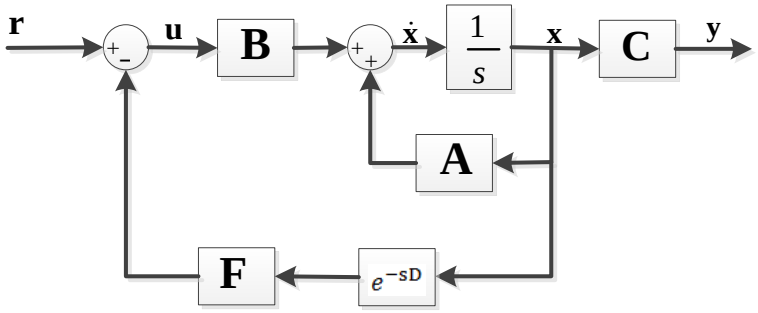

Figure 4.32 Feedback control system including delay in the measurements caused by inherent PMU and PDC latency.

In Figure 4.32 the state vector $\boldsymbol{x}$ is delayed by the D amount and fed as an input to the gain $\mathbf{F}$. The input $\boldsymbol{u}$ is composed by the difference of the reference signal $\boldsymbol{r}$ and the feedback signal. Assuming that a sample-and-hold circuit will be used this input can be defined as,

$$\boldsymbol{u}(t) = \boldsymbol{r}(kT) - \mathbf{F}\boldsymbol{x}(kT - dT) =: \boldsymbol{r}(k) - \mathbf{F}\boldsymbol{x}(k - d) \qquad (4.7)$$

$$\text{for, } kT \leq t < (k+1)T$$

where T is the sampling period, d and k are positive integers.

To simplify the simulation process the total delay is defined as $D =: dT$, i.e. it can be represented as an integer number of sampling periods.

At instant $t = kT$, (4.6) can be rewritten as,

$$\boldsymbol{x}[k] \coloneqq \boldsymbol{x}(kT) = e^{\mathbf{A}kT}\boldsymbol{x}(0) + \int_0^{kT} e^{\mathbf{A}(kT-\tau)}\mathbf{B}\boldsymbol{u}(\tau)d\tau \tag{4.8}$$

Similarly at instant $t = (k+1)T$, (4.6) would be,

$$\boldsymbol{x}[k+1] \coloneqq \boldsymbol{x}\big((k+1)T\big) = e^{\mathbf{A}(k+1)T}\boldsymbol{x}(0) + \int_0^{(k+1)T} e^{\mathbf{A}\left((k+1)T-\tau\right)}\mathbf{B}\boldsymbol{u}(\tau)d\tau \tag{4.9}$$

Rearranging (4.9),

$$\begin{aligned} x[k+1] = e^{\mathbf{A}T}\left[e^{\mathbf{A}kT}\boldsymbol{x}(0) + \int_0^{kT} e^{\mathbf{A}(kT-\tau)}\mathbf{B}\boldsymbol{u}(\tau)d\tau\right] \\ + \int_{kT}^{(k+1)T} e^{\mathbf{A}\left((k+1)T-\tau\right)}\mathbf{B}\boldsymbol{u}(\tau)d\tau \end{aligned} \tag{4.10}$$

On the right side of (4.10), the term in brackets is $\boldsymbol{x}[k]$ as obtained in (4.8). The second integral in (4.10) can be processed by making the change of variable $\alpha \coloneqq kT + T - \tau$; then this term becomes,

$$\int_T^0 e^{\mathbf{A}\alpha}\mathbf{B}\boldsymbol{u}(kT+T-\alpha)(-d\alpha) = \int_0^T e^{\mathbf{A}\alpha}\mathbf{B}\boldsymbol{u}(kT+T-\alpha)d\alpha \tag{4.11}$$

According to (4.7), the input $\boldsymbol{u}$ will be evaluated between $\alpha = 0$ and $\alpha = T$, and its value will be invariable except in the extremes. For $\alpha = 0$ the input will be $\boldsymbol{u}(kT+T)$, and for $\alpha = T$ the input results $\boldsymbol{u}(kT)$. Then according to (4.7), in the interval $t \in [kT, (k+1)T]$ the sample-and-hold circuit will give an output $\boldsymbol{u}(t) = \boldsymbol{r}(k) - \mathbf{F}\boldsymbol{x}(k-d)$. This being said, the term in (4.11) can be updated to $\int_0^T e^{\mathbf{A}\alpha}\mathbf{B}\big[\boldsymbol{r}[k] - \mathbf{F}\boldsymbol{x}[k-d]\big]d\alpha$, and (4.10) becomes,

$$x[k+1] = e^{\mathbf{A}T}x[k] + \left(\int_0^T e^{\mathbf{A}\alpha}d\alpha\right)\mathbf{B}\big[\boldsymbol{r}[k] - \mathbf{F}\boldsymbol{x}[k-d]\big] \tag{4.12}$$

Defining $\mathbf{A}_d \coloneqq e^{\mathbf{A}T}$ and $\mathbf{B}_d \coloneqq \left(\int_0^T e^{\mathbf{A}\alpha}d\alpha\right)\mathbf{B}$, the difference equation that represents the discretized system and includes delay in the measurements is,

$$\begin{aligned} \boldsymbol{x}[k+1] &= \mathbf{A}_{\boldsymbol{d}}\boldsymbol{x}[k] + \mathbf{B}_{\boldsymbol{d}}\big[\boldsymbol{r}[k] - \mathbf{F}\boldsymbol{x}[k-d]\big] \\ &= \mathbf{A}_{\boldsymbol{d}}\boldsymbol{x}[k] - \mathbf{B}_{\boldsymbol{d}}\mathbf{F}\boldsymbol{x}[k-d] + \mathbf{B}_{\boldsymbol{d}}\boldsymbol{r}[k] \end{aligned} \tag{4.13}$$

A closed solution for (4.13) can be found by expressing it at several discrete instants as follows,

$$k = 0;\ \boldsymbol{x}[1] = \mathbf{A}_{\boldsymbol{d}}\boldsymbol{x}[0] - \mathbf{B}_{\boldsymbol{d}}\mathbf{F}\boldsymbol{x}[-d] + \mathbf{B}_{\boldsymbol{d}}\boldsymbol{r}[0]$$

$$k=1;\ \boldsymbol{x}[2]=\mathbf{A}_{\boldsymbol{d}}\boldsymbol{x}[1]-\mathbf{B}_{\boldsymbol{d}}\mathbf{F}\boldsymbol{x}[1-d]+\mathbf{B}_{\boldsymbol{d}}\boldsymbol{r}[1]$$

$$=\mathbf{A}_{\boldsymbol{d}}^{2}\boldsymbol{x}[0]-\mathbf{A}_{d}\mathbf{B}_{d}\mathbf{F}\boldsymbol{x}[-d]-\mathbf{B}_{d}\mathbf{F}\boldsymbol{x}[1-d]+\mathbf{A}_{d}\mathbf{B}_{d}\boldsymbol{r}[0]+\mathbf{B}_{\boldsymbol{d}}\boldsymbol{r}[1]$$

$$k=2;\ \boldsymbol{x}[3]=\mathbf{A}_{\boldsymbol{d}}\boldsymbol{x}[2]-\mathbf{B}_{\boldsymbol{d}}\mathbf{F}\boldsymbol{x}[2-d]+\mathbf{B}_{\boldsymbol{d}}\boldsymbol{r}[2]$$

$$=\mathbf{A}_{\boldsymbol{d}}^{3}\boldsymbol{x}[0]-\mathbf{A}_{d}^{2}\mathbf{B}_{d}\mathbf{F}\boldsymbol{x}[-d]-\mathbf{A}_{d}\mathbf{B}_{d}\mathbf{F}\boldsymbol{x}[1-d]-\mathbf{B}_{d}\mathbf{F}\boldsymbol{x}[2-d]+\mathbf{A}_{d}^{2}\mathbf{B}_{d}\boldsymbol{r}[0]+\mathbf{A}_{d}\mathbf{B}_{d}\boldsymbol{r}[1]+\mathbf{B}_{\boldsymbol{d}}\boldsymbol{r}[2]$$

Then the closed solution of (4.13) is,

$$\boldsymbol{x}[k]=\mathbf{A}_{d}^{k}\boldsymbol{x}[0]-\sum_{n=0}^{k-1}\left(\mathbf{A}_{d}^{k-1-n}\mathbf{B}_{d}\mathbf{F}\boldsymbol{x}[n-d]\right)+\sum_{m=0}^{k-1}\left(\mathbf{A}_{d}^{k-1-m}\mathbf{B}_{d}\boldsymbol{r}[m]\right) \tag{4.14}$$

Appendix B includes the routine that was implemented to compute the effect of latency in the state vector. It introduces a small disturbance to machine shafts in order to excite the system to small signal conditions, then the effect of latency is measured by simulating 20 seconds and determining at what delay the system becomes unstable. As an approximation, variations in delay were done in steps of one sample period, going from 1 to 20 sampling periods, each one equal to 33.3 milliseconds, obtained at a sampling rate of 30 frames per second. The stability assessment was done by Prony analysis, as it is described in Subsection 4.4.2.

Each of the 39 operating conditions of Table 4-2 combined with the contingencies of Table 4-3, excluding the ones that produced non sustainable islands, generated 1248 cases that were tested for latency with every feedback gain of Table 4-4. A representative part of these results are compiled in Table 4-8, where only those cases that have an exclusive gain were considered, totalizing 144 combinations. These results reveal that when the applied gain is precisely the one designed for a specific operation point, then the tolerance to latency is greater than 433 milliseconds, but if a particular case is associated with some other gain then the system can handle latencies of 133 milliseconds in the worst case. In addition some combinations Case-Gain result in unstable behavior; these situations are expected to be avoided by recommendation of the decision tree-based scheme of Subsection 4.2.

In [106] it is found that the expected transmission delay is around 20ms between local PMUs and regional PDCs, and 40ms between PDCs and Super PDCs, totalizing an expected latency of 60ms for the measurement path. Similarly, [106] reports that time-critical applications require a maximum delay of 50ms to send control commands from control centers to substations. When this is considered it is expected that a total delay of 110ms can be expected in a wide area measurement and control system, and therefore the 133ms limit found in this simulations can easily be handled in real implementation.

In this sense, the results of this section are also useful to assess the applicability of the centralized control scheme in cases where measured latency is available. In the event that measured time data transmission delay exceeds the limits of Table 4-8, a suggested alternative to avoid latency-related instability would be to withdraw problematic gains from the controller. For instance, it can be verified in

Table 4-8 that Gain 3 consistently leads to low tolerance to latency in comparison with other gains, and therefore it would be a good candidate for elimination.

Table 4-8 Results of the latency test on all combinations of Case and Feedback Gain.

Case	Gain	Latency [ms]	Case	Gain	Latency [ms]	Case	Gain	Latency [ms]	Case	Gain	Latency [ms]
1	1	500	4	1	>667	7	1	>667	10	1	600
1	2	433	4	2	433	7	2	433	10	2	167
1	3	167	4	3	133	7	3	200	10	3	433
1	4	467	4	4	467	7	4	>667	10	4	>667
1	5	>667	4	5	>667	7	5	>667	10	5	Unstable
1	6	467	4	6	467	7	6	467	10	6	>667
1	7	467	4	7	467	7	7	467	10	7	Unstable
1	8	467	4	8	467	7	8	467	10	8	467
1	9	467	4	9	467	7	9	467	10	9	500
1	10	267	4	10	267	7	10	200	10	10	467
1	11	467	4	11	500	7	11	467	10	11	Unstable
1	12	500	4	12	467	7	12	>667	10	12	>667
2	1	467	5	1	>667	8	1	500	11	1	>667
2	2	433	5	2	433	8	2	467	11	2	433
2	3	167	5	3	167	8	3	167	11	3	167
2	4	467	5	4	467	8	4	467	11	4	>667
2	5	>667	5	5	>667	8	5	>667	11	5	667
2	6	467	5	6	467	8	6	467	11	6	500
2	7	467	5	7	467	8	7	467	11	7	467
2	8	433	5	8	467	8	8	467	11	8	433
2	9	467	5	9	467	8	9	467	11	9	467
2	10	200	5	10	333	8	10	233	11	10	Unstable
2	11	467	5	11	500	8	11	467	11	11	467
2	12	>667	5	12	>667	8	12	>667	11	12	>667
3	1	>667	6	1	500	9	1	>667	12	1	>667
3	2	433	6	2	433	9	2	433	12	2	433
3	3	433	6	3	167	9	3	467	12	3	133
3	4	>667	6	4	467	9	4	>667	12	4	467
3	5	>667	6	5	>667	9	5	>667	12	5	>667
3	6	467	6	6	467	9	6	>667	12	6	467
3	7	467	6	7	467	9	7	>667	12	7	467
3	8	467	6	8	467	9	8	467	12	8	467
3	9	467	6	9	467	9	9	467	12	9	467
3	10	200	6	10	267	9	10	200	12	10	267
3	11	467	6	11	467	9	11	467	12	11	467
3	12	>667	6	12	>667	9	12	>667	12	12	>667

CHAPTER 5 Conclusions and Future Work

Small signal oscillations in power systems are constantly present, as a consequence of the random natural excitation that originates from load movements followed by generation reactions, reconfiguration of transmission network, and disturbances affecting the system. Since this phenomenon cannot be eliminated, the best approach power engineers can take is to introduce damping to those modes that compromise the system's operation and integrity.

Nowadays this task is performed to a great extent by the use of power system stabilizers that are installed on specific generation plants, and tuned to tackle particular oscillation modes. The fact that the constituting filters of the stabilizer need to be adjusted for the frequency of interest, and that this oscillation frequency is not always the same for all operation scenarios, lead to the inconvenience of having PSSs with wrong parameters that put the system in risk of even worse oscillation problems than without PSSs. This is particularly true when the system experience conditions with notable deviations from the ones for which the PSS tuning was realized.

Another approach available to the power system industry to deal with small signal oscillations, is the use of supplementary control signals in HVDC transmission lines and in FACTS devices for series or shunt compensation. Although these lines of attack are effective, they are likely to remain of limited application since these elements are neither abundant nor economically accessible for most utilities, and for that reason they are only installed in cases of even more constraining restrictions to system's operation such as weak reactive power support, high variability of reactive power flows, or in the case of HVDC lines, economic benefits of interconnecting areas.

The centralized control scheme of power system stabilizers presented in this dissertation is based on the use of PSSs which are massively present in power systems and are affordable to any utility. These devices are proposed to be slightly modified to be able to receive an external control input without tampering with the current parameter values. This has been thought in consideration of two reasons: 1) The traditional reluctance of utilities to make modifications in the system unless indispensable, and 2) As a security measure that would increase confidence of utilities and operators, knowing that the system cannot be deteriorated if just the central controller was disabled in case of malfunction.

The current growing trend of WAMS has increased the possibility of centralized control implementation. The work done for this dissertation rests on the availability of PMU measurements at all generation plants in the system, and on the existence of a commensurate fiber optic communications network to transport feedback signals to the location of the central controller, and from the controller to all PSSs in the system.

Power system stabilizers are not generally equipped to receive external signals, other than rotor speed, line currents and voltages, or other synthesized products of these fundamental signals; therefore their action in increasing damping of small signal oscillations is limited to a specific frequency provided by the visibility they have of a single point of measurement. This dissertation presents an approach to adapt existing PSSs to receive a general purpose control signal, which can be used similarly to the control ports found in FACTS. This study demonstrates the implications of this new input on mathematical models, and the control functionality that is made available by its incorporation to stabilizers.

Readiness of dependable control, analysis, and design tools has facilitated the proposed design. The control actions are generated by robust state feedback. A series of representative operation points is selected such that a specialized gain is designed for each, ensuring beneficial pole displacement for damping increasing. Robustness of the centralized controller is accounted for by an enumeration gain scheduling methodology that is coordinated by decision trees. The results show that the accuracy of this decision approach implemented on the example Central American System model will be higher than 93%.

The effect of time delay in the feedback loop was assessed by finding the maximum latency that can be tolerated before resulting in unstable control. The results show that in the worst cases, that correspond to improbable combinations of operating point and applied gain, the delay limit before the control loop becomes unstable is 133ms. However the delay expected for a wide area measurement and control system is 110ms, and therefore data transmission delay is not expected to be an issue in real implementation. The determination of this limit was done by dynamic simulation, with an approximate assessment of stability by means of the Prony method.

Contributions

The main contributions of this dissertation are:

- A simple, efficient, and dependable methodology for robust centralized control of small signal oscillations that imposes much less computational burden than other nonlinear design approaches, making it a promising candidate for actual implementation by utilities and system operators.
- A detail description and recommendation of the way power system stabilizers can be modified to be included in external control tasks with minimum intrusion. This approach enables power system stabilizers to overcome their inherent limitation to act only on the basis of local measurements to damp a single target frequency. This study demonstrates the implications of this new input on mathematical models, and the control functionality that is made available by its incorporation to conventional stabilizers.
- A heuristic dynamic reduction methodology that preserves a physical equivalent model that can be interpreted by any commercial software package. The steps of this method are general, versatile, and of easy adaptation to any particular power system model, with the aggregated value of producing a physical model as final result, that makes the approach appealing for industry. The accuracy of the resulting reduced network has been demonstrated with the model of the Central American System.

Future Work

The completion of some additional tasks is required before the proposed centralized controller can be implemented in a real system. The following points fell beyond the scope of this dissertation due to time constraints:

- Development of a dynamic state observer to estimate non-measured state variables from available PMU measurements. This study assumed the availability of all the states pertaining to generators and their control systems. This assumption is considered only an initial step to verify the viability of the centralized control, but it is understood that in practice it is not yet possible to count with direct measurement of all the system's dynamic states; a full order state observer is an indispensable element to consider.
- Assessment of the latency effect on the performance of the centralized controller with dynamic state estimation. The latency effects on the controller have been studied when perfect measurement of all the system's states is taken for granted, however it remains the question of the repercussions of what can be seen as measurement imperfections introduced by a full order state observer.
- Study how the proximity of the actual operation point to the representative operation point, is correlated to the tolerance to latency. Determining if the tolerance to latency is correlated to the distance to the representative points would be of importance to decide if this metric should be considered for gain selection.
- Study how the latency tolerance results on all combinations of Case and Feedback Gain, can be used in the centralized controller to aid in the decision of the feedback gain to apply.
- Expansion of the range of operation conditions used to train the classification tools, including planned scenarios, a wide variety of system configurations, contingencies and power transfers. In this study the number of operation conditions and contingencies was considered to be broad enough to reflect the variety of conditions expected in real situations, nevertheless in a more detailed study for practical implementation it would be advisable to reevaluate the extent of case combinations to analyze, in order to account for all possibilities in the studied system.
- Study on the selection of operation points for which feedback gains will be designed. In this study, a set of representative operation points was defined based on the location of the eigenvalue exhibiting the lowest damping factor for the complete span of operation points. The reflection of the selected operation points on the eigenvalue with the second lowest damping factor was observed, but not considered for point selection. In further study, the span of more eigenvalues can be considered in order to have a more solid base to decide on the representative operation points.
- Consideration of alternative data mining tools for classification. Although decision trees produced good results and accuracy for case classification, it would be interesting and possibly beneficial to improve accuracy, to rehearse the classification tasks with random forests, since these have been reported to give good results in other power systems applications [107].

Bibliography

[1] P. Pourbeik, P. Kundur and C. W. Taylor, "The Anatomy of a Power Grid Blackout," *IEEE Power and Energy Magazine,* vol. September/October, pp. 22-29, 2006.

[2] J. DeLaRee, V. Centeno, J. S. Thorp and A. G. Phadke, "Synchronized Phasor Measurement Applications in Power Systems," *IEEE TRansactions on Smart Grid,* vol. 1, no. 1, 2010.

[3] G. T. Heydt, C. C. Liu, A. G. Phadke and V. Vittal, "Solutions for the Crisis in Electric Power Supply," *IEEE Computer Applications in Power,* 2001.

[4] D. J. Hill and I. A. Hiskens, "Robust, Adaptive or Nonlinear Control for Modern Power Systems," in *Proceedings of the 32nd Conference on Dcesion and Control*, San Antonio, Texas, 1993.

[5] L. Fan, "Review of Robust Feedback Control Applications in Power Systems," in *Proceedings of the IEEE PES Power Systems Conference and Exhibition*, Seattle, Washington, 2009.

[6] M. E. Aboul-Ela, A. A. Sallam, J. D. McCalley and A. A. Fouad, "Damping Controller Design for Power System Oscillations using Global Signals," *IEEE Transactions on Power Systems,* vol. 11, no. 2, pp. 767-773, 1996.

[7] A. Heniche, H. Bourles and M. P. Houry, "A Desensitized Controller for Voltage Regulation of Power Systems," *IEEE Transactions on Power Systems,* vol. 10, pp. 1461-1466, 1995.

[8] H. Bourles and A. Heniche, "The Inverse LQR problem and its Application to the Analysis of a Robust Coordinated AVR/PSS," in *Proceedings of the 12th Power Systems and Computers Conference*, Dresden, Germany, 1996.

[9] R. A. Elices, H. Bourles and T. Margotin, "Design of Robust Controllers for Damping Inter-area Oscillations: Application to the European Power System," *IEEE Transactions on Power Systems,* vol. 19, no. 2, pp. 1058-1067, 2004.

[10] J. Chang and J. H. Chow, "Time-Optimal Series Capacitor Control for Damping Interarea Modes in Interconnected Power Systems," *IEEE Transactions on Power Systems,* vol. 12, no. 1, pp. 215-221, 1997.

[11] J. Sanchez-Gasca, "Coordinated Control of Two FACS Devices for Damping Interarea Oscillations," *IEEE Transactions on Power Systems,* vol. 13, no. 2, pp. 428-434, 1998.

[12] G. Li, T. Lie, G. Shrestha and K. Lo, "Implementation of Coordinated FACTS Controllers for Damping

Oscillations," *Electrical Power and Energy Systems,* vol. 22, pp. 79-92, 1999.

[13] C. Balarko, R. Majumder and B. Pal, "Application of Multiple-Model Adaptive Control Strategy for Robust Damping of Interarea Oscillations in Power System," *IEEE Transactions on Control Systems Technology,* vol. 12, no. 5, pp. 727-736, 2004.

[14] J. Wang, F. Chuang and Z. Yao, "Design of WAMS-Based Multiple HVDC Damping Control System," *IEEE Transactions on Smart Grid,* vol. 2, no. 2, pp. 363-373, 2011.

[15] A. Pal and J. S. Thorp, "Co-ordinated Control of Interarea Oscillations using SMA and LMI," in *IEEE PES Innovative Smart Grid Technologies*, Washington DC, 2012.

[16] K. Vance, *Robust Control for Interarea Oscillations,* University Libraries, Virginia Polytechnic Institute and State University, 2011.

[17] J. Ma, S. Garlapati and J. S. Thorp, "Robust Wide Area Measurement System-Based Control of Interarea Oscillations," *Electric Power Components and Systems,* vol. 39, pp. 850-862, 2011.

[18] A. Chakrabortty, "Wide-Area Damping Control of Power Systems using Dynamic Clustering and TCSC-Based Redesigns," *IEEE Transactions on Smart Grid,* vol. 3, no. 3, pp. 1503-1513, 2012.

[19] M. Maghsoud, F. Aminifar, D. Nazarpour and S. Golshannavaz, "Wide-Area Power Oscillation Damping with a Fuzzy Controller Compensating the Coninuous Communication Delays," *IEEE Transactions on Power Systems,* vol. 28, no. 2, pp. 1997-2005, 2013.

[20] P. Robin, J. Milanovic, A. Almutairi and O. Marjanovic, "Damping of Interarea Oscillations in Mixed AC/DC Networks using WAMS Based Supplementary Controller," *IEEE Transactions on Power Systems,* vol. 28, no. 2, pp. 1160-1169, 2013.

[21] E. Gholipour and G. H. Isazadeh, "Design of a New Adaptive Wide Area IPFC Damping Controller in Iran Transmission Network," *Electric Power and Energy Systems,* vol. 53, pp. 529-539, 2013.

[22] H. Ni, G. T. Heydt and L. Mili, "Power System Stability Agents using Robust Wide Area Control," *IEEE Transactions on Power Systems,* vol. 17, no. 4, pp. 1123-1131, 2002.

[23] H. Wu, Q. Wang and X. Li, "PMU-Based Wide Area Damping Control of Power Systems," in *Joint International Conference on Power System Technology*, New Delhi, India, 2008.

[24] J. Ma, T. Wang, Z. Wang and J. Thorp, "Adaptive Damping Control of Interarea Oscillations Based on Federated Kalman Filter using Wide Area Signals," *IEEE Transactions on Power Systems,* vol. 28, no. 2, pp. 1627-1635, 2013.

[25] S. Kamalasadan and G. D. Swann, "A Novel System-Centric Intelligent Adaptive Control

Architecture for Damping Interarea Mode Oscillations in Power System," *IEEE Transactions on Industry Applications,* vol. 47, no. 3, pp. 1487-1497, 2011.

[26] J. Zhang, C. Y. Chung, S. Zhang and Y. Han, "Practical Wide Area Damping Controller Design Based on Ambient Signal Analysis," *IEEE Transactions on Power Systems,* vol. 28, no. 2, pp. 1687-1696, 2013.

[27] D. P. Ke and C. Y. Chung, "An Inter-Area Mode Oriented Pole-Shifting Method With Coordination of Control Efforts for Robust Tuning of Power Oscillation Damping Controllers," *IEEE Transactions on Power Systems,* vol. 27, no. 3, pp. 1422-1432, 2012.

[28] X. Xie, J. Xiao, C. Lu and Y. Han, "Wide-area stability control for damping interarea oscillations of interconnected power systems," *IEE Proceedings of Generation, Transmission and Distribution,* vol. 153, no. 5, pp. 507-514, 2006.

[29] Y. Zhang and A. Bose, "Design of Wide-Area Damping Controllers for Interarea Oscillations," *IEEE Transactions on Power System,* vol. 23, no. 3, pp. 1136-1143, 2008.

[30] R. Majumder, B. Chaudhuri and B. C. Pal, "Implementation and test results of a wide-area measurement-based controller for damping interarea oscillations considering signal-transmission delay," *IET Generation, Transmission&Distribution,* vol. 1, no. 1, pp. 1-7, 2007.

[31] G. L. Yu, B. H. Zhang, H. Xie and C. G. Wang, "Wide-Area Measurement-Based Nonlinear Robust Control of Power System Considering Signals' Delay and Incompleteness," in *IEEE Power Engineering Society General Meeting*, Tampa, Florida, 2007.

[32] H. Wu, H. Ni and G. Heydt, "The Impact of Time Delay on Robust Control Design in Power Systems," in *IEEE Power Engineering Society Winter Meeting*, Tempe, Arizona, 2002.

[33] L. Qi, L. W. Qian, S. Woodroff and D. Cartes, "Prony Analysis for Power System Harmonics," *EURASIP Journal onAdvances in Signal Processing,* vol. 2007, no. 1, pp. 1-13, 2007.

[34] A. Bracale, P. Caramia and G. Carpinelli, "Adaptive Prony Method for Waveform Distortion Detection in Power Systems," *International Journal of Electrical Power and Energy Systems,* vol. 29, no. 5, pp. 371-379, 2007.

[35] S. R. Nam, D. G. Lee, S. H. Kang, S. J. Ahn and J. H. Choi, "Fundamental Frequency Estimation in Power Systems using Complex Prony Analysis," *Journal of Electrical Engineering and Technology,* vol. 6, no. 2, pp. 154-160, 2011.

[36] S. Dunlap and M. M. Begovic, "State Tracking in Power Systems using DFT-Prony's Method," in *IEEE International Symposium on Circuits and Systems*, Chicago, IL, 1993.

[37] S. Vemuri and B. H. Chowdhury, "Performance Improvement of Power System Stabilizers using Prony Analysis," *International Journal of Power and Energy Systems,* vol. 28, no. 2, pp. 177-185, 2008.

[38] L. Wuxing, H. Kang, H. Kang and Y. Liangzhong, "Detection of Power System Oscillation using Moving Window Prony Method," in *International Conference on Power System Technology*, Hangzhou, China, 2010.

[39] J. DeLaOserna, "Synchrophasor Estimation Using Prony's Method," *IEEE Transactions on Instrumentation and Measurement,* vol. 62, no. 8, pp. 2119-2128, 2013.

[40] C. E. Grund, J. J. Parseba, J. F. Hauer and S. L. Nilsson, "Comparison of Prony and Eigenanalysis for Power System Control Design," *IEEE Transactions on Power Systems,* vol. 8, no. 3, pp. 964-971, 1993.

[41] C.-I. Cheng and G. W. Chang, "An Efficient Prony-Based Solution Procedure for Tracking of Power System Voltage Variations," *IEEE Transactions on Industrial Electronics,* vol. 60, no. 7, pp. 2681-2688, 2013.

[42] J. Qi, Q.-Y. Jiang and Y.-J. Cao, "General Prony Identification Algorithm for Power System Transfer Function," *Proceedings of the Chinese Society of Electrical Engineering,* vol. 28, no. 28, pp. 41-46, 2008.

[43] F. Solomonese, C. Barbulescu, S. Kilyeni and M. Litcantu, "Genetic Algorithms. Power System Applications," in *6th International Conference on Human System Interactions (HSI)*, Sopot, Poland, 2013.

[44] B. Sahu, A. Lall, S. Das, P. Kumar and T. Manoj, "Economic Load Dispatch in Power System using Genetic Algorithm," *International Journal of Computer Applications,* vol. 67, no. 7, 2013.

[45] J. Yao, Y.-J. Fang and Q. Li, "Multi-objective Genetic Algorithm for Power System Economic Load Dispatch," *East China Electric Power,* vol. 40, no. 4, pp. 648-651, 2012.

[46] U. Kilic, K. Ayan and U. Arifoglu, "Optimizing reactive power flow of HVDC systems using genetic algorithm," *International Journal of Electrical Power and Energy Systems,* vol. 55, no. 1, pp. 1-12, 2014.

[47] K. Nara, "Genetic Algorithm for Power Systems Planning," *IEE Conference Publications,* pp. 60-65, 1998.

[48] B. Liu, X. Lai, X.-Q. Kong, K.-W. Liu and Q.-R. Liu, "Application of Genetic Catastrophic Algorithm to Power Distribution System Reconfiguration," *Proceedings of the CSU-EPSA,* vol. 25, no. 2, pp. 31-35, 2013.

[49] A. Gupta and P. R. Sharma, "Optimization of Power System Performance Using Real Parameter Genetic Algorithm," *International Journal of Artificial Intelligence & Knowledge Discovery,* vol. 3, no. 3, pp. 16-22, 2013.

[50] Y. L. Abdel-Magid, M. A. Abido, S. Al-Biyat and A. H. Mantawi, "Simultaneous Stabilization of Multimachine Power Systems Via Genetic Algorithms," *IEEE Transactions on Power Systems,* vol. 14, no. 4, pp. 1428-1439, 1999.

[51] F. Shoorangis, M. Nikzad, M. Tabar, M. Naraghi and A. Javandian, "Multi-machine power system stabilizer adjustment using genetic algorithms," *Indian Journal of Science and Technology,* vol. 4, no. 4, 2011.

[52] A. Al-Hinai, "Dynamic stability enhancement using Genetic Algorithm Power System Stabilizer," in *International Conference on Power System Technology*, Hangzou, China, 2010.

[53] E. Bernabeu, *Methodology for a Security-Dependability Adaptive Protection Scheme Based on Data Mining,* Blacksburg, Virginia: University Libraries, Virginia Polytechnic Institute and State University, 2009.

[54] L. Wehenkel and M. Pavella, "Decision Tree Approach to Power Systems Security Assessment," *International Journal of Electrical Power and Energy Systems,* vol. 15, no. 1, pp. 13-36, 1993.

[55] V. Krishnan, J. McCalley, M. Henry and S. Issad, "Efficient Database Generation for Decision Tree Based Power System Security Assessment," *IEEE Transactions on Power Systems,* vol. 3, no. 4, pp. 2319-2327, 2011.

[56] Y. Xu, Z. Y. Dong, R. Zhang and K. P. Wong, "A Decision Tree-Based on-Line Preventive Control Strategy for Power System Transient Instability Prevention," *International Journal of Systems Science,* vol. 45, no. 2, pp. 176-186, 2014.

[57] Z. Rather, C. Liu, Z. Chen, C. Bak and P. Thogersen, "Dynamic Security Assessment of Danish Power System Based on Decision Trees: Today and Tomorrow," in *IEEE Grenoble Conference*, Grenoble, France, 2013.

[58] R. Sun, Z. Wu and V. A. Centeno, "Power system islanding detection & identification using topology approach and decision tree," in *IEEE Power and Energy Society General Meeting*, San Diego, California, 2011.

[59] P. Srikanth and A. Chandel, "Inverse S-Transform Based Decision Tree for Power System Faults Identification," *Telkomnica,* vol. 9, no. 1, pp. 99-106, 2011.

[60] P. Ray, S. Mohanty, N. Kishor and J. Catalao, "Optimal Feature and Decision Tree-Based Classification of Power Quality Disturbances in Distributed Generation Systems," *IEEE Transactions*

on Sustainable Energy, vol. 5, no. 1, pp. 200-208, 2014.

[61] A. Pal, J. S. Thorp, T. Khan and S. Young, "Classification Trees for Complex Synchrophasor Data," *Electric Power Components and Systems,* vol. 41, no. 14, pp. 1381-1396, 2013.

[62] E. Lobato, A. Ugedo, R. Rouco and F. M. Echavarren, "Decision Trees Applied to Spanish Power Systems Applications," in *International Conference on Probabilistic Methods Applied to Power Systems*, Stockolm, Sweden, 2006.

[63] A. M. Stankovic, A. T. Saric and M. Milosevic, "Identification of Nonparametric Dynamic Power System Equivalents with Artificial Neural Networks," *IEEE Transactions on Power Systems,* vol. 18, no. 4, pp. 1478-1486, 2003.

[64] L. Wang, M. Klein, S. Yirga and P. Kundur, "Dynamic Reduction of Large Power Systems for Stability Studies," *IEEE Transactions on Power Systems,* vol. 12, no. 2, pp. 889-895, 1997.

[65] J. S. Lawler and R. A. Schlueter, "Computational Algorithms for Constructing Modal-Coherent Dynamic Equivalents," *IEEE Transactions on Power Apparatus and Systems,* Vols. PAS-101, no. 5, pp. 1070-1080, 1982.

[66] W. W. Price, A. W. Hargrave, B. J. Hurysz, J. H. Chow and P. M. Hirsch, "Large Scale System Testing of a Power System Dynamic Equivalencing Program," *IEEE Transactions on Power Systems,* vol. 13, no. 3, pp. 768-774, 1998.

[67] J. J. Sánchez-Gasca and J. H. Chow, "Power System Reduction to Simplify the Design of Damping Controllers for Interarea Oscillations," *IEEE Transactions on Power Systems,* vol. 11, no. 3, pp. 1342-1349, 1996.

[68] A. Chang and M. Adibi, "Power System Dynamic Equivalents," *IEEE Transactions on Power Apparatus and Systems,* Vols. PAS-89, no. 8, pp. 1739-1744, 1970.

[69] S. Lee and F. Schweppe, "Distance Measures and Coherency Recognition for Transient Stability Equivalents," *IEEE Transactions on Power Apparatus and Systems,* Vols. PAS-92, no. 5, pp. 1550-1557, 1973.

[70] J. M. Ramírez and R. G. Valle, "A Technique to Reduce Power Systems Electromechanical Models," *IEEE Transactions on Energy Conversion,* vol. 19, no. 2, pp. 456-458, 2004.

[71] Y.-N. Yu and M. El-Sharkawi, "Estimation of External Dynamic Equivalents of a Thirteen Machine System," *IEEE Transactions on Power Apparatus and Systems,* Vols. PAS-100, no. 3, pp. 1324-1332, 1981.

[72] H. Rudnick, R. Patino and A. Brameller, "Power System Dynamic Equivalents: Coherency

Recognition via the Rate of Change of Kinetic Energy," *IEE Proceedings,* vol. 128, no. 6, pp. 325-333, 1981.

[73] J. L. Sancha and I. J. Perez-Arriaga, "Selective Modal Analysis of Power System Oscillatory Instability," *IEEE Transactions on Power Systems,* vol. 3, no. 2, pp. 429-438, 1988.

[74] P. Kundur, Power System Stability and Control, McGraw Hill, 1994.

[75] W. G. Heffron and R. A. Phillips, "Effect of Modern Amplidyne Voltage Regulators on Underexcited Operation of Large Turbine Generators," *Transactions of the American Institute of Electrical Engineers.,* 1952.

[76] F. P. DeMello and C. Concordia, "Concepts of Synchronous Machine Stability as Affected by Excitation Control," *IEEE Transactions on Power Apparatus and Systems,* 1969.

[77] C.-T. Chen, Linear System Theory and Design, Oxford University Press, 1999.

[78] W. J. Rough, Linear System Theory, Upper Saddle River: Prentice Hall, 1996.

[79] J. Kautski, N. K. Nichols and P. Van Doren, "Robust Pole Assignment in Linear State Feedback," *International Journal of Control,* 1985.

[80] J. H. Holland, Adaptation in Natural and Artificial Systems, Cambridge, MA: The MIT Press, 1992.

[81] M. Gestal and D. Rivero, Introducción a los Algoritmos Genéticos y a la Programación Genética, Universidade Da Coruña, 2010.

[82] T. Blickle and L. Thiele, "A Comparison of Selection Schemes used in Genetic Algorithms," Computer Engineering and Communication Network Lab (TIK), Zurich, 1995.

[83] The Mathworks, "Genetic Algorithm and Direct Search Toolbox," The MathWorks, Inc., Natick, MA, 2004.

[84] J. F. Hauer, C. L. Demeure and L. L. Scharf, "Initial Results in Prony Analysis of Power System Response Signals," *IEEE Transactions on Power Systems,* vol. 5, no. 1, 1990.

[85] S. L. Marple, Digital Spectral Analysis: With Applications, Englewood Clifs: Prentice Hall, 1987.

[86] A. Oppenheim and A. Willsky, Signals and Systems, Upper Saddle River: Prentice Hall, 1997.

[87] C. G. Verghese, I. J. Perez-Arriaga and F. C. Schweppe, "Selective Modal Analysis with Application to Electric Power Systems," *IEEE Transactions,* Vols. PAS-101, no. 9, pp. 3117-3134, 1982.

[88] J. Chow and G. Rogers, Power System Toolbox Version 3.0, Colborne, Ontario, 2008.

[89] M. Bramer, Principles of Data Minig, London: Springer-Verlag, 2007.

[90] J. R. Quinlan, "Induction of Decision Trees," *Machine Learning,* vol. 1, pp. 81-106, 1986.

[91] J. Mingers, "An Empirical Comparison of Pruning Methods for Decision Tree Induction," *Machine Learning,* vol. 4, pp. 227-243, 1989.

[92] B. Pal and B. Chaudhuri, Robust Control in Power Systems, Springer, 2005.

[93] P. W. Sauer and M. A. Pai, Power System Dynamics and Stability, Prentice Hall, Pearson Education, 1998.

[94] "Program Operation Manual. PSS/E-29," Power Technologies, Inc., 2002.

[95] G. Rogers, Power System Oscillations, Kluwer, 2000.

[96] "IEEE Committee Report: Excitation System Models for Power System Stability Studies," *IEEE Transactions on Power Apparatus and Systems,* Vols. PAS-100, no. No. 2, 1981.

[97] Ente Operador Regional, "Identificación de la Red de Transmisión Regional para el Año 2011," San Salvador, 2010.

[98] Ente Operador Regional, "Ente Operador Regional," 2014. [Online]. Available: http://www.enteoperador.org/. [Accessed 28 January 2014].

[99] Grupo Técnico de Seguridad Operativa. Ente Operador Regional., «Estudio de Seguridad Operativa: Máximas Transferencias de Potencia en el Sistema Eléctrico Regional. Época Seca, 2007.,» San Salvador, 2007.

[100] W. Rough and J. Shamma, "Research on Gain Scheduling," *Automatica,* vol. 36, pp. 1401-1425, 2000.

[101] M. Crow, Computational Methods for Electric Power Systems, Boca Raton: CRC Press, 2010.

[102] Matlab Statistics Toolbox. User's Guide, Natick, MA: MathWorks, 2013.

[103] A. Pal, G. Sanchez-Ayala, V. A. Centeno and J. S. Thorp, "A PMU Placement Scheme Ensuring Real-Time Monitoring of Critical Buses of the Network," *IEEE Transactions on Power Delivery,* 2013.

[104] G. Sanchez-Ayala, A. Pal, V. A. Centeno and W. C. Flores, "PMU Placement for the Central American Power Network and its Possible Impacts," in *ISGT-LA*, Medellin, 2012.

[105] Galina Antonova, "Guide for Phasor Data Concentrator Requirements for Power System Protecton, Control, and Monitoring," IEEE, 2011.

[106] Y. Deng, H. Lin, A. Phadke, S. Shukla, J. Thorp and L. Mili, "Communication Network Modeling and Simulation for Wide Area Measurement Applications," in *Innovative Smart Grid Technologies (ISGT)*, Washington, DC, 2012.

[107] N. Badayos, Machine Learning-Based Parameter Validation, Blacksburg: Virginia Tech. PhD Dissertation, 2014.

APPENDIX A

Information of Studied Systems

A.1 New England – New York System

Generator data:

Bus Number	MW	Base MVA	X Source (pu)	T'do	T"do	T'qo	T"qo	H	D
1	250	300	0.025	12.6	0.045	0.035	0.035	3.4	0
2	545	800	0.05	6.56	0.05	1.5	0.035	4.9494	0
3	650	800	0.045	5.7	0.05	1.5	0.035	4.9623	0
4	632	800	0.035	5.69	0.05	1.5	0.035	4.1629	0
5	505	700	0.05	5.4	0.05	0.44	0.035	4.7667	0
6	700	900	0.04	7.3	0.05	0.4	0.035	4.9107	0
7	560	800	0.04	5.66	0.05	1.5	0.035	4.3267	0
8	540	800	0.045	6.7	0.05	0.41	0.035	3.915	0
9	800	1000	0.045	4.79	0.05	1.96	0.035	4.0365	0
10	500	1200	0.04	9.37	0.05	1.5	0.035	2.9106	0
11	1000	1600	0.012	4.1	0.05	1.5	0.035	2.0053	0
12	1350	1900	0.025	7.4	0.05	1.5	0.035	5.1791	0
13	3591.6	12000	0.004	5.9	0.05	1.5	0.035	4.0782	8
14	1785	10000	0.0023	4.1	0.05	1.5	0.035	3	3
15	1000	10000	0.0023	4.1	0.05	1.5	0.035	3	6
16	4000	11000	0.0055	7.8	0.05	1.5	0.035	4.45	8.9

Bus Number	Xd	Xq	X'd	X'q	X"d	Xl	S(1.0)	S(1.2)
1	0.969	0.6	0.248	0.25	0.147	0.003	0.0654	0.5743
2	1.8	1.7207	0.42529	0.3661	0.30508	0.035	0.0654	0.5743
3	1.8	1.7098	0.38309	0.36072	0.32465	0.0304	0.0654	0.5743
4	1.8	1.7725	0.29954	0.27481	0.24046	0.0295	0.0654	0.5743
5	1.8	1.6909	0.36	0.32727	0.27273	0.027	0.0654	0.5743
6	1.8	1.7079	0.35433	0.3189	0.28346	0.0224	0.0654	0.5743
7	1.8	1.7817	0.29898	0.27458	0.24407	0.0322	0.0654	0.5743
8	1.8	1.7379	0.35379	0.31034	0.27931	0.028	0.0654	0.5743
9	1.8	1.7521	0.48718	0.42735	0.38462	0.0298	0.0654	0.5743
10	1.8	1.2249	0.48675	0.47929	0.42604	0.0199	0.0654	0.5743
11	1.8	1.7297	0.25312	0.21094	0.16875	0.0103	0.0654	0.5743
12	1.8	1.6931	0.55248	0.49901	0.44554	0.022	0.0654	0.5743
13	1.8	1.7392	0.33446	0.30405	0.24324	0.003	0.0654	0.5743
14	1.8	1.73	0.285	0.25	0.23	0.0017	0.0654	0.5743
15	1.8	1.73	0.285	0.25	0.23	0.0017	0.0654	0.5743
16	1.8	1.6888	0.35899	0.30337	0.27809	0.0041	0.0654	0.5743

Load data:

Bus Number	MW	MVAR
17	6000	300
18	2470	123
20	680	103
21	274	115
23	248	85
24	309	-92
25	224	47
26	139	17
27	281	76
28	206	28
29	284	27
33	112	0
36	102	-19.46
39	267	12.6
40	65.63	23.53
41	1000	250
42	1150	250

Bus Number	MW	MVAR
44	267.55	4.84
45	208	21
46	150.7	28.5
47	203.12	32.59
48	241.2	2.2
49	164	29
50	100	-147
51	337	-122
52	158	30
53	252.7	118.56
55	322	2
56	500	184
59	234	84
60	522	177
61	104	125
64	9	88
67	320	153
68	329	32

Exciters: ESDC1A

Bus Number	TR	KA	TA	TB	TC	VRMAX	VRMIN	KE
1	0	30	0.02	0	0	10	-10	1
2	0	30	0.02	0	0	10	-10	1
3	0	30	0.02	0	0	10	-10	1
4	0	30	0.02	0	0	10	-10	1
5	0	30	0.02	0	0	10	-10	1
6	0	30	0.02	0	0	10	-10	1
7	0	30	0.02	0	0	10	-10	1
8	0	30	0.02	0	0	10	-10	1
9	0	30	0.02	0	0	10	-10	1
10	0	30	0.02	0	0	10	-10	1
11	0	30	0.02	0	0	10	-10	1
12	0	30	0.02	0	0	10	-10	1

Bus Number	TE	KF	TF1	0	E1	SE(E1)	E2	SE(E2)
1	0.785	0.03	1	0	3.9267	0.07	5.2356	0.91
2	0.785	0.03	1	0	3.9267	0.07	5.2356	0.91
3	0.785	0.03	1	0	3.9267	0.07	5.2356	0.91
4	0.785	0.03	1	0	3.9267	0.07	5.2356	0.91
5	0.785	0.03	1	0	3.9267	0.07	5.2356	0.91
6	0.785	0.03	1	0	3.9267	0.07	5.2356	0.91
7	0.785	0.03	1	0	3.9267	0.07	5.2356	0.91
8	0.785	0.03	1	0	3.9267	0.07	5.2356	0.91
9	0.785	0.03	1	0	3.9267	0.07	5.2356	0.91
10	0.785	0.03	1	0	3.9267	0.07	5.2356	0.91
11	0.785	0.03	1	0	3.9267	0.07	5.2356	0.91
12	0.785	0.03	1	0	3.9267	0.07	5.2356	0.91

Stabilizers: IEE2ST

IBUS	ICS1	ICS2	K1	K2	T1	T2	T3	T4
1	1	3	0	0	0	0	1000	10
2	1	3	0	0	0	0	1000	10
3	1	3	0	0	0	0	1000	10
4	1	3	0	0	0	0	1000	10
5	1	3	0	0	0	0	1000	10
6	1	3	0	0	0	0	1000	10
7	1	3	0	0	0	0	1000	10
8	1	3	0	0	0	0	1000	10
9	1	3	0	0	0	0	1000	10
10	1	3	0	0	0	0	1000	10
11	1	3	0	0	0	0	500	10
12	1	3	0	0	0	0	1100	10

IBUS	T5	T6	T7	T8	T9	T10	LSMAX	LSMIN
1	0.1	0.02	0.08	0.02	0	0	0.2	-0.05
2	0.08	0.02	0.08	0.02	0	0	0.2	-0.05
3	0.08	0.02	0.08	0.02	0	0	0.2	-0.05
4	0.08	0.02	0.08	0.02	0	0	0.2	-0.05
5	0.08	0.02	0.08	0.02	0	0	0.2	-0.05
6	0.1	0.02	0.1	0.02	0	0	0.2	-0.05
7	0.08	0.02	0.08	0.02	0	0	0.2	-0.05
8	0.08	0.02	0.08	0.02	0	0	0.2	-0.05
9	0.08	0.03	0.05	0.01	0	0	0.2	-0.05
10	0.1	0.02	0.1	0.02	0	0	0.2	-0.05
11	0.08	0.03	0.05	0.01	0	0	0.2	-0.05
12	0.1	0.02	0.1	0.02	0	0	0.2	-0.05

Line data:

From Bus	To Bus	Id	Line R (pu)	Line X (pu)	Charging (pu)
7	23	1	0.0005	0.0272	0
17	36	1	0.0005	0.0045	0.32
17	43	1	0.0005	0.0276	0
18	42	1	0.004	0.06	2.25
18	49	1	0.0076	0.1141	1.16
18	50	1	0.0012	0.0288	2.06
19	68	1	0.0016	0.0195	0.304
21	22	1	0.0008	0.014	0.2565
21	68	1	0.0008	0.0135	0.2548
22	23	1	0.0006	0.0096	0.1846
23	24	1	0.0022	0.035	0.361
24	68	1	0.0003	0.0059	0.068
25	26	1	0.0032	0.0323	0.531
25	54	1	0.007	0.0086	0.146
26	27	1	0.0014	0.0147	0.2396
26	28	1	0.0043	0.0474	0.7802
26	29	1	0.0057	0.0625	1.029
27	37	1	0.0013	0.0173	0.3216
28	29	1	0.0014	0.0151	0.249
30	31	1	0.0013	0.0187	0.333
30	32	1	0.0024	0.0288	0.488
30	53	1	0.0008	0.0074	0.48
30	61	1	0.0019	0.0183	0.29
30	61	2	0.0019	0.0183	0.29
31	38	1	0.0011	0.0147	0.247
31	53	1	0.0016	0.0163	0.25
32	33	1	0.0008	0.0099	0.168
33	34	1	0.0011	0.0157	0.202
33	38	1	0.0036	0.0444	0.693
34	36	2	0.0033	0.0111	1.45
35	45	1	0.0007	0.0175	1.39
36	61	1	0.0022	0.0196	0.34
36	61	2	0.0022	0.0196	0.34
37	52	1	0.0007	0.0082	0.1319
37	68	1	0.0007	0.0089	0.1342
38	46	1	0.0022	0.0284	0.43
39	44	1	0	0.0411	0
39	45	1	0	0.0839	0
40	41	1	0.006	0.084	3.15
40	48	1	0.002	0.022	1.28

From Bus	To Bus	Id	Line R (pu)	Line X (pu)	Charging (pu)
41	42	1	0.004	0.06	2.25
43	44	1	0.0001	0.0011	0
44	45	1	0.0025	0.073	0
45	51	1	0.0004	0.0105	0.72
46	49	1	0.0018	0.0274	0.27
47	48	1	0.0025	0.0268	0.4
47	48	2	0.0025	0.0268	0.4
47	53	1	0.0013	0.0188	1.31
50	51	1	0.0009	0.0221	1.62
52	55	1	0.0011	0.0133	0.2138
53	54	1	0.0035	0.0411	0.6987
54	55	1	0.0013	0.0151	0.2572
55	56	1	0.0013	0.0213	0.2214
56	57	1	0.0008	0.0128	0.1342
56	66	1	0.0008	0.0129	0.1382
57	58	1	0.0002	0.0026	0.0434
57	60	1	0.0008	0.0112	0.1476
58	59	1	0.0006	0.0092	0.113
58	63	1	0.0007	0.0082	0.1389
59	60	1	0.0004	0.0046	0.078
60	61	1	0.0023	0.0363	0.3804
62	63	1	0.0004	0.0043	0.0729
62	65	1	0.0004	0.0043	0.0729
65	66	1	0.0009	0.0101	0.1723
66	67	1	0.0018	0.0217	0.366
67	68	1	0.0009	0.0094	0.171

Transformer data:

From Bus	To Bus	R (pu)	X (pu)	Wnd 1 Ratio (pu)
1	54	0	0.0181	1.025
2	58	0	0.025	1.07
3	62	0	0.02	1.07
4	19	0.0007	0.0142	1.07
5	20	0.0009	0.018	1.009
6	22	0	0.0143	1.025
8	25	0.0006	0.0232	1.025
9	29	0.0008	0.0156	1.025
10	31	0	0.026	1.04
11	32	0	0.013	1.04
12	36	0	0.0075	1.04
13	17	0	0.0033	1.04
14	41	0	0.0015	1
15	42	0	0.0015	1
16	18	0	0.003	1
19	20	0.0007	0.0138	1.06
27	53	0.032	0.32	1
34	35	0.0001	0.0074	0.946
63	64	0.0016	0.0435	1.06
64	65	0.0016	0.0435	1.06

A.2 Central American System

Generator data. Part 1:

Bus Number	MW	Base MVA	X Source (pu)	T'do	T"do	T"qo	H	D
14319	30001.69	35000	0.06	7	0.04	0.01	4.48	10
1101	77.1	112.5	0.0358	7	0.075	0.06	10.8	1
1103	256.3	276.5	0.00769	8.3	0.025	0.025	19.265	1
1105	219.8	309.3	0.055	5.4	0.036	0.141	19.52	1
1115	59.07	75	0.02149	5.3	0.04	0.06	7.98	1
1121	140.51	191.53	0.02831	5.2	0.038	0.145	12.992	0
1216	45.27	59.18	0.135	2.2	0.041	0.1	6.825	1
1648	58.22	85.21	0.05775	4.4	0.035	0.129	5.1	1
1651	128.06	160	0.081	10.56	0.048	1	0.06	3.5
27101	80.7	110.4	0.144	7.15	0.065	0.065	14.05	0.4
27131	72.9	106.4	0.2	5.2	0.038	0.145	7.218	0
27161	78.6	115	0.06	5.5	0.048	0.58	0.05	16.5
27171	160	192	0.2	1.21	0.05	0.021	11.85	0
27181	173.92	196	0.2	4	0.05	0.11	11	0
27211	92.5	149	0.02	6	0.05	1.5	0.07	18
27371	64.25	97.5	0.124	4.1	0.024	0.098	18.33	0
3019	44	60	0.05	5.1	0.034	0.126	4.44	0.1
3023	20	33.25	0.2547	4.25	0.046	0.046	10	0.1
3032	211.33	365	0.319	7.15	0.065	0.065	17.6	1.1
3059	80	56	0.319	4	0.066	0.158	11.36	0.1
3080	79.75	115.6	0.05232	5.4	0.036	0.146	6.32	0.1
3098	80	84.2	0.146	7	0.07	0.07	15.88	0.1
3204	216.43	299.45	0.27	6.5	0.043	0.141	11.44	0
3355	227.7	320.17	0.2	6.5	0.043	0.141	11.44	0
4023	18.24	28.32	0.09	3.6	0.018	0.043	4.74	0
4029	18.24	28.32	0.0525	3.6	0.018	0.043	4.74	0
4032	18.24	28.32	0.107	3.6	0.018	0.043	4.74	0
4033	18.24	28.32	0.105	3.6	0.018	0.043	4.74	0
4047	34.74	51.92	0.083	3.6	0.018	0.043	8.69	0
4048	17.52	28.32	0.249	3.6	0.018	0.043	4.74	0
4066	23.12	37.76	0.085	3.6	0.018	0.043	6.32	0
4341	10	24	0.04727	11.2	0.04	0.3	0.04	4.4
4405	92.1	124	0.0975	5	0.035	0.3	0.04	10
4600	30.89	45	0.16	4.274	0.043	0.041	13.5	0
4604	64.51	86.8	0.0975	5.989	0.05	0.04	5.824	0
4608	36	55.2	0.144	6.6	0.035	0.4	0.04	5
4615	16.8	31.5	0.05225	5.9	0.04	0.06	4	0
4619	47.9	72.25	0.05675	5.4	0.036	0.04	10	0
50100	83.67	136.48	0.145	6	0.024	0.05	6.5	0
50123	30	33.66	0.045	4.05	0.04	0.08	5.86	0
50200	96	123.46	0.145	9.6	0.023	0.06	6.32	0

Bus Number	MW	Base MVA	X Source (pu)	T'do	T"do	T"qo	H	D
50270	55.2	61.2	0.0175	6.3	0.031	1.3	0.05	4.06
50271	55.1	61.2	0.29	6.3	0.031	1.3	0.05	4.06
50700	83.6	99	0.135	5.35	0.05	0.01	12.36	0
50820	37.8	44.4	0.02888	6.9	0.04	0.08	8.48	0
50970	37.9	51.73	0.09	7.5	0.04	0.01	4.11	0
50971	37.9	51.73	0.07	7.5	0.04	0.01	4.11	0
53204	117.8	93.6	0.29	7.15	0.065	0.065	12.06	0.1
53854	120	166.86	0.29	5.5	0.045	0.077	12	1
54154	49.8	59.61	0.145	5.694	0.058	0.127	7.65	0
54500	40	47	0.27	5.8	0.06	0.1	11.4	0
58004	62	90	0.145	7.15	0.065	0.065	6	0.1
58021	31	45	0.208	6	0.02	0.01	3	0
54250	94	169.6	0.145	12.6	0.045	0.035	0.035	3.4
58106	102	135	0.01254	9.6	0.023	0.01	8.94	0
6060	114	141	0.01407	5.1	0.02	0.7	0.1	13.35
6096	139.99	222	0.1	9	0.06	0.09	9,1	0.51
6105	90.6	124	0.166	4.6	0.035	0.031	5.58	0
6124	81.11	128.9	0.27	5.3	0.038	0.149	3.884	0
6133	29.7	39	0.1155	5	0.02	0.09	4.194	1
6172	50.85	64.1	0.01983	5.3	0.038	0.149	2.913	0
6178	114	138	0.02975	5.65	0.08	0.16	6.36	1
6270	82.6	109	0.01983	6.2	0.029	0.12	8.2	0
6280	47.88	41.36	0.01983	2.06	0.0203	0.017	3.72	0

Generator data. Part 2

Bus Number	Xd	Xq	X'd	X"d	Xl	S(1.0)	S(1.2)
1431	1	0.7	0.28	0.2	0.1	0.1	0.4
1101	0.4067	0.2833	0.1133	0.06	0.0453	0.0841	0.43
1103	0.21	0.116	0.049	0.0358	0.0286	0.1	0.07
1105	0.0685	0.0384	0.0125	0.0078	0.0054	0.1757	0.4696
1115	0.4	0.21	0.09	0.055	0.0477	0.129	0.3441
1121	0.1633	0.0888	0.0408	0.0215	0.017	0.11	0.44
1216	0.2143	0.1114	0.0443	0.0278	0.0186	0.0733	0.2355
1648	0.322	0.1773	0.0773	0.0523	0.0353	0.25	0.5439
1651	1	2.422	2.3251	0.203	0.3553	0.146	0.0812
27101	0.854	0.635	0.275	0.18	0.125	0.11	0.48
27131	1.47	0.8	0.367	0.1934	0.153	0.11	0.44
27161	0	1.815	1.76	0.272	0.454	0.132	0.3423
27171	0.98	0.7	0.27	0.241	0.14	0.102	0.5438
27181	0.87	0.59	0.29	0.25	0.09	0.125	0.4375
27211	0	1.19	1.15	0.26	0.4	0.131	0.753
27371	1.62	0.88	0.337	0.227	0.135	0.1	0.4
3019	0.4175	0.2075	0.078	0.05225	0.0312	0.11	0.48
3023	0.35	0.25	0.0933	0.0567	0.0312	0.11	0.48
3032	0.2135	0.15875	0.06875	0.045	0.0312	0.11	0.48
3059	0.1875	0.1125	0.034	0.0175	0.0156	0.11	0.48
3080	0.2263	0.1175	0.04288	0.0288	0.0156	0.11	0.48
3098	0.245	0.155	0.0875	0.07	0.0312	0.11	0.48
3204	0.1092	0.0596	0.02292	0.0125	0.0105	0.11	0.48
3355	0.1092	0.0596	0.02292	0.0125	0.0105	0.11	0.48
4023	0.2542	0.1458	0.02492	0.0198	0.012	0.086	0.343
4029	0.2542	0.1458	0.02492	0.0198	0.012	0.086	0.343
4032	0.2542	0.1458	0.02492	0.0198	0.012	0.086	0.343
4033	0.2542	0.1458	0.02492	0.0198	0.012	0.086	0.343
4047	0.13865	0.0795	0.01359	0.0108	0.007	0.086	0.343
4048	0.2542	0.1458	0.02492	0.0198	0.012	0.086	0.343
4066	0.1906	0.1094	0.0431	0.0148	0.009	0.086	0.343
4341	0	1.115	0.415	0.175	0.23	0.084	0.48
4405	0	0.935	0.89	0.0815	0.265	0.065	0.48
4600	0.1222	0.0711	0.02444	0.0155	0.011	0.086	0.343
4604	0.343	0.234	0.08975	0.055	0.023	0.086	0.343
4608	0	1.6	0.88	0.337	0.338	0.22	0.48
4615	1	0.6	0.267	0.158	0.087	0.086	0.343
4619	0.362	0.188	0.0762	0.044	0.0286	0.086	0.343
50100	1.006	0.65	0.32	0.229	0.115	0.1	0.4
50123	0.95	0.69	0.29	0.2	0.1	0.1	0.4

Bus Number	Xd	Xq	X'd	X"d	Xl	S(1.0)	S(1.2)
50200	1.08	0.65	0.302	0.207	0.103	0.1	0.4
50270	0	1.63	1.58	0.31	0.47	0.235	0.42
50271	0	1.63	1.58	0.31	0.47	0.115	0.4
50700	1	0.62	0.25	0.221	0.091	0.1	0.4
50820	0.94	0.68	0.204	0.145	0.1	0.1	0.4
50970	1.16	0.7	0.3	0.18	0.1	0.1	0.4
50971	1.16	0.7	0.3	0.18	0.1	0.1	0.4
53204	0.2135	0.1587	0.0687	0.045	0.0312	0.11	0.48
53854	1.22	0.73	0.3	0.2	0.122	0.0685	0.2443
54154	1.096	0.696	0.285	0.219	0.1	0.11	0.48
54500	0.9	0.62	0.33	0.23	0.1	0.11	0.48
58004	0.2135	0.1587	0.0687	0.045	0.0312	0.11	0.48
58021	1.1066	0.715	0.352	0.15	0.1265	0.11	0.48
54250	0	0.969	0.6	0.248	0.25	0.147	0.5743
58106	1.08	0.65	0.302	0.207	0.103	0.1	0.4
6060	0	0.47	0.45	0.052	0.2	0.04	0.5
6096	0.27	0.25	0.155	0.06	0.2	0.67	0.5
6105	0.24	0.13	0.05	0.037	0.03	0.1	0.5
6124	0.3825	0.2075	0.183	0.128	0.09	0.1	0.5
6133	0.363	0.28	0.156	0.109	0.087	0.19	0.59
6172	0.51	0.28	0.111	0.077	0.06	0.1	0.5
6178	0.525	0.365	0.185	0.129	0.103	1.05	1.5
6270	0.152	0.0768	0.0257	0.017	0.013	0.1	0.5
6280	0.3825	0.3725	0.0775	0.0522	0.0415	0.1	0.5

Exciters. Part 1: ESDC1A

Bus Number	TR	KA	TA	TB	TC	VRMAX	VRMIN	KE
1101	0	30	0.02	0	0	10	-10	1
1103	0	30	0.02	0	0	10	-10	1
1105	0	30	0.02	0	0	10	-10	1
1115	0	30	0.02	0	0	10	-10	1
1121	0	30	0.02	0	0	10	-10	1
1216	0	30	0.02	0	0	10	-10	1
1648	0	30	0.02	0	0	10	-10	1
1651	0	30	0.02	0	0	10	-10	1
27101	0	30	0.02	0	0	10	-10	1
27131	0	30	0.02	0	0	10	-10	1
27161	0	30	0.02	0	0	10	-10	1
27171	0	30	0.02	0	0	10	-10	1
27181	0	30	0.02	0	0	10	-10	1
27211	0	30	0.02	0	0	10	-10	1
27371	0	30	0.02	0	0	10	-10	1
3032	0	30	0.02	0	0	10	-10	1
3080	0	30	0.02	0	0	10	-10	1
3098	0	30	0.02	0	0	10	-10	1
3204	0	30	0.02	0	0	10	-10	1
4023	0	30	0.02	0	0	10	-10	1
4029	0	30	0.02	0	0	10	-10	1
4032	0	30	0.02	0	0	10	-10	1
4033	0	30	0.02	0	0	10	-10	1
4047	0	30	0.02	0	0	10	-10	1
4048	0	30	0.02	0	0	10	-10	1
4066	0	30	0.02	0	0	10	-10	1
4341	0	30	0.02	0	0	10	-10	1
4405	0	30	0.02	0	0	10	-10	1
4600	0	30	0.02	0	0	10	-10	1
4604	0	30	0.02	0	0	10	-10	1
4608	0	30	0.02	0	0	10	-10	1
4615	0	30	0.02	0	0	10	-10	1
4619	0	30	0.02	0	0	10	-10	1
50100	0	30	0.02	0	0	10	-10	1
50123	0	30	0.02	0	0	10	-10	1

Bus Number	TR	KA	TA	TB	TC	VRMAX	VRMIN	KE
50200	0	30	0.02	0	0	10	-10	1
50270	0	30	0.02	0	0	10	-10	1
50271	0	30	0.02	0	0	10	-10	1
50700	0	30	0.02	0	0	10	-10	1
50820	0	30	0.02	0	0	10	-10	1
50970	0	30	0.02	0	0	10	-10	1
50971	0	30	0.02	0	0	10	-10	1
53204	0	30	0.02	0	0	10	-10	1
53854	0	30	0.02	0	0	10	-10	1
54154	0	30	0.02	0	0	10	-10	1
54250	0	30	0.02	0	0	10	-10	1
58004	0	30	0.02	0	0	10	-10	1
58021	0	30	0.02	0	0	10	-10	1
58106	0	30	0.02	0	0	10	-10	1
6060	0	30	0.02	0	0	10	-10	1
6096	0	30	0.02	0	0	10	-10	1
6105	0	30	0.02	0	0	10	-10	1
6133	0	30	0.02	0	0	10	-10	1
6172	0	30	0.02	0	0	10	-10	1
6178	0	30	0.02	0	0	10	-10	1

Exciters. Part 2: ESDC1A

Bus Number	TE	KF	TF1	0	E1	SE(E1)	E2	SE(E2)
1101	0.785	0.03	1	0	3.9267	0.07	5.2356	0.91
1103	0.785	0.03	1	0	3.9267	0.07	5.2356	0.91
1105	0.785	0.03	1	0	3.9267	0.07	5.2356	0.91
1115	0.785	0.03	1	0	3.9267	0.07	5.2356	0.91
1121	0.785	0.03	1	0	3.9267	0.07	5.2356	0.91
1216	0.785	0.03	1	0	3.9267	0.07	5.2356	0.91
1648	0.785	0.03	1	0	3.9267	0.07	5.2356	0.91
1651	0.785	0.03	1	0	3.9267	0.07	5.2356	0.91
27101	0.785	0.03	1	0	3.9267	0.07	5.2356	0.91
27131	0.785	0.03	1	0	3.9267	0.07	5.2356	0.91
27161	0.785	0.03	1	0	3.9267	0.07	5.2356	0.91
27171	0.785	0.03	1	0	3.9267	0.07	5.2356	0.91
27181	0.785	0.03	1	0	3.9267	0.07	5.2356	0.91
27211	0.785	0.03	1	0	3.9267	0.07	5.2356	0.91
27371	0.785	0.03	1	0	3.9267	0.07	5.2356	0.91
3032	0.785	0.03	1	0	3.9267	0.07	5.2356	0.91
3080	0.785	0.03	1	0	3.9267	0.07	5.2356	0.91
3098	0.785	0.03	1	0	3.9267	0.07	5.2356	0.91
3204	0.785	0.03	1	0	3.9267	0.07	5.2356	0.91
4023	0.785	0.03	1	0	3.9267	0.07	5.2356	0.91
4029	0.785	0.03	1	0	3.9267	0.07	5.2356	0.91
4032	0.785	0.03	1	0	3.9267	0.07	5.2356	0.91
4033	0.785	0.03	1	0	3.9267	0.07	5.2356	0.91
4047	0.785	0.03	1	0	3.9267	0.07	5.2356	0.91
4048	0.785	0.03	1	0	3.9267	0.07	5.2356	0.91
4066	0.785	0.03	1	0	3.9267	0.07	5.2356	0.91
4341	0.785	0.03	1	0	3.9267	0.07	5.2356	0.91
4405	0.785	0.03	1	0	3.9267	0.07	5.2356	0.91
4600	0.785	0.03	1	0	3.9267	0.07	5.2356	0.91
4604	0.785	0.03	1	0	3.9267	0.07	5.2356	0.91
4608	0.785	0.03	1	0	3.9267	0.07	5.2356	0.91
4615	0.785	0.03	1	0	3.9267	0.07	5.2356	0.91
4619	0.785	0.03	1	0	3.9267	0.07	5.2356	0.91
50100	0.785	0.03	1	0	3.9267	0.07	5.2356	0.91
50123	0.785	0.03	1	0	3.9267	0.07	5.2356	0.91
50200	0.785	0.03	1	0	3.9267	0.07	5.2356	0.91
50270	0.785	0.03	1	0	3.9267	0.07	5.2356	0.91
50271	0.785	0.03	1	0	3.9267	0.07	5.2356	0.91
50700	0.785	0.03	1	0	3.9267	0.07	5.2356	0.91
50820	0.785	0.03	1	0	3.9267	0.07	5.2356	0.91

Bus Number	TE	KF	TF1	0	E1	SE(E1)	E2	SE(E2)
50970	0.785	0.03	1	0	3.9267	0.07	5.2356	0.91
50971	0.785	0.03	1	0	3.9267	0.07	5.2356	0.91
53204	0.785	0.03	1	0	3.9267	0.07	5.2356	0.91
53854	0.785	0.03	1	0	3.9267	0.07	5.2356	0.91
54154	0.785	0.03	1	0	3.9267	0.07	5.2356	0.91
54250	0.785	0.03	1	0	3.9267	0.07	5.2356	0.91
58004	0.785	0.03	1	0	3.9267	0.07	5.2356	0.91
58021	0.785	0.03	1	0	3.9267	0.07	5.2356	0.91
58106	0.785	0.03	1	0	3.9267	0.07	5.2356	0.91
6060	0.785	0.03	1	0	3.9267	0.07	5.2356	0.91
6096	0.785	0.03	1	0	3.9267	0.07	5.2356	0.91
6105	0.785	0.03	1	0	3.9267	0.07	5.2356	0.91
6133	0.785	0.03	1	0	3.9267	0.07	5.2356	0.91
6172	0.785	0.03	1	0	3.9267	0.07	5.2356	0.91
6178	0.785	0.03	1	0	3.9267	0.07	5.2356	0.91

PSSs : IEE2ST

IBUS	ICS1	ICS2	K1	K2	T1	T2	T3	T4
1103	1	3	1.584394	0	0	0	1.061181	0.9074
27181	1	3	4.369585	0	0	0	4.494686	0.3647
3204	1	3	2.426225	0	0	0	4.879754	2.4747
4032	1	3	0.668297	0	0	0	3.303737	0.2711
4033	1	3	0.968085	0	0	0	1.969993	0.081
4048	1	3	0.768569	0	0	0	1.933405	0.0204
4066	1	3	1.343913	0	0	0	1.948767	0.1951
4604	1	3	0.98742	0	0	0	1.291159	0.1339
4619	1	3	1.124356	0	0	0	2.91081	0.3296
50820	1	3	2.932009	0	0	0	1.581163	0.3437
50970	1	3	0.542694	0	0	0	2.115794	0.0178
53854	1	3	0.837803	0	0	0	2.855781	0.6625
58021	1	3	0.968085	0	0	0	1.969993	0.081
58106	1	3	3.707115	0	0	0	0.3176	0.011
6060	1	3	2.426225	0	0	0	4.879754	2.4747
6096	1	3	4.369585	0	0	0	4.494686	0.3647

IBUS	T5	T6	T7	T8	T9	T10	LSMAX	LSMIN
1103	0.730824	0.021735	0.57258	0.055211	0	0	0.1	-0.1
27181	0.611795	0.01295	1.518259	0.057149	0	0	0.1	-0.1
3204	0.458181	0.039922	1.345561	0.067378	0	0	0.1	-0.1
4032	0.081555	0.006141	0.677972	0.027118	0	0	0.1	-0.1
4033	0.295417	0.05912	0.327727	0.143938	0	0	0.1	-0.1
4048	0.120694	0.036101	0.310502	0.100671	0	0	0.1	-0.1
4066	0.175484	0.043612	0.210488	0.017899	0	0	0.1	-0.1
4604	0.343608	0.013679	0.515703	0.158011	0	0	0.1	-0.1
4619	0.442731	0.017249	0.893142	0.075606	0	0	0.1	-0.1
50820	0.14281	0.08656	0.584172	0.077582	0	0	0.1	-0.1
50970	0.286437	0.036048	0.24821	0.067025	0	0	0.1	-0.1
53854	0.183709	0.017217	0.478991	0.068903	0	0	0.1	-0.1
58021	0.295417	0.05912	0.327727	0.143938	0	0	0.1	-0.1
58106	0.331946	0.01839	0.345593	0.086234	0	0	0.1	-0.1
6060	0.458181	0.039922	1.345561	0.067378	0	0	0.1	-0.1
6096	0.611795	0.01295	1.518259	0.057149	0	0	0.1	-0.1

APPENDIX B

Computational Routines

B.1 Matlab Routine for Dynamic Reduction

```
function obj_fun=ssat_acc(xn)
pause(15)
xb=[1 2 2 0.2 0.04 0.39 0.12];
X0={'1.00' '2.00' '2.0' '0.2' '0.04' '0.39' '0.12'};
x=xn.*xb;
for i=1:length(x);
  X{i}=num2str(x(i));
end
for i=1:length(x)
  LX(i)=length(X{i});
end
for i=1:length(x)
  LX0(i)=length(X0{i});
end
data=fopen('CAMAX_RED4_b_DYN.dyr','r');
fid=fopen('CAMAX_RED4_DYN.dyr','w');
formatSpec = '%s\n';
line=1;
n=1;
while 1
  if line==-1
    break
  else
    line=fgetl(data);
    if line~=-1
      % Write line 158:
      if n==158
        for c=1:length(line)
          if strcmp(line(c:c+LX0(1)-1),X0{1})
            line(c:c+LX0(1)-1)=' ';
            line(c:c+LX(1)-1)=X{1};
          elseif strcmp(line(c:c+LX0(2)-
1),X0{2})
            line(c:c+LX0(2)-1)=' ';
            line(c:c+LX(2)-1)=X{2};
          elseif % Repeat for all characters in X
            break
          else
          end
        end
      else
      end
      fprintf(fid,formatSpec,line);
      n=n+1;
    else
    end
  end
end
fclose(data);
fclose(fid);
dos('ssat_batch CAMAX_RED4.ssa');
dos CAMAX_RED_SSAT.exe;
data=fopen('eigenv01.txt','r');
line=1;
n=1;
e_line=0;
while e_line<2
  line=fgetl(data);
  if and(line==-1,e_line==0)
    L(n,:)=[100 100 100 100 11 1];
    n=n+1;
    display('Eigenvalue 1 empty')
    break
  else
  end
  if length(line)>1
    e_line=0;
    if strcmp(line(1:10),'Eigenvalue')
      for c=11:length(line)
        if strcmp(line(c),':')
          ci=c+2;
        elseif strcmp(line(c),'+')
          cf=c-1;
          break
```

```
      else
      end
    end
    L(n,1)=str2double(line(ci:cf));
    ci=cf+3;
    for c=ci:length(line)
      if strcmp(line(c),' ')
        cf=c-1;
        break
      else
      end
    end
    L(n,1)=L(n,1)+1i*str2double(line(ci:cf));
    ci=cf+2;
    for c=ci:length(line)
      if strcmp(line(c),'H')
        cf=c-1;
        break
      else
      end
    end
    L(n,2)=str2double(line(ci:cf));
    ci=cf+4;
    cf=length(line)-1;
    L(n,3)=str2double(line(ci:cf))/100;
  else
    ci=25;
    for c=ci:length(line)
      if strcmp(line(c),' ')
        cf=c-1;
        break
      else
      end
    end
    L(n,4)=str2double(line(ci:cf));
    for c=cf:length(line)
      if strcmp(line(c:c+4),'Model')
        ci=c+8;
        break
      else
      end
    end
    for c=ci:length(line)
      if strcmp(line(c),' ')
        cf=c-1;
        break
      else
      end
    end
    model=line(ci:cf);
    if strcmp(model,'GAST')
      L(n,5)=1;
    elseif % Repeat for all dynamic models
    else
    end
    L(n,6)=str2double(line(length(line)));
    n=n+1;
  end
else
  e_line=e_line+1;
end
end
data=fopen('eigenv02.txt','r');
line=1;
e_line=0;
while e_line<2
  line=fgetl(data);
  if and(line==-1,e_line==0)
    L(n,:)=[100 100 100 100 11 1];
    n=n+1;
    display('Eigenvalue 2 empty')
    break
  else
  end
  if length(line)>1
    e_line=0;
    if strcmp(line(1:10),'Eigenvalue')
      for c=11:length(line)
        if strcmp(line(c),':')
          ci=c+2;
        elseif strcmp(line(c),'+')
          cf=c-1;
          break
        else
```

```
        end
    end
    L(n,1)=str2double(line(ci:cf));
    ci=cf+3;
    for c=ci:length(line)
        if strcmp(line(c),' ')
            cf=c-1;
            break
        else
        end
    end
    L(n,1)=L(n,1)+1i*str2double(line(ci:cf));
    ci=cf+2;
    for c=ci:length(line)
        if strcmp(line(c),'H')
            cf=c-1;
            break
        else
        end
    end
    L(n,2)=str2double(line(ci:cf));
    ci=cf+4;
    cf=length(line)-1;
    L(n,3)=str2double(line(ci:cf))/100;
else
    ci=25;
    for c=ci:length(line)
        if strcmp(line(c),' ')
            cf=c-1;
            break
        else
        end
    end
    L(n,4)=str2double(line(ci:cf));
    for c=cf:length(line)
        if strcmp(line(c:c+4),'Model')
            ci=c+8;
            break
        else
        end
    end
    for c=ci:length(line)
        if strcmp(line(c),' ')
            cf=c-1;
            break
        else
        end
    end
    model=line(ci:cf);
    if strcmp(model,'GAST')
        L(n,5)=1;
    elseif strcmp(model,'ESAC8B')
        L(n,5)=2;
    elseif % Repeat for all dynamic models
    else
    end
    L(n,6)=str2double(line(length(line)));
    n=n+1;
  end
else
  e_line=e_line+1;
end
end
fclose('all');
S=size(L);
j=1;
for i=1:S(1)
  if or(L(i,5)==7,L(i,5)==11)
    L_(j,:)=L(i,:);
    j=j+1;
  elseif or(L(i,5)==16,L(i,5)==17)
    L_(j,:)=L(i,:);
    j=j+1;
  else
  end
end
S=size(L_);
j=1;
for i=1:S(1)
  if or(L_(i,6)==1,L_(i,6)==2)
    L_rotor(j,:)=L_(i,:);
    j=j+1;
  else
  end
```

```
end
L_f0=[11;11;11;11;11;11;11;11;11;11;11;11;
11;11]/100;
S=size(L_rotor);
if S(1)==15
   obj_fun_=zeros(15,1);
   for n=1:15
      obj_fun_(n)=abs(L_rotor(n,3)-
L_f0(n))/L_f0(n);
   end
   obj_fun=sum(obj_fun_);
else
   obj_fun=500;
   size(L)
   L
end
```

B.2 Matlab Routine to Compute the Effect of Latency

```
case_idx=[1019 117 323 1031 1216 1018 506
2225 1524 2615 2000 1123];
T=1/(30);
Bc=xlsread('centro_am.xlsx','B','A1:P597');
dist=0.1;
count=2;
for m=1:length(case_idx)
   file_A=num2str(case_idx(1,m),'%4.4u');
   caso1=strcat('ACA',file_A,'.mat');
   load(caso1);
   Ac=a_mat;
   N=length(Ac);
   [Ad Bd]=c2d(Ac,Bc,T);

current(1,:)={'point','gain','stab','latency','state'}
;
   for q=1:12
      file_B=num2str(q-1,'%2.2u');
      caso2=strcat('KCA',file_B,'.mat');
      load(caso2);
      l=0;
      while l<=20 % Number of delayed samples
to consider
         k=1;
         c=1;
         while k<=10 % State to disturb. Ideally
this should be N
            x=zeros(N,1);
            x(k,1)=dist;
            for n=1:600
               %x(:,n+1)=Ad*x(:,n);
               if n-l<1
                  x(:,n+1)=Ad*x(:,n);
               else
                  x(:,n+1)=Ad*x(:,n)-Bd*K*x(:,n-l);
               end
            end
            for p=1:2 % Signals on which stability
will be assessed. Ideally should be N
               [Num,Den] = prony(x(p,:),3,6);
               stab_idx(p)=max(abs(roots(Den)));
               if stab_idx(p)>10.001
                  L(c)=l;
                  c=c+1;
                  est=k;
                  k=N;
                  break
               else
               end
            end
            plot(x','LineWidth',2)
            grid

current(count,:)={caso1,caso2,max(stab_idx),l,k
}
            k=k+1;
         end
         if c>1
            l=20;
         else
         end
         l=l+1;
      end
      if c==1
         disp('Latency does not affect stability')

current(count,:)={caso1,caso2,max(abs(roots(D
en))),'l>20','any'}
         count=count+1;
      else
         disp('The maximum delay tollerated is:')
         disp(min(L)-1)

current(count,:)={caso1,caso2,max(abs(roots(D
en))),min(L)-1,est}
         count=count+1;
      end
   end
end
```

APPENDIX C

Selected Decision Trees

Decision Tree 1:

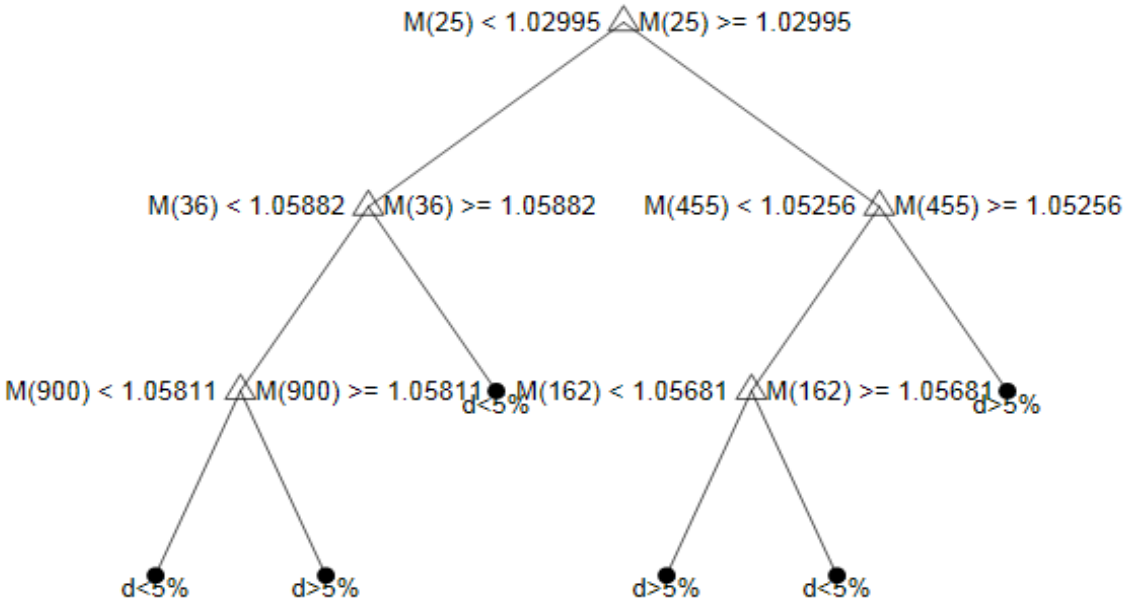

Decision Tree 4:

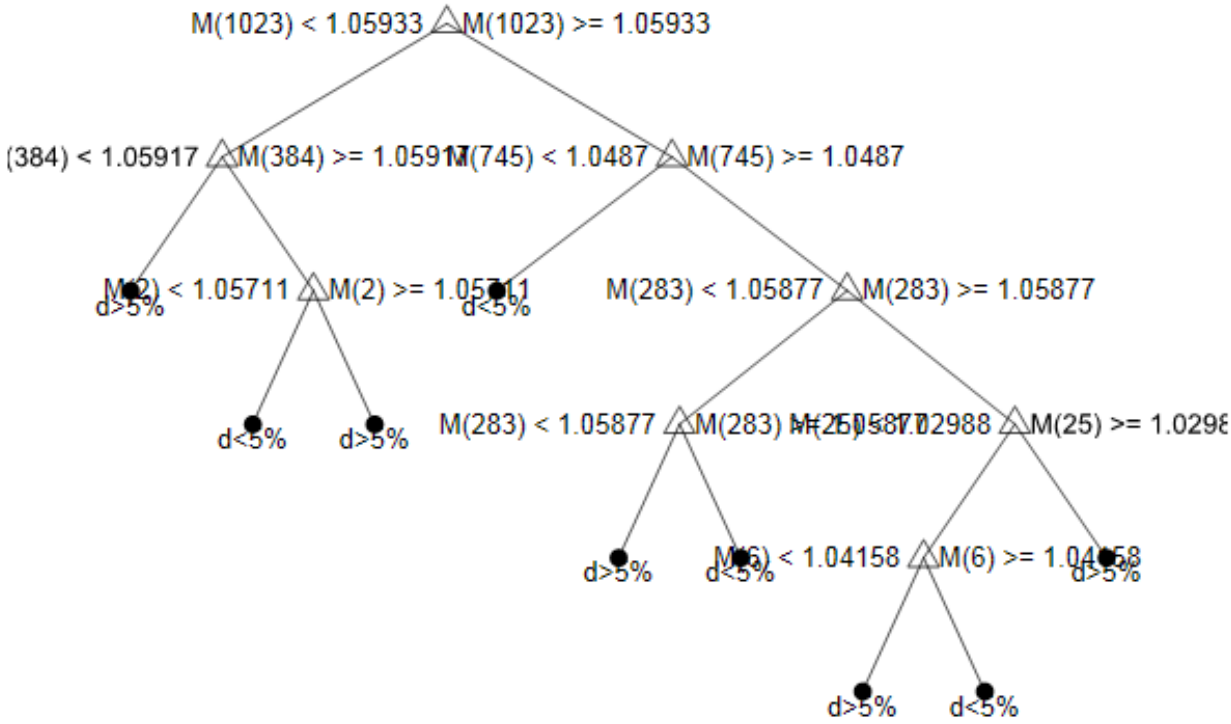

Decision Tree 5:

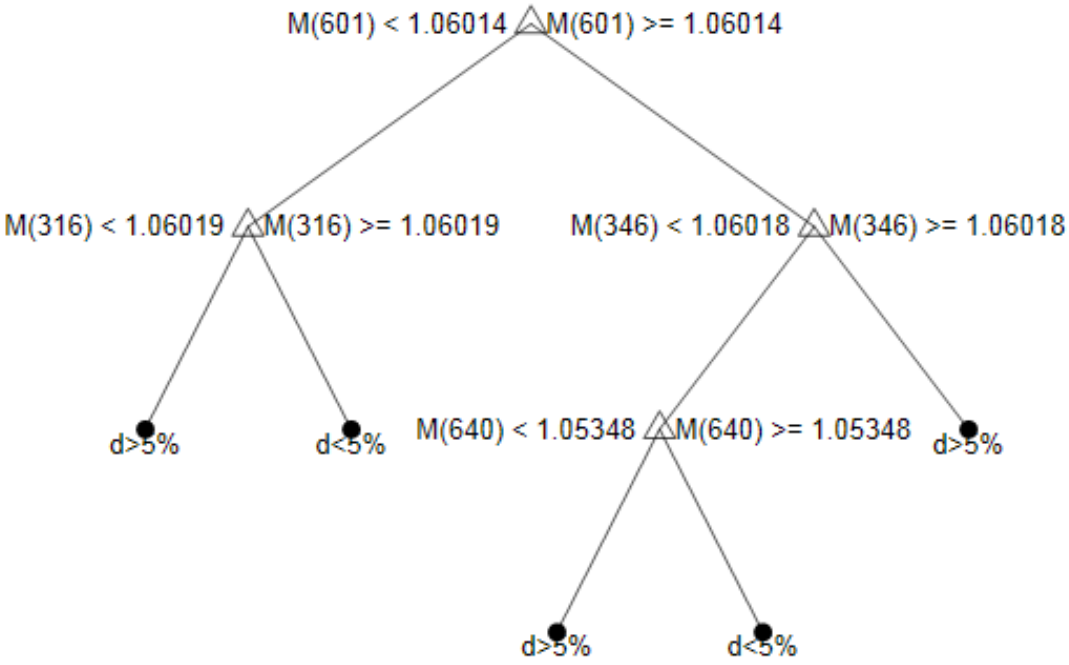

Decision Tree 6:

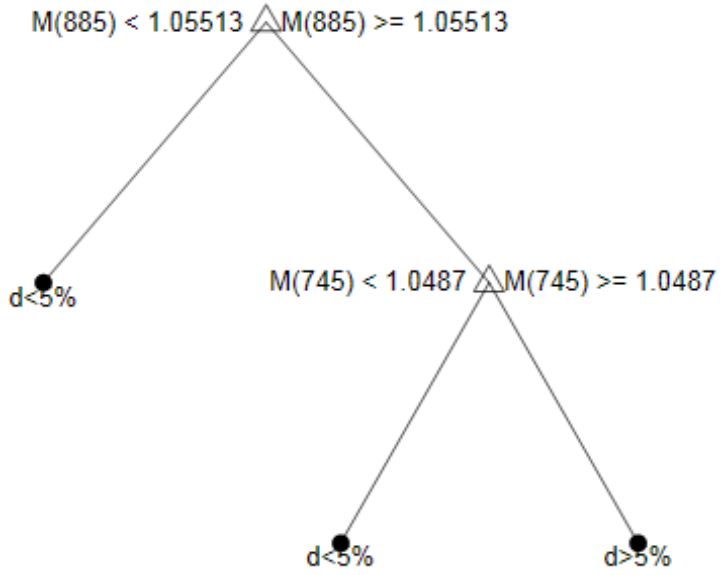

Decision Tree 7: